

Elastic pion-nucleon scattering in chiral perturbation theory: Explicit $\Delta(1232)$ degrees of freedom

D. Siemens^{1,*}

¹*Independent*

Abstract

For the first time, elastic pion-nucleon scattering is analyzed in the framework of chiral perturbation theory up to fourth order with explicit Δ degrees of freedom. The analysis is performed within the heavy-baryon expansion as well as in a covariant approach based on an extended on-mass-shell renormalization scheme. The renormalization of low-energy constants in both chiral approaches is discussed in detail and the explicit expressions to cancel both power-counting breaking as well as decoupling breaking terms are given. The low-energy constants from the $2\pi\bar{N}N$ interaction as well as additional constants from the Δ sector are reliably constrained by fits to experimental data. The traditional K -matrix unitarization is employed in the near threshold region, whereas a complex mass approach is used to extend the applicability of the theory up to the Δ pole region. Additionally, we estimate a theoretical error based on the truncation of the chiral series as employed in recent analyses of nuclear forces as well as pion-nucleon scattering. The obtained results provide a clear evidence that the explicit inclusion of Δ degrees of freedom is fundamental to describe pion-nucleon physics at threshold. The resulting predictions for the subthreshold and threshold parameters as well as phase shifts are in excellent agreement with the ones determined by the recent Roy-Steiner analysis of pion-nucleon scattering.

*dmitrij.siemens@rub.de

I. INTRODUCTION

Relying on the approximate chiral symmetry of QCD and its strong constraints on low-energy hadronic dynamics, Chiral perturbation theory (χ PT), an effective field theory of the strong interactions, provides the toolkit to perform a systematically improvable expansion of low-energy hadronic observables around the chiral and zero-energy limit. Starting with the pioneering work in the meson sector [1–3], χ PT has been extended to the single-baryon and few baryon sectors [4–11], including numerous applications and extensions like the heavy baryon (HB) approach, the infrared renormalization scheme or the extended on-mass shell scheme [12–17]. The interested reader is referred to Ref. [7] for a detailed discussion and comparison of the various formulations of χ PT.

One of the most studied hadronic processes in χ PT is low-energy pion-nucleon scattering. The recent interest in this reaction stems from the observation that the pion-nucleon LECs enter the two-pion exchange contributions to the two- and three-nucleon forces [18–22]. Thus, these pion-nucleon LECs are vital inputs for nuclear chiral EFT [23] and a reliable extraction of these LECs becomes a crucial task in understanding the long-range behavior of nuclear forces

In this paper, elastic low-energy pion-nucleon scattering is analyzed in detail within the HB and covariant baryon χ PT formulation at the full one-loop order. In particular, the effects of including the Δ resonance as an explicit degree of freedom in a consistent power counting is the focus of this analysis. In this work, we employ the so called small scale expansion ε , where the difference between the $\Delta(1232)$ mass and the nucleon mass is counted as of the same order as the pion mass [24]. Mainly due to the analytic complexity of calculating loop graphs including the Δ resonance, previous analyses of pion-nucleon scattering in the framework of baryon χ PT are shy of including explicit Δ degrees of freedom or only study the effects of leading-order Δ contributions [13, 25–35]. Within the small scale expansion, the first calculations of loop contributions to the πN amplitude were performed in the HB approach two decades ago [36] and only a couple years ago in the covariant approach as well [37]. In both analyses, the amplitudes are determined up to the leading-loop order ε^3 and fits to the S - and P -wave phase shifts are performed to extract the πN -LECs.

The analysis carried out in this paper is strongly motivated by the obstacles encountered in Ref. [37]. Thus, we give a brief summary of this paper in the following. In Ref. [37], we calculated the pion-nucleon scattering amplitude in the small scale expansion up to order ε^3 and renormalized $2\pi\bar{N}N$ -LECs within the EOMS scheme [16, 17], such that only the LECs c_i are shifted to absorb power counting breaking terms (PCBTs). In addition, we employed a complex Δ mass in the amplitudes. Finally, the unknown LECs are extracted from fits to the Roy-Steiner (RS) phase shifts including their uncertainties. Given that the RS analysis provides parametrization for the S - and P -waves, equidistant points are generated and then the corresponding mean values are normally distributed, such that the reduced χ^2 gets the proper definition of $\chi^2/\text{dof} \sim 1$. The outcome of this analysis is a good agreement with the RS values [38] regarding the fitted phase shifts and predicted threshold parameters. Unfortunately, the LECs extracted from the fits to the phase shifts turn out to be strongly correlated. Note that the above

mentioned Δ -less analyses exhibited strong correlations only at order Q^4 . Compared to a Δ -less analysis at order Q^3 , only two more LECs are introduced by the explicit Δ degrees of freedom at order ε^3 . All in all, a reliable determination of LECs from fitting to phase shifts seems problematic, especially when considering even higher-order calculations like the one carried out in this work.

Encouraged by our analysis in Ref. [26], this paper follows the more tedious path of studying the large amount of available data on pion-nucleon scattering observables at low energies. Furthermore, we employ a systematic approach of including the theoretical uncertainty stemming from the truncation of the chiral expansion into the fitting procedure, which was motivated in Ref. [39]. Note that recently a more sophisticated approach for estimating the truncation errors was introduced in Refs. [40, 41]. In contrast to the analyses where phase shifts are used as inputs in the fitting routine, we are able to give predictions for the phase shifts based on experimental scattering data employing χ PT amplitudes. In addition, two different unitarization prescriptions for the π N amplitudes are employed in this paper. First, we study the near threshold region and employ the standard K -matrix unitarization. Second, when increasing the energy up to the Δ pole region, we employ a complex mass for the Δ resonance instead. To the best of our knowledge, this is the first full one-loop order calculation including Δ degrees of freedom within the HB and covariant baryon framework of χ PT. In the small scale expansion this corresponds to order ε^4 . At this time, it is practically not feasible to perform calculations beyond one-loop level, mainly due to the complexity of multi-loop amplitudes. Another achievement of this work is the first time discussion of the complete renormalization procedure of the leading-order coupling constants and the pion-nucleon amplitude up to order ε^4 in both chiral approaches.

Given the motivation above, it is natural that we extend the Δ -less analysis in Ref. [26] in this paper. Thus, we refer the unfamiliar reader for details on kinematics, observables, renormalization and fitting procedure to this reference. For the sake of brevity, only the fundamental differences due to the explicit inclusion of the Δ degrees of freedom are discussed in the following sections.

The organization of this paper is as follows. In section II, we describe the two different unitarization prescriptions, K -matrix unitarization and complex mass approach. Then, in section III, the renormalization schemes including explicit Δ dynamics are discussed in detail for both chiral approaches. The specifics of the fitting procedure are explained in section IV. In section V, the predicted observables in both unitarization schemes are visualized and discussed. Finally, we summarize the main results of this analysis in section VI. In the appendix we give explicit expressions for the renormalized LECs in the HB framework and refer to the supplementary material in the form of a Mathematica notebook for the covariant expressions.

II. BASIC DEFINITIONS

The extraction of real-valued phase shifts demands an unitarization prescription for the perturbative partial wave amplitudes. Whereas the standard approach is to use the K -matrix unitarization for all partial waves, we employ a second additional unitarization prescription in the analysis presented here. In the following, we review the general idea

of an unitarized perturbative amplitude. In particular, we demonstrate the breakdown of the K -matrix unitarization and emphasize the need of another more general unitarization prescription.

For an elastic scattering process, the transition matrix is given by

$$T_{l\pm}(s) = |\mathbf{q}|f_{l\pm}(s) = \frac{1}{2i} (e^{2i\delta_{l\pm}(s)} - 1) , \quad (1)$$

where \mathbf{q} is the center-of-mass three-momentum. Phase shifts can be extracted from the partial wave amplitude via

$$\delta_{l\pm}^I(s) = \text{Arg}(f_{l\pm}^I(s)) . \quad (2)$$

Below the inelastic threshold, partial wave unitarity

$$\text{Im } f_{l\pm}^I(s) = |\mathbf{q}||f_{l\pm}^I(s)|^2 \quad (3)$$

can be used to write Eq. (2) as

$$\delta_{l\pm}^I(s) = \arctan \left(\frac{|\mathbf{q}|(\text{Re}(f_{l\pm}^I(s))^2 + \text{Im}(f_{l\pm}^I(s))^2)}{\text{Re}(f_{l\pm}^I(s))} \right) = \arctan \left(\frac{|\mathbf{q}|}{\text{Re}(f_{l\pm}^I(s)^{-1})} \right) . \quad (4)$$

In χ PT, however, the partial wave amplitude up to chiral order n

$$f = f^{(1)} + f^{(2)} + \dots + f^{(n)} \quad (5)$$

fulfils the unitarity condition in Eq. (3) not exactly but only perturbatively, e.g., for $n = 4$ one has

$$\begin{aligned} \text{Im } f^{(3)} + \text{Im } f^{(4)} &= |\mathbf{q}||f^{(1)} + f^{(2)} + f^{(3)} + f^{(4)}|^2 \\ &= |\mathbf{q}|[(\text{Re}f^{(1)})^2 + 2\text{Re}f^{(1)}\text{Re}f^{(2)}] + \dots \end{aligned} \quad (6)$$

Thus, the idea is to enforce the unitarity condition on the perturbative amplitude by employing Eq. (4) instead of Eq. (2) such that the extracted phase shifts are real-valued. For the special case of non-resonant partial waves, Eq. (4) can be expanded in $\text{Im } f_{l\pm}^I(s)$ such that to leading-order one gets

$$\delta_{l\pm}^I(s) = \arctan(|\mathbf{q}|\text{Re } f_{l\pm}^I(s)) . \quad (7)$$

The above equality assumes that imaginary parts do not need to be resummed and are always suppressed compared to the real parts. To be more precise, Eq. (6) is equivalent to the so-called K -matrix unitarization, where one chooses

$$f^K = \frac{\text{Re}f}{1 - i|\mathbf{q}|\text{Re}f} \quad (8)$$

such that inserting in Eq. (2) yields

$$\delta = \text{Arg}(f^K) = \arctan \left(\frac{\text{Im}f^K}{\text{Re}f^K} \right) = \arctan(|\mathbf{q}|\text{Re}f) . \quad (9)$$

Note that for the sake of simplicity, all indices have been suppressed in the last two equations. We will use the same notation in the following as well. In the case of resonant partial waves,

the K -matrix unitarization prescription in Eq. (8) generates the respective resonance width by an infinite resummation of self-energy contributions. This can be seen by considering only the pole contribution f^{Pole} of a resonance and employing the geometric series for Eq. (8), such that one has

$$f^K = \frac{\text{Re}f^{Pole}}{1 - i|\mathbf{q}|\text{Re}f^{Pole}} \simeq \text{Re}f^{Pole}(1 + i|\mathbf{q}|\text{Re}f^{Pole} + (i|\mathbf{q}|\text{Re}f^{Pole})^2 + \dots) . \quad (10)$$

One can also take into account further contributions from the amplitude f , which will give an infinite resummation of many different topologies. This approach is clearly not based on a power counting scheme but non-perturbatively resums higher-order contributions. However, for smaller values of the phase shifts this modification is negligible. To be more precise, the condition is

$$|\mathbf{q}|\text{Re}f = \tan \delta \ll 1 \quad (11)$$

or translating into a rule of thumb for the phase shifts

$$\tan \delta \simeq \delta , \quad (12)$$

which is a good approximation for $|\delta| \ll \pi/6$.

In the following, to extract real-valued phase shifts the partial wave amplitudes deduced from the T -matrix of $\pi N \rightarrow \pi N$ are unitarized in two different ways:

- K -matrix approach: The standard K -matrix unitarization given in Eq. (7) is used for all partial waves. This approach is used in the threshold region, especially far below the Δ pole region. Here, we employ the real-valued Breit-Wigner mass of the $\Delta(1232)$ in our amplitudes.
- Complex mass approach: To extend the applicability of the theory to the Δ pole region the complex mass renormalization scheme [42–44] is employed. Like in Ref. [37], only the P_{33} partial wave is unitarized by the prescription in Eq. (4), whereas for all the remaining non-resonant partial waves the K -matrix unitarization in Eq. (7) is used. Here, we employ the complex-valued pole mass of the $\Delta(1232)$ in our amplitudes, which is equivalent to a resummation of graphs corresponding to the Δ width based on a consistent power counting.

At this point, we emphasize that the K -matrix unitarization should not be used for the P_{33} partial wave in combination with a complex-valued Δ mass in the amplitudes. This would lead to a double counting of particular graphs due to the additional resummation by the K -matrix unitarization, see Eq. (10). However, it is fine to employ the K -matrix unitarization for non-resonant partial waves, given that for these partial waves the difference between Eq. (4) and Eq. (7) is of higher order only.

III. RENORMALIZATION PROCEDURE

A. Pion-Nucleon Scattering Amplitudes

In this work, the chiral amplitudes for pion-nucleon scattering including explicit Δ degrees of freedom are calculated in the small scale expansion with the expansion parameter

$$\varepsilon = \left\{ \frac{q}{\Lambda_b}, \frac{M_\pi}{\Lambda_b}, \frac{\Delta}{\Lambda_b} \right\} , \quad \text{where} \quad \Lambda_b \in \{\Lambda_\chi, 4\pi F, m\} . \quad (13)$$

Note that the explicit expansion in inverse powers of m is only carried out in the HB framework. To be precise the T -matrix for $\pi^a(q) N(p) \rightarrow \pi^b(q') N'(p')$ can be decomposed in the following way

$$T^{ba} = \chi_{N'}^\dagger (\delta^{ab} T^+ + i\epsilon^{bac} \tau_c T^-) \chi_N, \quad (14)$$

where in the covariant approach

$$T^\pm = \bar{u}^{(s')} \left(D^\pm - \frac{1}{4m_N} [\not{q}', \not{q}] B^\pm \right) u^{(s)} \quad (15)$$

and in the HB approach

$$T^\pm = \bar{u}_v^{(s')} (g^\pm + 2i \mathbf{S} \cdot \mathbf{q} \times \mathbf{q}' h^\pm) u_v^{(s)}. \quad (16)$$

The Mandelstam variables are defined in the standard way

$$s = (p + q)^2, \quad t = (q - q')^2, \quad u = (p' - q)^2, \quad s + t + u = 2m_N^2 + 2M_\pi^2. \quad (17)$$

The effective chiral Lagrangian to describe pion-nucleon dynamics at the full one-loop level with explicit Δ resonances thus reads

$$\begin{aligned} \mathcal{L}_{\text{eff}} = & \mathcal{L}_{\pi\pi}^{(2)} + \mathcal{L}_{\pi\pi}^{(4)} + \mathcal{L}_{\pi N}^{(1)} + \mathcal{L}_{\pi N}^{(2)} + \mathcal{L}_{\pi N}^{(3)} + \mathcal{L}_{\pi N}^{(4)} \\ & + \mathcal{L}_{\pi\Delta}^{(1)} + \mathcal{L}_{\pi\Delta}^{(2)} + \mathcal{L}_{\pi\Delta}^{(4)} \\ & + \mathcal{L}_{\pi N\Delta}^{(1)} + \mathcal{L}_{\pi N\Delta}^{(2)} + \mathcal{L}_{\pi N\Delta}^{(3)} + \mathcal{L}_{\pi N\Delta}^{(4)} \end{aligned} \quad (18)$$

with the individual terms presented in appendix A. Note that the notation for coupling constants and other quantities used in the following is explained in the above mentioned appendix as well. Thus, before continuing reading this section, we refer the reader to look through this appendix first.

In the following, we sketch the routine employed to calculate the full ε^4 results in both chiral frameworks. At tree-level, the covariant amplitudes were determined based on the corresponding covariant Lagrangian. Then, to get the HB expressions, we expanded those covariant amplitudes in inverse powers of the nucleon mass m . In principle, one could proceed at loop-level in analogy and perform a strict expansion of loop-level amplitudes in small parameters. However, this is a non-trivial task, in particular, for loop functions including several propagators. Instead, we calculated both sets of loop-level amplitudes based on the corresponding effective Lagrangians. At this point, we emphasize the redundant dependence of the Lagrangian presented in appendix A on the off-shell parameters z_i and y_i [45–47]. To be precise, in the loop-level amplitudes, we only kept track of z_0 , whereas the dependence on y_1 and z_1 is a higher-order effect and thus was neglected. In the tree-level amplitudes, the off-shell parameters y_i and z_i would show up in $1/m$ corrections to the LECs b_i and h_i . However, these LECs can be absorbed into the $2\pi NN$ -LECs and the renormalization of h and thus are redundant in the πN amplitude. In Appendix B, we present all the necessary shifts to cancel the redundant LECs b_3 , b_6 , c_i^Δ and h_i and the off-shell parameter z_0 in the amplitudes. Note that the shifts are given in the strict HB expansion only. In the covariant approach, we just set $z_0 = z_1 = z_2 = y_1 = y_3 = 0$ and $b_3 = b_6 = h_i = c_i^\Delta = 0$.

B. Coupling Constants

As a next step, we consider the renormalization of coupling constants. We start with the bare quantities in the leading-order Lagrangian which are renormalized on mass-shell. The renormalization of the quantities from the nucleon sector, mass m and coupling g , is extended by explicit Δ contributions. Additionally, the quantities from the Δ sector, mass \mathbf{m} and coupling h , have to be considered. In Appendix C, we give the explicit expressions for m_N , Z_N , g_A and m_Δ , Z_Δ , h_A in both chiral approaches.

After performing all the redundancy shifts and the renormalization of the leading-order couplings, both discussed above, the remaining $2\pi\bar{N}N$ -LECs are renormalized. In particular, we choose to absorb UV divergent pieces as well as additional finite pieces. The main steps necessary to identify both types of these pieces are:

- Perform a Taylor series of the full amplitude in powers of small scales while interchanging the loop integration with a power series of the integrand
- After performing this power series, absorb all remaining parts of the loop amplitude order-by-order into the corresponding LECs
- Return to the full amplitude and redefine the LECs as constrained in the previous step
- Absorb all remaining UV divergent pieces in the full amplitude into corresponding LECs

In the following, we discuss the results for both chiral approaches after performing the above steps. Considering the HB framework, we have

$$\begin{aligned} c_i &= \bar{c}_i + \delta c_i^{(3,\Delta)} + \delta c_i^{(4,\Delta)} , \\ d_i &= \bar{d}_i + \delta d_i + \delta d_i^{(3,\Delta)} + \delta d_i^{(4,\Delta)} , \\ e_i &= \bar{e}_i + \delta e_i + \delta e_i^{(4,\Delta)} , \end{aligned} \tag{19}$$

where for $x \in \{c, d, e\}$ one has

$$\begin{aligned} \delta x_i &= \frac{\beta_{x_i} + \beta_{x_i}^\Delta}{F_\pi^2} \left(\bar{\lambda} + \frac{1}{32\pi^2} \ln \left(\frac{M_\pi^2}{\mu^2} \right) \right) , \\ \delta x_i^{(n,\Delta)} &= \frac{\delta \bar{x}_{i,f}^{(n,\Delta)}}{F_\pi^2} + \frac{\beta_{x_i}^{(n,\Delta)}}{F_\pi^2} \left(\bar{\lambda} + \frac{1}{16\pi^2} \ln \left(\frac{2\Delta}{\mu} \right) \right) \end{aligned} \tag{20}$$

with

$$\bar{\lambda} = \frac{\mu^{d-4}}{16\pi^2} \left(\frac{1}{d-4} + \frac{1}{2}(\gamma_E - 1 - \ln 4\pi) \right) . \tag{21}$$

The additional finite pieces are denoted by $\delta \bar{x}_{i,f}^{(n,\Delta)}$. They are needed to absorb decoupling breaking pieces, which are generated by loop functions. According to the decoupling theorem, all Δ contributions in the amplitude have to vanish in the decoupling limit $\Delta \rightarrow \infty$. As already pointed out in Ref. [48], this theorem is explicitly satisfied for tree-level contributions of resonances like the Δ or Roper resonances. At loop-level, however, loop functions

generate terms with positive power of the mass splitting Δ , which do not vanish explicitly in the decoupling limit. We emphasize that these decouplings breaking terms (DBTs) are very similar to the PCBTs in the covariant formalism of baryon χ PT [16, 17]. The difference to the PCBTs is that the DBTs in the HB framework obey the naive power counting, simply because the mass splitting Δ is regarded as a small scale and not as a large scale like the nucleon mass m_N . However, if one chose a counting scheme where the mass splitting is a large scale $\Delta \sim O(\varepsilon^0)$, then the DBTs would violate the naive power counting. Clearly, this counting scheme coincides with the decoupling limit. At this point, we also would like to point out a feature of the HB framework. In the construction of the Lagrangian, we employ an expansion around $m_N \sim O(\varepsilon^0)$ and $\Delta \sim O(\varepsilon^1)$, but then for the decoupling limit we need to take $\Delta \rightarrow \infty$ in the amplitudes. Thus, terms proportional to e.g., Δ/m_N which seem to break decoupling, actually vanish in the decoupling limit

$$\Delta/m_N \xrightarrow{\Delta \rightarrow \infty} 0, \quad (22)$$

because $\Delta \ll m_N$ by construction. In summary, the DBTs in the d -dimensional HB amplitude are cancelled by absorbing all IR regular contributions from loops into the $2\pi\bar{N}N$ -LECs. To be precise, we expand in the following scales

$$\omega \sim M_\pi \sim O(\varepsilon^1), \quad t \sim O(\varepsilon^2), \quad m_N \sim \Delta \sim O(\varepsilon^0). \quad (23)$$

Note that this is in evident analogy to EOMS in the covariant formalism. To calculate the IR regular part of a loop function, the loop momentum integration is interchanged with a Taylor expansion of the integrand in powers of the small scales in Eq. (23) and the loop momentum $l \sim O(\varepsilon^0)$, see Ref. [49] for the analogous approach in EOMS. At this point, we emphasize that the IR regular contributions that are absorbed into the LECs e_i do not violate decoupling. Instead, the motivation at this point is that loop contributions should only saturate the loop-level LECs and none of the tree-level LECs. Finally, the renormalized HB amplitude fulfills

- UV finiteness: amplitude is free from UV divergencies
- decoupling theorem: amplitude is free from DBTs
- natural saturation: tree-level (loop-level) amplitudes with Δ saturate the $2\pi\bar{N}N$ -LECs at tree-level (loop-level).

Considering the covariant framework, we have

$$\begin{aligned} c_i &= \bar{c}_i + \delta c_i^{(3)} + \delta c_i^{(3,\Delta)} + \delta c_i^{(4)} + \delta c_i^{(4,\Delta)}, \\ d_i &= \bar{d}_i + \delta d_i + \delta d_i^{(3)} + \delta d_i^{(3,\Delta)} + \delta d_i^{(4)} + \delta d_i^{(4,\Delta)}, \\ e_i &= \bar{e}_i + \delta e_i + \delta e_i^{(4)} + \delta e_i^{(4,\Delta)} \end{aligned} \quad (24)$$

with

$$\begin{aligned} \delta x_i &= \frac{\beta_{x_i} + \beta_{x_i}^\Delta}{F_\pi^2} \left(\bar{\lambda} + \frac{1}{32\pi^2} \ln \left(\frac{M_\pi^2}{\mu^2} \right) \right), \\ F_\pi^2 \delta x^{(n)} &= a_0 + a_1 A_0(m_N^2), \\ F_\pi^2 \delta x^{(n,\Delta)} &= a_0 + a_1 A_0(m_N^2) + a_2 A_0(m_\Delta^2) + b_1 B_0(m_N^2, 0, m_\Delta^2) + b_2 B_0(m_\Delta^2, 0, m_N^2) \\ &\quad + c_1 C_0(m_N^2, 0, m_\Delta^2, 0, m_N^2, m_N^2) + c_2 C_0(m_N^2, 0, m_\Delta^2, 0, m_\Delta^2, m_\Delta^2) \\ &\quad + c_3 C_0(m_\Delta^2, 0, m_N^2, 0, m_N^2, m_\Delta^2) + c_4 C_0(m_\Delta^2, 0, m_\Delta^2, 0, m_N^2, m_\Delta^2), \end{aligned} \quad (25)$$

where for the only IR divergent C_0 -function we get in dimensional regularization

$$C_0(m_N^2, 0, m_\Delta^2, 0, m_N^2, m_\Delta^2) = \frac{(d-2) \left(m_\Delta^2 A_0(m_N^2) - m_N^2 A_0(m_\Delta^2) \right)}{2(-4+d)m_N^2 m_\Delta^2 (m_N^2 - m_\Delta^2)} \quad (26)$$

$$\simeq -\frac{\text{Log} \left(\frac{m_N^2}{m_\Delta^2} \right) \left(2 + 64\pi^2 \bar{\lambda} + \ln \left(\frac{m_N^2 m_\Delta^2}{\mu^4} \right) \right)}{4(m_N^2 - m_\Delta^2)} + O(d-4) . \quad (27)$$

In Eq. (24), the terms $\delta x^{(n)}$ correspond to the renormalization of the LECs in the Δ -less theory, which is discussed extensively in Ref. [26]. However, due to explicit Δ degrees of freedom, the order-by-order renormalization of the LECs has to be extended. Those additional redefinitions of couplings are denoted by $\delta x^{(n,\Delta)}$. It has to be stressed that both set of terms are calculated in complete analogy. The idea is to expand the d -dimensional amplitudes D and B in small parameters

$$M_\pi \sim \mathcal{O}(\varepsilon^1) , \quad s - m_N^2 \sim \mathcal{O}(\varepsilon^1) , \quad u - m_N^2 \sim \mathcal{O}(\varepsilon^1) , \quad t \sim \mathcal{O}(\varepsilon^2) \quad (28)$$

and additionally in the Δ -ful theory

$$m_N \sim m_\Delta \sim m_\Delta - m_N \sim \mathcal{O}(\varepsilon^0) \quad (29)$$

such that the IR regular parts of the amplitudes are identified. Note again that the IR regular part of a loop function can be extracted by interchanging loop integration with a Taylor series in powers of the small parameters [49]. At this point we have to emphasize that the nucleon- Δ mass splitting is a small scale in the power counting used in this analysis, see Eq.(13). However, in our renormalization procedure the mass splitting is treated as a large scale. This apparent contradiction is easily resolved. In the covariant approach, the motivation is to absorb PCBTs and DBTs. Both set of terms only appear in the IR regular part of loop functions given by an expansion as specified by Eqs. (28) and (29). Thus, one has to treat the mass splitting as a large scale. Furthermore, note the employed notation for the terms δx , $\delta x^{(n)}$ and $\delta x^{(n,\Delta)}$ in Eq. (25). In these expressions, the loop functions A_0 , B_0 and the IR divergent function C_0 in Eq. (26) include finite and divergent pieces. The parameters a_i , b_i and c_i are functions of baryonic masses and lower-order coupling constants. It has to be stressed that only UV and no IR divergencies are included in the renormalization procedure. In particular, the IR divergent piece in the C_0 function is exactly cancelled by the divergence proportional to $\beta_{x_i}^\Delta$ in δx_i . To be precise, the β -functions $\beta_{x_i}^\Delta$ are determined after performing the shifts $\delta x^{(n)}$ and $\delta x^{(n,\Delta)}$ in the pion-nucleon scattering amplitude by demanding that the amplitude is free of divergencies. Finally, the renormalized covariant amplitude fulfills (up to $\mathcal{O}(\varepsilon^4)$)

- UV finiteness: amplitude is free from UV divergencies
- proper power counting: amplitude is free from PCBTs
- decoupling theorem: amplitude is free from DBTs
- natural saturation: tree-level (loop-level) amplitudes with Δ saturate the $2\pi\bar{N}N$ -LECs at tree-level (loop-level).

In Appendix C and in the supplementary material, we give the explicit expressions for the renormalization of the LECs c_i , d_i and e_i in both chiral approaches. We performed the following check on our results. The covariant d -dimensional expressions were expanded in the mass splitting $\Delta \sim \mathcal{O}(\varepsilon^1)$ and the corresponding Δ singular parts were successfully matched to the HB expressions. Note that we define the Δ singular part of a loop function in Eq. (25) in analogy to the IR singular part used in EOMS. In particular, it is the contribution, which is non-analytic in the mass splitting Δ in d dimensions. The Δ singular part can be extracted from a loop function by interchanging loop integration with an expansion of the integrand in $l \sim \Delta \sim \mathcal{O}(\varepsilon^1)$ and $m_N \sim \mathcal{O}(\varepsilon^0)$. Note that l is the loop momentum.

C. Complex and Real Counter Terms

In Ref. [26], we already discussed the pertinent tree- and loop-level graphs for $\pi N \rightarrow \pi N$ up to order Q^4 . As shown exemplarily in Fig. 1, the additional graphs including Δ are generated by substituting intermediate nucleon propagators by Δ propagators. Note that this example does not show graphs with redundant contributions. Finally, the renormalized pion-nucleon scattering amplitude depends on the following masses and couplings:

- pion sector: M_π and F_π from $\mathcal{L}_{\pi\pi}^{(2)}$
- nucleon sector: m_N and g_A from $\mathcal{L}_{\pi N}^{(1)}$, \bar{c}_i from $\mathcal{L}_{\pi N}^{(2)}$, \bar{d}_i from $\mathcal{L}_{\pi N}^{(3)}$ and \bar{e}_i from $\mathcal{L}_{\pi N}^{(4)}$
- Δ sector: h_A from $\mathcal{L}_{\pi N \Delta}^{(1)}$, m_Δ and g_1 from $\mathcal{L}_{\pi \Delta}^{(1)}$ and $b_{4,5}$ from $\mathcal{L}_{\pi N \Delta}^{(2)}$

At this point, we have to emphasize that in our renormalization procedure the real-valued bare quantities in the effective Lagrangian are renormalized complex. This is a general consequence when decaying particles are considered explicitly. A prominent example is the Δ mass which can be parametrized via

$$m_\Delta = m_\Delta^{\text{Re}} - \frac{i\Gamma}{2} , \quad (30)$$

where Γ denotes the strong decay width of the Δ . Note that $\Gamma \sim \mathcal{O}(\varepsilon^3)$, because Γ receives its leading contribution at loop-level. For our calculation, this means that in a loop contribution the bare Δ mass \mathbf{m} does not need to be replaced by the complex-valued quantity m_Δ . In a loop contribution, the imaginary part proportional to Γ counts as $\mathcal{O}(\varepsilon^5)$, such that for our purposes it is already sufficient to replace \mathbf{m} by m_Δ^{Re} . Of course, one can also take the full complex-valued mass m_Δ in all loop amplitudes. However, the trick above makes loop calculations easier and is justified based on the power counting. If we now consider only the real part m_Δ^{Re} in loop contributions, we see that the renormalized quantities m_Δ , h_A , \bar{c}_i , \bar{d}_i and \bar{e}_i in Appendix C still remain complex. In contrast, the quantities m_N and g_A are real-valued now. We emphasize that the given renormalization rules completely determine the imaginary parts of the complex-valued quantities, because the initial bare quantities are real-valued. Clearly, such an imaginary part is generated in the renormalization procedure, in particular, by a splitting between the renormalized quantity and the corresponding counter term, e.g., for the Δ mass up to order ε^4 one gets the condition

$$\text{Im } m_\Delta = -\text{Im } \delta \mathbf{m}^{(3)} - \text{Im } \delta \mathbf{m}^{(4)} . \quad (31)$$

This means that these imaginary parts do not need to be constrained by data, because they are fixed by the theory and, in particular, do not represent additional degrees of freedom.

As mentioned in section II, two different unitarization schemes are employed in this work. To be more precise, in the K -matrix unitarization, which is closely related to the extraction of the Breit-Wigner masses, we set the Δ mass m_Δ in the leading-order amplitudes to its real-valued Breit-Wigner mass m_Δ^{BW} . This means that the imaginary parts of the renormalized mass m_Δ and of the counterterms $\delta\mathbf{m}^{(3)}$ and $\delta\mathbf{m}^{(4)}$ are neglected in our amplitudes. As can be seen in Eq. (7), only the real part of the partial wave amplitude is considered in the K -matrix unitarization anyway. Thus, within this unitarization scheme, only the real parts of the renormalized quantities m_Δ , h_A and the LECs \bar{c}_i , \bar{d}_i and \bar{e}_i have to be taken into account in our calculation of the πN scattering amplitudes up to order ε^4 . Note that we could also keep all imaginary parts in the amplitude and instead fix them to the negative of their corresponding counter terms, e.g., as for the Δ mass in Eq. (31). This would be an equivalent procedure, however, the former one might be more intuitive to the reader. In the complex mass approach, the Δ mass in the leading-order amplitudes is set to its complex-valued pole mass m_Δ^{Pole} , where the imaginary part is fixed by its experimental value. As mentioned before, the complex mass unitarization scheme is employed in this work to extend the applicability of the chiral EFT to the Δ pole region, where a dressing of the Δ is inevitable. In particular, the real-valued Δ propagator is divergent in the Δ pole region

$$\frac{1}{\not{p} - m_\Delta^{\text{Re}}} \xrightarrow{\not{p} \rightarrow m_\Delta^{\text{Re}}} \infty. \quad (32)$$

However, as we are going to demonstrate, this is only an artifact of the employed power counting. The resummed or dressed Δ propagator is the initial starting point. This propagator is expanded around the renormalization point $\not{p} = m_\Delta^{\text{Re}}$, which gives

$$\frac{1}{\not{p} - m_\Delta^{\text{Re}} - \Sigma(\not{p})} \simeq \frac{1}{\not{p} - m_\Delta^{\text{Re}} - \Sigma(m_\Delta^{\text{Re}}) - \Sigma'(m_\Delta^{\text{Re}})(\not{p} - m_\Delta^{\text{Re}}) + \mathcal{O}((\not{p} - m_\Delta^{\text{Re}})^2)}. \quad (33)$$

Here, the self-energy of the Δ is denoted by $-\text{i}\Sigma(\not{p})$, which is given by the sum of all one-particle-irreducible contributions to the two-point function of the Δ . If we employ the following renormalization conditions

$$\text{Re } \Sigma(m_\Delta^{\text{Re}}) = 0, \quad \text{Im } \Sigma(m_\Delta^{\text{Re}}) = -\frac{\Gamma}{2}, \quad \Sigma'(m_\Delta^{\text{Re}}) = 0, \quad (34)$$

we are left with

$$\frac{1}{\not{p} - m_\Delta^{\text{Re}} - \Sigma(\not{p})} \simeq \frac{1}{\not{p} - m_\Delta^{\text{Re}} + \text{i}\frac{\Gamma}{2}} + \mathcal{O}((\not{p} - m_\Delta^{\text{Re}})^2), \quad (35)$$

which is well-defined in the limit $\not{p} \rightarrow m_\Delta^{\text{Re}}$. In particular, this is the appropriate behavior in the Δ pole region. Note that a Taylor expansion of Eq. (35) in Γ is equivalent to the expression in Eq. (32) to leading order. To be precise, a strict power counting even demands such an expansion, because $\not{p} - m_\Delta^{\text{Re}} \sim \mathcal{O}(\varepsilon^1)$ and $\Gamma \sim \mathcal{O}(\varepsilon^3)$ such that $\Gamma \ll \not{p} - m_\Delta^{\text{Re}}$. In contrast, one has $\not{p} \simeq m_\Delta^{\text{Re}}$ in the Δ pole region. This means that $\Gamma \gtrsim \not{p} - m_\Delta^{\text{Re}}$, which clearly does not justify the expansion of Eq. (35) in powers of Γ . Thus, for practical calculations,

it is advantageous to renormalize the Δ mass complex. In particular, one has in the on-mass-shell renormalization scheme

$$\frac{1}{\not{p} - m_\Delta - \Sigma(\not{p})} \simeq \frac{1}{\not{p} - m_\Delta} + \mathcal{O}((\not{p} - m_\Delta)^2), \quad (36)$$

where the conditions

$$\Sigma(m_\Delta) = 0, \quad \Sigma'(m_\Delta) = 0 \quad (37)$$

give the desired dressed Δ propagator. At one-loop order, we can simplify the above conditions to

$$\Sigma(m_\Delta^{\text{Re}}) = 0, \quad \Sigma'(m_\Delta^{\text{Re}}) = 0, \quad (38)$$

where $m_\Delta = m_\Delta^{\text{Re}} - i\Gamma/2$. In particular, $m_\Delta^{\text{Re}} \sim \mathcal{O}(\varepsilon^0)$ and $\Gamma \sim \mathcal{O}(\varepsilon^3)$ such that the higher-order effects of Γ , namely $\mathcal{O}(\varepsilon^5)$, are neglected. Note that in the discussion above, the tensorial structure of the numerator of the covariant Δ propagator was suppressed, see Eq. (A28). In the HB approach, we proceed in very close analogy to the covariant case. Here, we expand the dressed Δ propagator around $v \cdot p = \Delta$ such that

$$\frac{1}{v \cdot p - \Delta - \Sigma(v \cdot p)} \simeq \frac{1}{v \cdot p - \Delta - \Sigma(\Delta) - \Sigma'(\Delta)(v \cdot p - \Delta) + \mathcal{O}((v \cdot p - \Delta)^2)} \quad (39)$$

with the conditions at one-loop order

$$\Sigma(\Delta^{\text{Re}}) = 0, \quad \Sigma'(\Delta^{\text{Re}}) = 0, \quad (40)$$

where $\Delta = \Delta^{\text{Re}} - i\Gamma/2$.

As mentioned before, in the K -matrix approach, the Δ width is generated by the unitarization prescription. However, this unitarization is not reliable in the Δ region, because it is simply an approximation for low energies and small phase shifts. Instead, in the complex mass approach, the complex-valued Δ mass is used in the leading-order amplitudes and the P_{33} partial wave is unitarized as given in Eq. (4). In addition, we also would like to avoid Δ pole contributions at loop-level. Thus, we employ a complex-valued coupling h_A with its imaginary part fixed by its counter term, namely

$$\text{Im } h_A = -\text{Im } \delta h^{(3)} - \text{Im } \delta h^{(4)}. \quad (41)$$

We emphasize that both quantities m_Δ and h_A are only complex-valued in the leading-order Δ pole graphs. At loop-level, the imaginary parts of those quantities are regarded as higher-order effects, such that only the real parts are used. E.g., in the s -channel, the Δ pole contributions at tree-level scale as

$$\frac{h_A^2}{s - m_\Delta^2} = \frac{(h_A^{\text{Re}} + i h_A^{\text{Im}})^2}{s - m_\Delta^2} \simeq \frac{(h_A^{\text{Re}})^2 + 2i h_A^{\text{Re}} h_A^{\text{Im}}}{s - m_\Delta^2} + \dots, \quad (42)$$

where the ellipsis denotes terms neglected in our calculation, which are at least two-loop-level contributions. Furthermore, we fix the imaginary parts of the $2\pi\bar{N}N$ -LECs in the tree-level diagrams by their counter terms, namely

$$\text{Im } \bar{x}_i = -\text{Im } \delta x_i^{(3,\Delta)} - \text{Im } \delta x_i^{(4,\Delta)} \quad \text{with } x \in \{c, d, e\}. \quad (43)$$

Instead of employing Eq. (43), we can also follow an equivalent approach, where we neglect from the beginning the imaginary parts of the LECs in the renormalization procedure. This means just considering $\text{Re } \delta x_i^{(n,\Delta)}$, see Appendix C. We emphasize that due to the complex leading-order Δ pole the above statement holds for the coupling h_A only modulo higher order, as seen in Eq. (42).

Furthermore, we use in the HB formalism the covariant leading-order Δ pole amplitudes instead of the HB ones. This modification is motivated by two arguments. First, the strict HB expansion is not justified in the Δ pole region. Obviously, this can be corrected for by considering the resummed expressions in the covariant framework. Second, the convergence of the quantities Γ and $\text{Im } h_A$ in inverse powers of m_N is very poor, see Table I. Thus, the HB framework does not seem to work well if we consider those imaginary parts explicitly like in the complex mass approach. Note that the two breakdowns discussed above, the breakdown of the HB expansion in the vicinity of the Δ pole and the breakdown of the expansion of the covariant propagator in the Δ width, are closely related. In particular, they are both artifacts of the employed power counting. For a different treatment of the resummations on the pole region see Ref. [50].

D. Final Amplitudes and Checks

In this analysis we have calculated the amplitudes of a total of 60 tree-level and 618 loop-level graphs (including crossed and redundant ones). Due to the enormous size of those amplitudes, we refrain from showing them explicitly and instead prefer to present them upon request. In addition, we calculated the 13 leading subthreshold parameters and the 8 leading threshold parameters in both chiral approaches based on those amplitudes. The explicit expressions are given in Ref. [51].

We emphasize that this is the first full one-loop order calculation of $\pi N \rightarrow \pi N$ including explicit Δ degrees of freedom in the small scale expansion. We are therefore not in the position to cross check all of our results with references in the literature. However, some lower-order calculations are available. Up to order ε^3 , we performed a cross check with the HB expressions given in Ref. [36]. Except for obvious typos and the absent renormalization of the coupling h_A , we agree with the expressions in that work. In our analysis of Ref. [37], two groups calculated the covariant expressions up to order ε^3 independently. Both sets of amplitudes were successfully matched. Note that the $2\pi\bar{N}N$ -LECs in the above references are renormalized differently compared to the same LECs in this work. In addition, our ε^4 results passed the following checks:

- The explicit independence of the off-shell parameters α , z_0 and of the redundant LECs b_3 , b_6 , h_i was verified.
- The renormalized amplitudes exhibit the correct analytic structure. To be precise, only the leading-order nucleon and Δ amplitudes have physical poles corresponding to their masses.
- The renormalization rules of the $2\pi\bar{N}N$ -LECs in the covariant and HB frameworks were successfully matched after an appropriate expansion in inverse powers of m_N .

- The subthreshold and threshold parameters in the covariant and HB frameworks were successfully matched after an appropriate expansion in inverse powers of m_N .

IV. FITTING PROCEDURE

As explained in the previous section, the amplitudes for elastic pion-nucleon scattering including explicit Δ degrees of freedom depend on several LECs. Throughout this section, we employ the following numerical values for the leading-order quantities: $M_\pi = 139.57$ MeV, $F_\pi = 92.2$ MeV, $m_N = 938.27$ MeV, $m_\Delta^{\text{BW}} = 1232$ MeV or $m_\Delta^{\text{Pole}} = 1210 - i50$ MeV [52] and $g_A = 1.289$ [26]. Furthermore, the leading- and higher-order LECs are renormalized as discussed in section III. Note that we suppress in the following the bars in the notation of the renormalized LECs \bar{c}_i , \bar{d}_i and \bar{e}_i . Keep in mind that the numerical values of these LECs are given in units of GeV^{-1} , GeV^{-2} and GeV^{-3} , respectively.

The fits described below are performed to πN scattering data given in terms of the two observables $d\sigma/d\Omega$ and P of all three channels. Note that we proceed in very close analogy to the Δ -less fits in Ref. [26], where the reader is referred to for more details. The first step is the minimization of the quantity

$$\chi^2 = \chi_{\pi N}^2 + \chi_C^2, \quad (44)$$

where the information from the πN scattering data [53] including an estimated theoretical uncertainty [39] are incorporated in the first term, in particular,

$$\chi_{\pi N}^2 = \sum_i \left(\frac{\mathcal{O}_i^{\text{exp}} - N_i \mathcal{O}_i^{(n)}}{\delta \mathcal{O}_i} \right)^2 \quad \text{with} \quad \delta \mathcal{O}_i = \sqrt{(\delta \mathcal{O}_i^{\text{exp}})^2 + (\delta \mathcal{O}_i^{(n)})^2}. \quad (45)$$

The experimental data $\mathcal{O}_i^{\text{exp}}$, experimental errors $\delta \mathcal{O}_i^{\text{exp}}$ and normalization factors N_i are taken from the GWU-SAID data base [53]. The quantity $\mathcal{O}_i^{(n)}$ is the corresponding observable \mathcal{O}_i but calculated from our chiral amplitudes at order n . The theoretical error $\delta \mathcal{O}_i^{(n)}$ is based on the truncation of the chiral expansion and is estimated as

$$\delta \mathcal{O}_i^{(n)} = \max(|\mathcal{O}_i^{(\text{LO})}| Q^{n-\text{LO}+1}, \{|\mathcal{O}_i^{(k)} - \mathcal{O}_i^{(j)}| Q^{n-j}\}) \quad \text{with} \quad j < k \leq n. \quad (46)$$

Here, we use $Q = \omega_{\text{CMS}}/\Lambda_b$, where the energy of the incoming pion in the CMS frame is denoted by ω_{CMS} . The acronym LO refers to leading nonvanishing chiral order of the observable \mathcal{O}_i . Furthermore, the second term in Eq. (44) is defined as

$$\chi_C^2 = \sum_i \left(\frac{a_i^2 - \bar{a}_i^2}{\delta a_i^2} \right)^2, \quad (47)$$

where we employ $\mathbf{a} = \{g_1, b_4, b_5\}$, $\bar{\mathbf{a}} = \{9/5 g_A, 1, 1\}$ and $\delta a_i = 1$. In these conditions we assume the large N_c prediction for g_1 , naturalness for b_4 and b_5 and altogether rather conservative errors δa_i . In particular, we use the quantity χ_C^2 to enforce additional constraints on the LECs g_1 and b_4, b_5 due to their first appearance in loops only at order ε^3 and ε^4 , respectively. Unfortunately, we were not able to reliably constrain these LECs by mere scattering data such that additional constraints were needed in the fitting procedure. In contrast to

the Δ -less analysis in Ref. [26], where we used a conservative estimate for the breakdown scale Λ_b , we adopted in this analysis a more aggressive estimate for the breakdown scale, namely $\Lambda_b = 700$ MeV. This value is justified due to explicit Δ resonances in our calculation. The second step, after minimizing the quantity in Eq. (44) and extracting a preferred set of LECs, we included additional information from the subthreshold region and minimized the following quantity

$$\hat{\chi}^2 = \chi_{\pi N}^2 + \chi_{\text{RS}}^2 + \chi_C^2. \quad (48)$$

The quantities $\chi_{\pi N}^2$ and χ_C^2 are defined above and the quantity χ_{RS}^2 is defined in close analogy to $\chi_{\pi N}^2$ as

$$\chi_C^2 = \sum_i \left(\frac{\mathcal{O}_i^{\text{RS}} - \mathcal{O}_i^{(n)}}{\delta \mathcal{O}_i} \right)^2 \quad \text{with} \quad \delta \mathcal{O}_i = \sqrt{(\delta \mathcal{O}_i^{\text{RS}})^2 + (\delta \mathcal{O}_i^{(n)})^2}, \quad (49)$$

where $\mathcal{O}^{\text{RS}} = \{d_{00}^\pm, d_{10}^\pm, d_{01}^\pm, b_{00}^\pm\}$ denotes the set of the 8 leading subthreshold parameters taken from Ref. [38]. Note that we took the set of LECs extracted from minimizing χ^2 in Eq. (44) as the starting point in the iterative minimization procedure of $\hat{\chi}^2$ in Eq. (48).

In the following section, we study pion-nucleon scattering data in three chiral approaches employing two different unitarization prescriptions, K -matrix and complex mass approach. The chiral approaches are the two HB formalisms called HB-NN and HB- π N in the following, which differ by the treatment of the $1/m$ corrections, and the fully covariant formalism denoted by Cov. See Ref. [26] for more details.

V. FIT RESULTS, PREDICTIONS, AND DISCUSSION

A. K -Matrix Approach

We first start our discussion with the more commonly used K -matrix approach. In this approach, we performed fits to all available data for all scattering angles and incoming pion kinetic energy of $T_\pi < \{100, 125, 150, 175, 200\}$ MeV, which corresponds to $\{1704, 1854, 2176, 2399, 2564\}$ data points, respectively. In Fig. 2, the reduced χ^2 and $\bar{\chi}^2$ values for these set of fits are presented as functions of the maximum fit energy T_π . In Figs. 3 and 4, the extracted LECs as functions of T_π are plotted as well. As can be seen in these figures, we get a plateau-like behavior of the extracted LECs and the reduced χ^2 is close to 1 in the energy range between 100 MeV and 150 MeV. Interestingly, the reduced χ^2 and $\bar{\chi}^2$ slightly decrease for fits including data at higher energies, however, the extracted LECs start to deviate from their plateaus. This behavior is clearly attributed to the K -matrix unitarization, which is used in this analysis in the calculation of the phase shifts. As can be seen in Eq. (7), the employed unitarization prescription modifies the perturbative amplitude, where the modification is getting stronger with an increase in the magnitude of the phase shift. As mentioned before, the reliability of the K -matrix unitarization is only ensured for small phase shifts ($|\delta| < \pi/6$). Thus, guided by arguments above, we choose the fits with $T_\pi < 125$ MeV as representative results for the following discussion.

In Table II, the extracted LECs at different chiral orders are compared for the three chiral approaches. Every set of LECs is also supplemented by values of the reduced $\chi_{\pi N}^2$ and $\bar{\chi}_{\pi N}^2$ of the corresponding fit. Additionally, the same set of values but including the

constraints χ_{RS}^2 are given as comparison. Fortunately, we can observe that an increase in the chiral order leads to a decrease of the reduced $\bar{\chi}_{\pi N}^2$. This clearly demonstrates an improved description of the scattering data when higher chiral orders are taken into account. Due to large theoretical uncertainties at lower orders, we can see that the reduced $\chi_{\pi N}^2$, unfortunately, has the opposite rising behavior. Note that this was also observed in the previous Δ -less analysis. Furthermore, the values for $\bar{\chi}_{\pi N}^2/\text{dof}$ at fourth order show that all three considered chiral approaches give a similar description of the scattering data. When considering the additional constraints χ_{RS}^2 from the subthreshold region, we observe on the one hand a negligible increase of $\bar{\chi}_{\pi N}^2/\text{dof}$. Meaning that the description quality of the scattering data is only slightly degraded. But, on the other hand, as seen in Tables VII and VIII, that the determined values for the subthreshold and threshold parameters are substantially closer to the RS results. Given these findings, we decided to select fits including the constraints from the subthreshold region as representative results of the approach employing the K -matrix unitarization. In what follows, we only discuss predictions based on the LECs extracted from Eq. (48) with $T_\pi < 125$ MeV. In Tables IV - VI, we provide for these selected fits the corresponding correlation and covariance matrices. Although some stronger correlations occur in the two HB approaches, it is comforting that in the covariant approach these stronger correlations are visibly reduced.

Next, we focus on the predictions of the numerous πN scattering observables. See Ref. [26] for an extensive summary of these observables. All predictions are based on the values of LECs taken from Table II in the columns denoted by $\pi N + \text{RS}$. Furthermore, we present all results with a statistical error and a theoretical error.

In the columns denoted by $\pi N + \text{RS}$ in Tables VII and VIII, the determined values for the subthreshold and threshold parameters are given at order ε^4 . Unfortunately, both HB counting schemes give rather disappointing results, where the HB-NN counting seems to be slightly superior to the HB- πN counting. In addition, a majority of these parameters have rather large theoretical errors, which is directly contributed to strong changes in between the determined values at lower chiral orders. Note, however, that many parameters only coincide with the RS values when considering more than one standard deviation. We only get a good agreement with the RS values for the four leading parameters d_{00}^+ , d_{10}^+ , d_{01}^+ and b_{00}^- . Fortunately, for the covariant approach we get a better results, where most of the 8 leading parameters agree closely with the RS analysis. Only b_{00}^+ turns out too small. Additionally, the theoretical errors estimated for these parameters are relatively small, which is an indication for a superior convergence in the covariant approach. Finally, we turn to the predictions for the threshold parameters. As can be seen, these predicted parameters are in good agreement with the RS results. This can be observed for all three considered chiral approaches, where the covariant one gives slightly better predictions. Only a_{0+}^- turns out too large.

Next, we turn to our results for the scattering observables, in particular, the differential cross sections $d\sigma/d\Omega$ and polarizations P . In Figs. 5 and 6, we show our results for these observables up to pion energies $T_\pi = 170$ MeV. Note that we only visualize the dominant theoretical error in these figures. Furthermore, the theoretical curves for $d\sigma/d\Omega$ and P are calculated at the mean energies $T_\pi = \{42, 90, 121, 140, 167\}$ MeV and $T_\pi = \{68, 90, 117, 139, 167\}$ MeV, respectively. The experimental data, however are shown

in an additional energy range of ± 5 MeV around the above mentioned mean values. As can be seen, we get an excellent agreement between theory and experiment even above the fitted data, namely for energies higher than $T_\pi = 125$ MeV. Note that we only show the results calculated based on the covariant framework. These results should, however, be understood as representative for all three chiral approaches.

Finally, the predictions for the S -, P -, D - and F -wave phase shift are shown in Figs. 7 - 9, where we see an excellent agreement with the RS values for the S - and P -waves up to energies $T_\pi = 100$ MeV. For higher energies, however, the phase shifts of the S_{11} -wave in the HB approaches, the S_{31} -wave in the covariant approach and of the P_{13} -wave in all approaches behave rather different compared to the RS results. Due to the relatively small magnitude of the phase shifts of the P_{13} -wave, the observed deviation should be taken with care. In contrast, the strong deviations for the leading S -waves is quite surprising. The higher order phase shifts for the D - and F -wave are compared with the results from GWU-SAID. We are able to reproduce these results with some exceptions. In particular, we get stronger discrepancies for the D_{33} -wave in the covariant approach, the D_{35} -wave in the HB- π N approach and the F_{35} -, F_{17} -waves in both HB approaches. Note, however, that the contributions from the D , F (and higher) partial waves are negligible at the considered low energies. This is also explicitly demonstrated in the RS analysis. In contrast, the D - and F -waves in the GWU-SAID analysis are constrained by scattering data at higher energies and then continuously extended to lower energies, in particular, the threshold region. Unfortunately, they do not provide any error estimates of their approach. Thus, minor deviations for higher partial waves should be taken with caution.

B. Complex Mass Approach

As discussed in the previous section, the K -matrix approach has only a limited energy range of applicability. In contrast, the complex mass approach should be applicable at higher energies as well. Thus, in the complex mass approach, we extend the energy region by performing fits to all available scattering data with energy $T_\pi < \{150, 175, 200, 225, 250, 275, 300\}$ MeV corresponding to $\{2176, 2399, 2564, 2727, 3004, 3147, 3413\}$ data points, respectively. In Figs. 2, 10 and 11, we present the reduced χ^2 , $\bar{\chi}^2$ and the extracted LECs as functions of the maximum energy T_π , respectively. As can be seen in these figures, by employing the complex mass approach we are able to extend the plateau-like behavior of the extracted LECs to higher energies of up to $T_\pi \simeq 225$ MeV. We also observe that the reduced χ^2 slightly decreases with increasing energy in the two HB approaches. In the covariant counting scheme the reduced χ^2 is minimal at $T_\pi \simeq 200$ MeV. At this point, we remind the reader of the discussion in the end of section III, where we pointed out that we had to modify the amplitudes in both HB approaches by replacing the Δ pole contribution by the covariant expression. Thus, these result should be taken with care and we rather focus on the results in the covariant formalism from now on. In particular, as representative results of the first step of the fitting procedure we choose the fits with $T_\pi < 200$ MeV.

Next, we turn to the results of the fitting procedure. The extracted LECs at different chiral orders are shown in Table III for all three chiral approaches. Additionally, we give the corresponding reduced $\chi^2_{\pi N}$ and $\bar{\chi}^2_{\pi N}$. As in the K -matrix approach, additional

constraints from the subthreshold region (χ_{RS}^2) are considered in the fitting routine and the results without and with these constraints are compared. As can be seen, the reduced $\bar{\chi}^2$ decreases with an increasing chiral order, which is a clear indicator of an improving description of the scattering data. Furthermore, we observe rather large theoretical uncertainties at lower orders, which explains the increasing values of the reduced χ^2 with increasing chiral order. In summary, the three chiral approaches give a similar fit quality. However, the convergence pattern in the covariant framework, seen in the small changes of the reduced $\chi_{\pi N}^2$ between chiral orders, seems to be superior to the other approaches. Note the small difference between the values at order ε^3 and ε^4 . Including the constraints χ_{RS}^2 visibly impacts the values of the LECs but only slightly effects the value of the reduced $\chi_{\pi N}^2$. In addition, we also get an improved description of the subthreshold and threshold parameters given in Tables VII and VIII. Unfortunately, most of the subthreshold parameters still exhibit rather strong deviations from the RS values. It is surprising that not even the leading subthreshold parameters are properly reproduced. Even the covariant result turn out poorly, although this approach worked quite well within the K -matrix unitarization studied in the previous section. Similar conclusions can also be drawn for the threshold parameters. The observed inability to describe the threshold and subthreshold region properly is due to the employed complex mass approach. By construction, we use a constant Δ width in the amplitudes. But this is only a good approximation in the vicinity of the renormalization point $\not{p} = m_{\Delta}^{\text{Re}}$, which corresponds to what we labeled as the Δ region. Clearly, if we move away from the renormalization point, this approximation becomes less reliable. In particular, the energy-dependent width vanishes at the threshold and subthreshold point, which is not the case for the constant width employed in our amplitudes. Thus, in the analysis of the subthreshold and threshold parameters, it was necessary to perform an additional expansion of the amplitudes in powers of the Δ width. This clearly modifies the amplitudes constrained by fits to experimental data. Note that these modifications are strictly speaking of higher chiral order. We have to stress that it was not necessary to perform such kind of modification in the K -matrix approach. Instead, we were able to use the same amplitudes as input for the fits to the experimental data and for the subthreshold and threshold parameters. Another difference between both approaches, is that in the the K -matrix unitarization only the real part of the partial wave amplitude is considered, whereas in the complex mass approach the full amplitude including the imaginary parts is taken into account. In particular, the imaginary part of the amplitude, not considering the Δ pole dressing for a moment, is only calculated up to its next-to-leading order in the ε^4 πN -amplitudes. Taken our observations for the real part contributions at next-to-leading order into account, it is highly unlikely that the we have reasonably well converged next-to-leading order expressions for the imaginary parts. Additionally, in the Δ pole region, the dressed Δ pole amplitude are enhanced to order ε^{-1} and other parts of the amplitude keep their original chiral order.¹ Thus, the Δ pole contributions become extremely important and the specific treatment of these contributions is crucial, see Eq. (42). To sum up, it should not be surprising that we observe superior results in the K -matrix approach when connecting threshold and subthreshold region. The motivation of the complex mass approach is to extend the applicability of the theory to

¹ The enhancement is due to the different countings of the denominator of the Δ propagator in both kinematical regions. In the threshold region, one has $\not{p} - m_{\Delta} \sim \mathcal{O}(\varepsilon^1)$ and in the vicinity of the Δ pole, one has $\not{p} - m_{\Delta} \sim \Gamma \sim \mathcal{O}(\varepsilon^3)$.

higher energies and the Δ pole region. The cost of this extension is the reduced accuracy of describing subthreshold and threshold parameters. Based on this discussion, we prefer the fits without additional constraints from the subthreshold region as representative results. In particular, we only discuss in what follows the results from the complex mass approach based on the LECs extracted from Eq. (44) with $T_\pi < 200$ MeV. In Tables IV - VI, the corresponding correlation and covariance matrices can be found. Note the rather small correlations between the extracted LECs in the covariant approach.

Like in the previous section on the K -matrix approach, we discuss the predicted observables once again. In particular, the LECs collected in Table III in the columns denoted by πN are employed. In Tables VII and VIII, we show the predictions for the subthreshold and threshold parameters. The results are quite unsatisfactory which is, as we already mentioned, a consequence of the employed scheme. We refer the reader to the previous section for a more consistent determination of these parameters.

Next, we turn to the predictions for the differential cross sections $d\sigma/d\Omega$ and polarizations P . In Figs. 12 and 14 we show the predicted values up to $T_\pi = 170$ MeV. In Figs. 13 and 15 we extend the energy range up to $T_\pi = 300$ MeV. Note that we calculate the theoretical curves based on mean values, whereas the experimental data are shown in an additional energy range of ± 5 MeV around those means. For $d\sigma/d\Omega$ the mean energies are $T_\pi = \{42, 90, 121, 140, 167, 194, 218, 241, 267, 290\}$ MeV and for P we have chosen $T_\pi = \{68, 90, 117, 139, 167, 194, 218, 241, 267, 290\}$ MeV. In these figures we only show the results in the covariant framework, which should be taken as representative examples. As can be seen, the theoretical curves match the experimental data perfectly up to energies $T_\pi = 220$ MeV, whereas for higher energies the predictions deviate from the experimental values. Note the stronger deviations for the observable P .

Finally, we present the predictions for the phase shifts in all three chiral approaches. The predicted S -, P -, D - and F -wave phase shifts are shown in Figs. 16 - 18. Considering the fitting region, the S - and P -waves in all approaches agree very well with the RS results, except the P_{13} -wave in the HB-NN counting. Going to higher energies, we observe stronger deviations for both S -waves and the P_{31} -wave. In the covariant approach, we see an agreement of the D - and F -waves with the GWU-SAID mean values, in particular up to $T_\pi = 200$ MeV. The only exception is the F_{17} -wave, which exhibits the opposite behavior as indicated by the data. Except for the D_{33} -wave, the predicted values for higher energies are reasonable as well. The HB approaches are not able to describe the D_{35} - and F_{35} -wave properly and the HB-NN counting is not able to predict F_{17} -wave. For the rest of the partial waves, both countings give a fair description.

VI. SUMMARY AND OUTLOOK

The main results of this paper are summarized as follows:

- We calculated the pion-nucleon scattering amplitudes in two heavy baryon and in the covariant framework of baryon χ PT with explicit $\Delta(1232)$ degrees of freedom. In particular, the calculation was performed up to order ε^4 in the small scale expansion. Additionally, we discussed in detail the renormalization procedure including Δ contri-

butions of the pion-nucleon LECs. The explicit expressions for the UV divergent parts and additional finite shifts are given in the appendix and/or in the supplementary material.

- We performed fits to low-energy pion-nucleon scattering observables employing three different countings of relativistic corrections, labeled as HB-NN, HB- π N and Cov. Furthermore, we used a systematical approach to account for the theoretical uncertainties due to the truncation of the chiral series. The LECs were extracted from two kinematical regions, the threshold and the Δ pole region. In particular, for each region we employed different unitarization procedures, the K -matrix and the complex mass approach, respectively. Additionally, we studied the impact of the 8 leading subthreshold parameters when included as additional constraints in the fitting procedure. All in all, the extracted LECs turned out to be of natural size.
- In the K -matrix approach, we chose the LECs extracted from fits to experimental data with $T_\pi < 125$ MeV including the constraints from the subthreshold region as the representative and most reliable values. With these LECs we get an excellent description of the low-energy experimental data up to $T_\pi = 170$ MeV and a very good agreement with the threshold and subthreshold parameters of the RS analysis. In addition, our predictions for the phase shifts of the S - and P -waves are in agreement with the RS values near threshold. However, some of the higher-order partial waves show a different behavior compared to the GWU results. Comparing the different chiral approaches, we were able to observe that the covariant approach is far more superior in connecting the threshold and subthreshold region.
- In the complex mass approach, we chose the LECs extracted from fits to experimental data with $T_\pi < 200$ MeV and without the constraints from the subthreshold region as the representative and most reliable values. Given these LECs we get an excellent agreement of the theoretical values with the low-energy data up to $T_\pi = 220$ MeV. Thus, employing this approach we were able to extend the applicability of χ PT to higher energies up to the Δ pole region. However, we had to pay a price for this extension. The theory fails to predict the threshold and subthreshold parameters. Like in the K -matrix approach, we observed superior results in the covariant framework.

The extensive analysis in this paper is a fundamental step in the study of pion-nucleon- Δ physics. In particular, this analysis should be extended by performing a combined analysis of $\pi N \rightarrow \pi N$ and $\pi N \rightarrow \pi\pi N$.

-
- [1] S. Weinberg, *Physica A* **96**, 327 (1979).
 - [2] J. Gasser and H. Leutwyler, *Annals Phys.* **158**, 142 (1984).
 - [3] J. Gasser and H. Leutwyler, *Nucl. Phys. B* **250**, 465 (1985).
 - [4] J. Gasser, M. E. Sainio and A. Svarc, *Nucl. Phys. B* **307**, 779 (1988).
 - [5] V. Bernard, N. Kaiser and U.-G. Meißner, *Int. J. Mod. Phys. E* **4**, 193 (1995) [hep-ph/9501384].
 - [6] V. Bernard and U.-G. Meißner, *Ann. Rev. Nucl. Part. Sci.* **57**, 33 (2007) [hep-ph/0611231].
 - [7] V. Bernard, *Prog. Part. Nucl. Phys.* **60**, 82 (2008) [arXiv:0706.0312 [hep-ph]].
 - [8] S. Weinberg, *Phys. Lett. B* **251**, 288 (1990).
 - [9] C. Ordonez, L. Ray and U. van Kolck, *Phys. Rev. C* **53**, 2086 (1996) [hep-ph/9511380].
 - [10] E. Epelbaum, H. W. Hammer and U.-G. Meißner, *Rev. Mod. Phys.* **81**, 1773 (2009) [arXiv:0811.1338 [nucl-th]].
 - [11] R. Machleidt and D. R. Entem, *Phys. Rept.* **503**, 1 (2011) [arXiv:1105.2919 [nucl-th]].
 - [12] E. E. Jenkins and A. V. Manohar, *Phys. Lett. B* **255**, 558 (1991).
 - [13] V. Bernard, N. Kaiser, J. Kambor and U.-G. Meißner, *Nucl. Phys. B* **388**, 315 (1992).
 - [14] T. Becher and H. Leutwyler, *Eur. Phys. J. C* **9**, 643 (1999) [hep-ph/9901384].
 - [15] P. J. Ellis and H. B. Tang, *Phys. Rev. C* **57**, 3356 (1998) [hep-ph/9709354].
 - [16] J. Gegelia and G. Japaridze, *Phys. Rev. D* **60**, 114038 (1999) [hep-ph/9908377].
 - [17] T. Fuchs, J. Gegelia, G. Japaridze and S. Scherer, *Phys. Rev. D* **68**, 056005 (2003) [hep-ph/0302117].
 - [18] H. Krebs, A. Gasparyan and E. Epelbaum, *Phys. Rev. C* **85**, 054006 (2012) [arXiv:1203.0067 [nucl-th]].
 - [19] K. A. Wendt, B. D. Carlsson and A. Ekström, [arXiv:1410.0646 [nucl-th]].
 - [20] D. R. Entem, N. Kaiser, R. Machleidt and Y. Nosyk, *Phys. Rev. C* **91**, no. 1, 014002 (2015) [arXiv:1411.5335 [nucl-th]].
 - [21] D. R. Entem, N. Kaiser, R. Machleidt and Y. Nosyk, *Phys. Rev. C* **92**, no. 6, 064001 (2015) [arXiv:1505.03562 [nucl-th]].
 - [22] E. Epelbaum, H. Krebs and U.-G. Meißner, *Phys. Rev. Lett.* **115**, no. 12, 122301 (2015) [arXiv:1412.4623 [nucl-th]].
 - [23] E. Epelbaum, [arXiv:1510.07036 [nucl-th]].
 - [24] T. R. Hemmert, B. R. Holstein and J. Kambor, *J. Phys. G* **24**, 1831 (1998) [hep-ph/9712496].
 - [25] N. Fettes, U.-G. Meißner, M. Mojzsis and S. Steininger, *Annals Phys.* **283**, 273 (2000) [*Annals Phys.* **288**, 249 (2001)] [hep-ph/0001308].
 - [26] D. Siemens, V. Bernard, E. Epelbaum, A. Gasparyan, H. Krebs and U.-G. Meißner, *Phys. Rev. C* **94**, no. 1, 014620 (2016) [arXiv:1602.02640 [nucl-th]].
 - [27] M. Mojzsis, *Eur. Phys. J. C* **2**, 181 (1998) [hep-ph/9704415].
 - [28] N. Fettes, U.-G. Meißner and S. Steininger, *Nucl. Phys. A* **640**, 199 (1998) [hep-ph/9803266].
 - [29] P. Buettiker and U.-G. Meißner, *Nucl. Phys. A* **668**, 97 (2000) [hep-ph/9908247].
 - [30] N. Fettes and U.-G. Meißner, *Nucl. Phys. A* **676**, 311 (2000) [hep-ph/0002162].
 - [31] T. Becher and H. Leutwyler, *JHEP* **0106**, 017 (2001) [hep-ph/0103263].
 - [32] M. Hoferichter, B. Kubis and U.-G. Meißner, *Nucl. Phys. A* **833**, 18 (2010) [arXiv:0909.4390 [hep-ph]].
 - [33] A. Gasparyan and M. F. M. Lutz, *Nucl. Phys. A* **848**, 126 (2010) [arXiv:1003.3426 [hep-ph]].
 - [34] J. M. Alarcon, J. Martin Camalich and J. A. Oller, *Annals Phys.* **336**, 413 (2013)

- [arXiv:1210.4450 [hep-ph]].
- [35] Y. H. Chen, D. L. Yao and H. Q. Zheng, Phys. Rev. D **87**, 054019 (2013) [arXiv:1212.1893 [hep-ph]].
 - [36] N. Fettes and U.-G. Meißner, Nucl. Phys. A **679**, 629 (2001) [hep-ph/0006299].
 - [37] D. L. Yao, D. Siemens, V. Bernard, E. Epelbaum, A. M. Gasparyan, J. Gegelia, H. Krebs and U.-G. Meißner, JHEP **1605**, 038 (2016) [arXiv:1603.03638 [hep-ph]].
 - [38] M. Hoferichter, J. Ruiz de Elvira, B. Kubis and U. G. Meiner, Phys. Rept. **625**, 1 (2016) [arXiv:1510.06039 [hep-ph]].
 - [39] E. Epelbaum, H. Krebs and U.-G. Meißner, Eur. Phys. J. A **51**, no. 5, 53 (2015) [arXiv:1412.0142 [nucl-th]].
 - [40] E. Epelbaum *et al.*, arXiv:1907.03608 [nucl-th].
 - [41] J. A. Melendez, S. Wesolowski and R. J. Furnstahl, Phys. Rev. C **96**, no. 2, 024003 (2017) [arXiv:1704.03308 [nucl-th]].
 - [42] R. G. Stuart, in Z^0 physics, J. Tran Thanh Van ed., Editions Frontieres, Gif-sur-Yvette France, 41 (1990)
 - [43] A. Denner, S. Dittmaier, M. Roth and D. Wackeroth, Nucl. Phys. B **560**, 33 (1999) [hep-ph/9904472].
 - [44] J. Gegelia, private communication.
 - [45] H. B. Tang and P. J. Ellis, Phys. Lett. B **387**, 9 (1996) [hep-ph/9606432].
 - [46] V. Pascalutsa, Phys. Lett. B **503**, 85 (2001) [hep-ph/0008026].
 - [47] H. Krebs, E. Epelbaum and U.-G. Meissner, Phys. Lett. B **683**, 222 (2010) [arXiv:0905.2744 [hep-th]].
 - [48] D. Siemens, V. Bernard, E. Epelbaum, A. M. Gasparyan, H. Krebs and U. G. Meiner, Phys. Rev. C **96**, no. 5, 055205 (2017) [arXiv:1704.08988 [nucl-th]].
 - [49] M. R. Schindler, J. Gegelia and S. Scherer, Phys. Lett. B **586**, 258 (2004) [hep-ph/0309005].
 - [50] B. Long and U. van Kolck, Nucl. Phys. A **840**, 39 (2010) [arXiv:0907.4569 [hep-ph]].
 - [51] D. Siemens, J. Ruiz de Elvira, E. Epelbaum, M. Hoferichter, H. Krebs, B. Kubis and U.-G. Meiner, Phys. Lett. B **770**, 27 (2017) [arXiv:1610.08978 [nucl-th]].
 - [52] K. A. Olive *et al.* [Particle Data Group Collaboration], Chin. Phys. C **38**, 090001 (2014).
 - [53] R. L. Workman, R. A. Arndt, W. J. Briscoe, M. W. Paris and I. I. Strakovsky, Phys. Rev. C **86**, 035202 (2012) [arXiv:1204.2277 [hep-ph]].
 - [54] V. Pascalutsa and D. R. Phillips, Phys. Rev. C **67**, 055202 (2003) [nucl-th/0212024].
 - [55] L. M. Nath, B. Etemadi and J. D. Kimel, Phys. Rev. D **3**, 2153 (1971).
 - [56] T. R. Hemmert, UMI-98-09346.
 - [57] V. Bernard, T. R. Hemmert and U.-G. Meißner, Phys. Lett. B **565**, 137 (2003) [hep-ph/0303198].
 - [58] C. Zöller, Master Thesis, Ruhr University Bochum (2014).
 - [59] D. Siemens, V. Bernard, E. Epelbaum, H. Krebs and U.-G. Meißner, Phys. Rev. C **89**, no. 6, 065211 (2014) [arXiv:1403.2510 [nucl-th]].
 - [60] I. I. Strakovsky, private communication.

Appendix A: Effective Lagrangian

The effective pion-nucleon Lagrangian with explicit Δ degrees of freedom consists of four parts: pion-pion ($\pi\pi$), pion-nucleon (πN), pion- Δ ($\pi\Delta$), and pion-nucleon- Δ ($\pi N\Delta$) interactions. Thus, at a given chiral order n one has

$$\mathcal{L}^{(n)} = \mathcal{L}_{\pi\pi}^{(n)} + \mathcal{L}_{\pi N}^{(n)} + \mathcal{L}_{\pi\Delta}^{(n)} + \mathcal{L}_{\pi N\Delta}^{(n)}, \quad (\text{A1})$$

where the chiral order of an interaction term is determined by the small scale expansion with the expansion parameter [24]

$$\varepsilon = \left\{ \frac{q}{\Lambda_b}, \frac{M}{\Lambda_b}, \frac{\Delta_0}{\Lambda_b} \right\} \quad \text{with} \quad \Lambda_b \in \{\Lambda_\chi, 4\pi F, m\}. \quad (\text{A2})$$

Furthermore, the chiral order D of a Feynman diagram with L loops, V_d^M mesonic vertices and V_d^B baryonic vertices is given by

$$D = 2L + 1 + \sum_d (d-2)V_d^M + \sum_d (d-1)V_d^B, \quad (\text{A3})$$

where Δ and nucleonic vertices are treated on the same footing. In the following, we only discuss terms contributing to pion nucleon scattering up to chiral order $n = 4$ and in the case of $\text{SU}(2)$. Thus, we set the external sources to $p = a_\mu = v_\mu = 0$ and $s = \mathcal{M}$.

1. Chiral Perturbation Theory for Pions

The pion fields are conveniently collected in a matrix U , whose most general parametrization constrained by unitarity is given by

$$\begin{aligned} U = 1 + i \frac{\boldsymbol{\tau} \cdot \boldsymbol{\pi}}{F} - \frac{\boldsymbol{\pi}^2}{2F^2} - i\alpha \frac{\boldsymbol{\pi}^2 \boldsymbol{\tau} \cdot \boldsymbol{\pi}}{F^3} + \frac{(8\alpha - 1)}{8F^4} \boldsymbol{\pi}^4 \\ - i\beta \frac{\boldsymbol{\pi}^4 \boldsymbol{\tau} \cdot \boldsymbol{\pi}}{F^5} + \frac{-1 + 8\alpha - 8\alpha^2 + 16\beta}{16F^6} \boldsymbol{\pi}^6 + \dots \end{aligned} \quad (\text{A4})$$

with

$$\boldsymbol{\tau} \cdot \boldsymbol{\pi} = \begin{pmatrix} \pi^3 & \pi^1 - i\pi^2 \\ \pi^1 + i\pi^2 & -\pi^3 \end{pmatrix} \equiv \begin{pmatrix} \pi^0 & \sqrt{2}\pi^+ \\ \sqrt{2}\pi^- & -\pi^0 \end{pmatrix}, \quad (\text{A5})$$

where we used the Pauli matrices τ_i and denoted the unphysical off-shell parameters by α , β . Employing the above matrix notation for the pion fields, the effective pion Lagrangian up to next-to-leading order reads [1, 2]

$$\begin{aligned} \mathcal{L}_{\pi\pi}^{(2)} &= \frac{F^2}{4} \langle \partial_\mu U^\dagger \partial^\mu U \rangle + \frac{F^2}{4} \langle \chi_+ \rangle, \\ \mathcal{L}_{\pi\pi}^{(4)} &= \frac{l_1}{4} \langle \partial_\mu U \partial^\mu U^\dagger \rangle^2 + \frac{l_2}{4} \langle \partial_\mu U \partial_\nu U^\dagger \rangle \langle \partial^\mu U \partial^\nu U^\dagger \rangle + \frac{l_3}{16} \langle \chi_+ \rangle^2 \\ &\quad + \frac{l_4}{16} \left(2 \langle \partial_\mu U \partial^\mu U^\dagger \rangle \langle \chi_+ \rangle + 2 \langle \chi^\dagger U \chi^\dagger U + U^\dagger \chi U^\dagger \chi \rangle - 4 \langle \chi^\dagger \chi \rangle - \langle \chi_- \rangle^2 \right) \end{aligned} \quad (\text{A6})$$

where

$$\chi = 2B_0\mathcal{M} \quad \text{with} \quad \mathcal{M} = \text{diag}(m_u, m_d) \quad (\text{A7})$$

and

$$\chi_{\pm} = u^{\dagger}\chi u^{\dagger} \pm u\chi^{\dagger}u, \quad (\text{A8})$$

where we used the definition $u(\boldsymbol{\pi}) = \sqrt{U(\boldsymbol{\pi})}$. Note the explicit chiral symmetry breaking by the non-zero quark masses m_u and m_d .

2. Chiral Perturbation Theory for Pions and Nucleons

The proton p and neutron n fields are conveniently written in the isodoublet representation

$$\Psi = \begin{pmatrix} p \\ n \end{pmatrix}. \quad (\text{A9})$$

Given the introduced notation for the pion and nucleon fields, the covariant pion-nucleon Lagrangian up to fourth chiral order reads [25]

$$\begin{aligned} \mathcal{L}_{\pi N}^{(1)} &= \bar{\Psi} \left[i\not{D} - m + \frac{g}{2}\not{u}\gamma_5 \right] \Psi, \\ \mathcal{L}_{\pi N}^{(2)} &= \bar{\Psi} \left[c_1 \langle \chi_+ \rangle + \frac{c_2}{8m^2} (-\langle u_\mu u_\nu \rangle D^{\mu\nu} + \text{h.c.}) + \frac{c_3}{2} \langle u \cdot u \rangle - \frac{c_4}{2} \sigma^{\mu\nu} [u_\mu, u_\nu] \right] \Psi, \\ \mathcal{L}_{\pi N}^{(3)} &= \bar{\Psi} \left[-\frac{d_1}{2m} [u_\mu, [D_\nu, u^\mu]] D^\nu - \frac{d_2}{2m} [u_\mu, [D^\mu, u_\nu]] D^\nu + \frac{d_3}{12m^3} [u_\mu, [D_\nu, u_\rho]] D^{\mu\nu\rho} \right. \\ &\quad + \frac{d_4}{2m} \epsilon^{\mu\nu\alpha\beta} \langle u_\mu u_\nu u_\alpha \rangle D_\beta + \frac{d_5}{2m} i[\chi_-, u_\mu] D^\mu - \frac{d_{12}}{8m^2} \gamma^\mu \gamma_5 \langle u_\lambda u_\nu \rangle u_\mu D^{\lambda\nu} \\ &\quad - \frac{d_{13}}{8m^2} \gamma^\mu \gamma_5 \langle u_\mu u_\nu \rangle u_\lambda D^{\lambda\nu} - \frac{d_{14}}{2m} \sigma^{\mu\nu} \langle [D_\lambda, u_\mu] u_\nu \rangle D^\lambda - \frac{d_{15}}{2m} \sigma^{\mu\nu} \langle u_\mu [D_\nu, u_\lambda] \rangle D^\lambda + \text{h.c.} \left. \right] \Psi \\ &\quad + \bar{\Psi} \left[\frac{d_{10}}{2} \gamma^\mu \gamma_5 \langle u \cdot u \rangle u_\mu + \frac{d_{11}}{2} \gamma^\mu \gamma_5 \langle u_\mu u_\nu \rangle u^\nu + \frac{d_{16}}{2} \gamma^\mu \gamma_5 \langle \chi_+ \rangle u_\mu + \frac{d_{18}}{2} i\gamma^\mu \gamma_5 [D_\mu, \chi_-] \right] \Psi, \\ \mathcal{L}_{\pi N}^{(4)} &= \bar{\Psi} \left[\left(\frac{e_{10}}{4m^2} \langle h_{\lambda\mu} u_\nu \rangle u_\rho \epsilon^{\mu\nu\rho} D^{\lambda\tau} + \text{h.c.} \right) + \left(\frac{e_{11}}{4m} \langle h_{\lambda\mu} [u^\lambda, u_\nu] \rangle \gamma_5 \gamma^\mu D^\nu + \text{h.c.} \right) \right. \\ &\quad + \left(\frac{e_{12}}{4m} \langle h_{\lambda\mu} [u^\lambda, u_\nu] \rangle \gamma_5 \gamma^\nu D^\mu + \text{h.c.} \right) + \left(-\frac{e_{13}}{24m^3} \langle h_{\lambda\mu} [u_\nu, u_\rho] \rangle \gamma_5 \gamma^\rho D^{\lambda\mu\nu} + \text{h.c.} \right) \\ &\quad + e_{14} \langle h_{\mu\nu} h^{\mu\nu} \rangle + \left(-\frac{e_{15}}{4m^2} \langle h_{\lambda\mu} h^\lambda{}_\nu \rangle D^{\mu\nu} + \text{h.c.} \right) + \left(\frac{e_{16}}{48m^4} \langle h_{\lambda\mu} h_{\nu\rho} \rangle D^{\lambda\mu\nu\rho} + \text{h.c.} \right) \\ &\quad - e_{17} [h_{\lambda\mu}, h^\lambda{}_\nu] \sigma^{\mu\nu} + \left(\frac{e_{18}}{4m^2} [h_{\lambda\mu}, h_{\nu\rho}] \sigma^{\mu\nu} D^{\lambda\rho} + \text{h.c.} \right) + e_{19} \langle \chi_+ \rangle \langle u_\mu u^\mu \rangle \\ &\quad + \left(-\frac{e_{20}}{4m^2} \langle \chi_+ \rangle \langle u_\mu u_\nu \rangle D^{\mu\nu} + \text{h.c.} \right) - e_{21} \langle \chi_+ \rangle [u_\mu, u_\nu] \sigma^{\mu\nu} + e_{22} [D_\mu, [D^\mu, \langle \chi_+ \rangle]] \\ &\quad + \left(\frac{e_{34}}{4m} i \langle \tilde{\chi}_- [u_\mu, u_\nu] \rangle \gamma_5 \gamma^\mu D^\nu + \text{h.c.} \right) + \left(-\frac{e_{35}}{4m^2} i \langle \tilde{\chi}_- h_{\mu\nu} \rangle D^{\mu\nu} + \text{h.c.} \right) \\ &\quad + e_{36} i \langle u_\mu [D^\mu, \tilde{\chi}_-] \rangle - e_{37} i [u_\mu, [D_\nu, \tilde{\chi}_-]] \sigma^{\mu\nu} + e_{38} \langle \chi_+ \rangle \langle \chi_+ \rangle \\ &\quad + \frac{e_{115}}{4} \langle \chi_+^2 - \chi_-^2 \rangle - \frac{e_{116}}{4} (\langle \chi_-^2 \rangle - \langle \chi_- \rangle^2 + \langle \chi_+^2 \rangle - \langle \chi_+ \rangle^2) \left. \right] \Psi, \end{aligned} \quad (\text{A10})$$

where we employed the chiral vielbein

$$u_\mu = i(u^\dagger \partial_\mu u - u \partial_\mu u^\dagger), \quad (\text{A11})$$

the chiral connection

$$\Gamma_\mu = \frac{1}{2}(u^\dagger \partial_\mu u + u \partial_\mu u^\dagger) , \quad (\text{A12})$$

the covariant derivative

$$D_\mu = \partial_\mu + \Gamma_\mu , \quad (\text{A13})$$

the totally symmetrized product of covariant derivatives $D_{\mu\nu\dots}$ and additionally

$$\begin{aligned} h_{\mu\nu} &= [D_\mu, u_\nu] + [D_\nu, u_\mu] , & \tilde{\chi}_- &= \chi_- - \langle \chi_- \rangle , \\ [\tau_a, \tau_b] &= 2i\epsilon_{abc}\tau_c , & \{\gamma_\mu, \gamma_\nu\} &= 2g_{\mu\nu} , & \sigma_{\mu\nu} &= \frac{1}{4}[\gamma_\mu, \gamma_\nu] . \end{aligned} \quad (\text{A14})$$

We emphasize two differences between Eq. (A10) and the effective Lagrangian in Ref. [25]. In that reference, one defines $\sigma_{\mu\nu} = \frac{i}{2}[\gamma_\mu, \gamma_\nu]$ and uses the opposite sign for the interaction terms proportional to the LECs d_4 , e_{10} and e_{34} .

In the HB approach, the nucleon momentum is split into two parts

$$p_\mu = m v_\mu + k_\mu , \quad (\text{A15})$$

where the first summand is a large contribution close to on-shell kinematics, with v_μ the four-velocity of the nucleon, and the second summand is a residual contribution k_μ . Additionally, a decomposition of the nucleon field Ψ into eigenstates of $\not{\psi}$ is employed, where

$$N = e^{imv \cdot x} P_v^+ \Psi , \quad h = e^{imv \cdot x} P_v^- \Psi \quad (\text{A16})$$

are the so-called light and heavy fields, respectively. Note that the projection operators are given by

$$P_v^\pm = \frac{1}{2}(1 \pm \not{\psi}) . \quad (\text{A17})$$

In our analysis, we employ the HB Lagrangian only to calculate the loop-level amplitudes, whereas the tree-level contributions are directly determined by an expansion of the covariant amplitudes in inverse powers of the nucleon mass. Thus, for our purpose, we only need to consider the HB Lagrangian up to next-to-leading order [25]

$$\begin{aligned} \hat{\mathcal{L}}_{\pi N}^{(1)} &= \bar{N} [\not{v} \cdot D + gS \cdot u] N , \\ \hat{\mathcal{L}}_{\pi N}^{(2)} &= \bar{N} \left[c_1 \langle \chi_+ \rangle + \frac{c_2}{2} \langle (v \cdot u)^2 \rangle + \frac{c_3}{2} \langle u \cdot u \rangle + \frac{c_4}{2} [S^\mu, S^\nu][u_\mu, u_\nu] \right] N \\ &\quad + \frac{1}{2m} \bar{N} \left[(v \cdot D)^2 - D^2 - ig\{S \cdot D, v \cdot u\} - \frac{g^2}{8} \langle (v \cdot u)^2 \rangle + \frac{1}{4} [S^\mu, S^\nu][u_\mu, u_\nu] \right] N \end{aligned} \quad (\text{A18})$$

with the Pauli-Lubanski spin vector

$$S_\mu = -\gamma_5 \sigma_{\mu\nu} v^\nu = -\frac{1}{2} \gamma_5 (\gamma_\mu \not{v} - v_\mu) , \quad (\text{A19})$$

which inherits the Dirac spin structure. This spin vector has the properties

$$S \cdot v = 0 , \quad S^2 = \frac{1-d}{4} , \quad \{S_\mu, S_\nu\} = \frac{1}{2}(v_\mu v_\nu - g_{\mu\nu}) , \quad [S_\mu, S_\nu] = i\epsilon_{\mu\nu\alpha\beta} v^\alpha S^\beta , \quad (\text{A20})$$

with the space-time dimension d and the Levi-Civita symbol $\epsilon^{\mu\nu\alpha\beta}$, where $\epsilon^{0123} = -1$.

3. Chiral Perturbation Theory for Pions, Nucleons, and $\Delta(1232)$ Resonances

The $\Delta(1232)$ resonance has four physical states $(\Delta^{++}, \Delta^+, \Delta^0, \Delta^-)$, which are conveniently collected in three isospin doublets

$$\Psi_\mu^1 = \frac{1}{\sqrt{2}} \begin{pmatrix} \Delta^{++} - \frac{1}{\sqrt{3}}\Delta^0 \\ \frac{1}{\sqrt{3}}\Delta^0 - \Delta^- \end{pmatrix}_\mu, \quad \Psi_\mu^2 = \frac{i}{\sqrt{2}} \begin{pmatrix} \Delta^{++} + \frac{1}{\sqrt{3}}\Delta^0 \\ \frac{1}{\sqrt{3}}\Delta^+ + \Delta^- \end{pmatrix}_\mu, \quad \Psi_\mu^3 = -\sqrt{\frac{2}{3}} \begin{pmatrix} \Delta^+ \\ \Delta^0 \end{pmatrix}_\mu, \quad (\text{A21})$$

where the field Ψ_μ^i is a Rarita-Schwinger-like isospurion, a spin-3/2 field constructed via coupling of a spin-1 to a spin-1/2 field. Additionally, each spin component is an isodoublet with its own isovector index and with the constraint

$$\tau^i \Psi_\mu^i = 0 \quad (\text{A22})$$

to reduce the number of independent states from six to four. Note that to ensure the independence of unobservable off-shell parameters, the Lagrangian of the Δ resonance has to be invariant under the so-called point transformation [55]

$$\Psi_\mu \rightarrow \Psi_\mu + a\gamma_\mu\gamma_\nu\Psi^\nu, \quad A \rightarrow \frac{A-2a}{1+4a}, \quad (\text{A23})$$

where the unphysical gauge parameter A appears in the most general leading-order Lagrangian. A convenient choice for this parameter is $A = -1$, resulting in a more compact form for the Δ propagator. However, in the original formulation of the HB Lagrangian [24] the Δ fields are redefined to absorb the dependence on the parameter A . This is equivalent to the choice $A = 0$. We discuss the matching of coupling constants between these two choices at the end of this section, after introducing the HB Lagrangian. In the following, we employ the convenient choice $A = -1$. Thus, employing the above notation, the covariant pion- Δ Lagrangian up to fourth order reads [24, 56]

$$\begin{aligned} \mathcal{L}_{\pi\Delta}^{(1)} &= -\bar{\Psi}_\mu^i \left[(i\not{D}^{ij} - \mathbf{m}\delta^{ij})g_{\mu\nu} - i(\gamma_\mu D_\nu^{ij} + \gamma_\nu D_\mu^{ij}) + i\gamma_\mu \not{D}^{ij}\gamma_\nu + \mathbf{m}\delta^{ij}\gamma_\mu\gamma_\nu \right. \\ &\quad \left. + \frac{\mathbf{g}_1}{2}g_{\mu\nu}\not{u}^{ij}\gamma_5 + \frac{\mathbf{g}_2}{2}(\gamma_\mu u_\nu^{ij} + u_\mu^{ij}\gamma_\nu)\gamma_5 + \frac{\mathbf{g}_3}{2}\gamma_\mu\not{u}^{ij}\gamma_5\gamma_\nu \right] \Psi_\nu^j, \\ \mathcal{L}_{\pi\Delta}^{(2)} &= \bar{\Psi}_\mu^i \Theta^{\mu\alpha}(y_1) \left[c_1^\Delta \sigma_{\alpha\beta} \delta^{ij} \langle \chi_+ \rangle + \frac{c_2^\Delta}{16\mathbf{m}^2} g_{\alpha\beta} \langle u^\rho u^\lambda \rangle D_{\rho\lambda}^{ij} - \frac{c_3^\Delta}{4} g_{\alpha\beta} \langle u \cdot u \rangle \delta^{ij} \right. \\ &\quad \left. + \frac{c_4^\Delta}{4} g_{\alpha\beta} [u_\rho, u_\lambda] \sigma^{\rho\lambda} \delta^{ij} - \frac{c_{11}^\Delta}{4} \langle u^\alpha u^\beta \rangle \delta^{ij} - \frac{c_{12}^\Delta}{2} (w_\alpha^i w_\beta^j + w_\alpha^j w_\beta^i) \right. \\ &\quad \left. - \frac{c_{13}^\Delta}{8\mathbf{m}^2} (w_\rho^i w_\lambda^k + w_\lambda^i w_\rho^k) D_{kj}^{\rho\lambda} \right] \Theta^{\beta\nu}(y_1) \Psi_\nu^j + \text{h.c.}, \\ \mathcal{L}_{\pi\Delta}^{(3)} &= \bar{\Psi}_\mu^i \Theta^{\mu\alpha}(y_2) \left[d_1^\Delta i w_{\alpha\beta}^k \tau^k \gamma_5 + d_2^\Delta \langle \chi_- \tau^k \rangle \tau^k \gamma_5 \delta^{ij} g_{\alpha\beta} + d_3^\Delta \langle \chi_+ \rangle w_\lambda^k \tau^k \gamma_5 \gamma^\lambda g_{\alpha\beta} \right. \\ &\quad \left. + d_4^\Delta w_{\rho\tau\lambda}^k g^{\rho\tau} \tau^k \gamma_5 \gamma^\lambda g_{\alpha\beta} + d_5^\Delta w_{\alpha\beta\lambda}^k \tau^k \gamma_5 \gamma^\lambda \right] \delta^{ij} \Theta^{\beta\nu}(y_2) \Psi_\nu^j, \\ \mathcal{L}_{\pi\Delta}^{(4)} &= \bar{\Psi}_\mu^i \Theta^{\mu\alpha}(y_3) \left[e_{38}^\Delta \langle \chi_+ \rangle \langle \chi_+ \rangle + \frac{e_{115}^\Delta}{4} \langle \chi_+^2 - \chi_-^2 \rangle \right. \\ &\quad \left. - \frac{e_{116}^\Delta}{4} (\langle \chi_-^2 \rangle - \langle \chi_- \rangle^2 + \langle \chi_+^2 \rangle - \langle \chi_+ \rangle^2) \right] g_{\alpha\beta} \delta^{ij} \Theta^{\beta\nu}(y_3) \Psi_\nu^j, \end{aligned} \quad (\text{A24})$$

with $\Theta^{\mu\alpha}(z) = g^{\mu\alpha} + z\gamma^\mu\gamma^\alpha$ and the off-shell parameters y_i , \mathbf{g}_2 and \mathbf{g}_3 . Additionally, we used the covariant derivative

$$D_\mu^{ij} = \partial_\mu \delta^{ij} + \Gamma_\mu^{ij} \quad (\text{A25})$$

with the chiral connection

$$\Gamma_\mu^{ij} = \Gamma_\mu \delta^{ij} - i\epsilon^{ijk} \langle \tau^k \Gamma_\mu \rangle \quad (\text{A26})$$

and the following set of definitions

$$w_\alpha^i = \frac{1}{2} \text{Tr} [\tau^i u_\alpha] \ , \quad w_{\alpha\beta}^i = \frac{1}{2} \text{Tr} [\tau^i [D_\alpha, u_\beta]] \ , \quad w_{\alpha\beta\tau}^i = \frac{1}{2} \text{Tr} [\tau^i [D_\alpha, [D_\beta, u_\tau]]] \ . \quad (\text{A27})$$

The Δ propagator constrained by the leading-order Lagrangian $\mathcal{L}_{\pi\Delta}^{(1)}$ is given by [57]

$$\begin{aligned} \mathcal{G}_{ij,\Delta}^{\mu\nu}(p) &= -\frac{\not{p} + \mathbf{m}}{p^2 - \mathbf{m}^2} \left(g^{\mu\nu} - \frac{1}{d-1} \gamma^\mu \gamma^\nu + \frac{1}{d-1} \frac{p^\mu \gamma^\nu - p^\nu \gamma^\mu}{\mathbf{m}} - \frac{d-2}{d-1} \frac{p^\mu p^\nu}{\mathbf{m}^2} \right) \xi_{3/2}^{ij} \\ &= -\frac{\not{p} + \mathbf{m}}{p^2 - \mathbf{m}^2} \left(P_{33}^{3/2} \right)^{\mu\nu} \xi_{3/2}^{ij} - \frac{1}{\sqrt{d-1} \mathbf{m}} \left(\left(P_{12}^{1/2} \right)^{\mu\nu} + \left(P_{21}^{1/2} \right)^{\mu\nu} \right) \xi_{3/2}^{ij} \\ &\quad + \frac{d-2}{d-1} \frac{\not{p} + \mathbf{m}}{\mathbf{m}^2} \left(P_{22}^{1/2} \right)^{\mu\nu} \xi_{3/2}^{ij} \end{aligned} \quad (\text{A28})$$

with the spin projection operators

$$\begin{aligned} \left(P_{33}^{3/2} \right)_{\mu\nu} &= g_{\mu\nu} - \frac{1}{d-1} \gamma_\mu \gamma_\nu - \frac{1}{(d-1)p^2} (\not{p} \gamma_\mu p_\nu + p_\mu \gamma_\nu \not{p}) - \frac{d-4}{d-1} \frac{p_\mu p_\nu}{p^2} \ , \\ \left(P_{12}^{1/2} \right)_{\mu\nu} &= \frac{1}{\sqrt{d-1} p^2} (p_\mu p_\nu - \not{p} p_\nu \gamma_\mu) \ , \\ \left(P_{21}^{1/2} \right)_{\mu\nu} &= \frac{1}{\sqrt{d-1} p^2} (\not{p} p_\mu \gamma_\nu - p_\mu p_\nu) \ , \\ \left(P_{22}^{1/2} \right)_{\mu\nu} &= \frac{p_\mu p_\nu}{p^2} \ , \\ \left(P_{11}^{1/2} \right)_{\mu\nu} &= \frac{1}{d-1} \gamma_\mu \gamma_\nu + \frac{1}{(d-1)p^2} (\not{p} \gamma_\mu p_\nu + p_\mu \gamma_\nu \not{p}) - \frac{3}{d-1} \frac{p_\mu p_\nu}{p^2} \ , \end{aligned} \quad (\text{A29})$$

which obey

$$\left(P_{33}^{3/2} \right)_{\mu\nu} + \left(P_{11}^{1/2} \right)_{\mu\nu} + \left(P_{22}^{1/2} \right)_{\mu\nu} = g_{\mu\nu} \ , \quad (P_{ij}^I)_{\mu\nu} (P_{kl}^J)^{\nu\rho} = \delta^{IJ} \delta_{jk} (P_{il}^I)_\mu{}^\rho \quad (\text{A30})$$

and the isospin projection operators

$$\xi_{ij}^{3/2} = \frac{2}{3} \delta_{ij} - \frac{i}{3} \epsilon_{ijk} \tau^k \ , \quad \xi_{ij}^{1/2} = \frac{1}{3} \delta_{ij} + \frac{i}{3} \epsilon_{ijk} \tau^k \ , \quad (\text{A31})$$

which obey

$$\xi_{ij}^{3/2} + \xi_{ij}^{1/2} = \delta_{ij} \ , \quad \xi_{ij}^I \xi_{jk}^J = \delta^{IJ} \xi_{ik}^J \ . \quad (\text{A32})$$

The covariant pion-nucleon- Δ Lagrangian up to third order reads [56, 58]

$$\mathcal{L}_{\pi N \Delta}^{(1)} = h \bar{\Psi}_\mu^i \Theta^{\mu\alpha}(z_0) w_\alpha^i \Psi + \text{h.c.} \ ,$$

$$\begin{aligned}
\mathcal{L}_{\pi N \Delta}^{(2)} &= \bar{\Psi}_\mu \Theta^{\mu\alpha}(z_1) \left[i b_3 w_{\alpha\beta}^i \gamma^\beta + \frac{b_4}{2} w_\alpha^i w_\beta^j \gamma^\beta \gamma_5 \tau^j + \frac{b_5}{2} w_\alpha^j w_\beta^i \gamma^\beta \gamma_5 \tau^j - \frac{b_6}{m} w_{\alpha\beta}^i D^\beta \right] \Psi + \text{h.c.} \\
\mathcal{L}_{\pi N \Delta}^{(3)} &= \bar{\Psi}_\mu \Theta^{\mu\nu}(z_2) \left[\frac{h_4}{2} w_\nu^i \langle \chi_+ \rangle + h_7 i \langle [D_\nu, \chi_-] \tau^i \rangle + h_{58} i \langle [D_\alpha, u_\nu] \tau^i \rangle w_\beta^j \tau^j \sigma^{\alpha\beta} \gamma_5 \right. \\
&\quad - \frac{h_{59}}{2m} \langle [D_\alpha, u_\nu] \tau^i \rangle w_\beta^j \tau^j \gamma^\beta \gamma_5 D^\alpha + h_{60} i \langle [D_\alpha, u_\nu] \tau^j \rangle w_\beta^i \tau^j \sigma^{\alpha\beta} \gamma_5 \\
&\quad - \frac{h_{61}}{2m} \langle [D_\alpha, u_\nu] \tau^j \rangle w_\beta^i \tau^j \gamma^\alpha \gamma_5 D^\beta - \frac{h_{62}}{2m} \langle [D_\alpha, u_\beta] \tau^j \rangle w_\nu^i \tau^j \gamma^\alpha \gamma_5 D^\beta \\
&\quad - \frac{h_{63}}{2m} \langle [D_\alpha, u_\nu] \tau^j \rangle w_\beta^i \tau^j \gamma^\beta \gamma_5 D^\alpha - \frac{h_{64}}{2m^2} \langle [D_\nu, [D_\alpha, u_\beta]] \tau^i \rangle D^{\alpha\beta} \\
&\quad \left. - \frac{h_{65}}{2m^2} \langle [D_\alpha, [D_\beta, u_\nu]] \tau^i \rangle D^{\alpha\beta} \right] \Psi + \text{h.c.} .
\end{aligned} \tag{A33}$$

At this point we emphasize that the terms contributing to $\mathcal{L}_{\pi\Delta}^{(3)}$ and $\mathcal{L}_{\pi\Delta}^{(4)}$ in Eq. (A24) do not appear in Refs. [24, 56], but instead were constructed for our purpose based on the rules provided in these papers. Also, the full Lagrangian $\mathcal{L}_{\pi N \Delta}^{(3)}$ is constructed in the unpublished work [58] and only the terms of interest are shown above. Furthermore, the Lagrangian $\mathcal{L}_{\pi N \Delta}^{(4)}$ is omitted, because there are no terms or only redundant ones which contribute to elastic pion-nucleon scattering. For the sake of brevity, we refrain from showing the construction and verification of these terms in detail. However, the interested reader can check that these terms fulfill all the necessary symmetry and power counting requirements. Additionally, we would like to preempt, that these terms turn out to be redundant in the final pion-nucleon amplitude. Next, we turn to the dependence on the off-shell parameters z_i, y_i in Eqs. (A24) and (A33). In these equations, we constrained the off-shell parameters to be equal for all LECs at a given chiral order. As shown in Ref. [47], it is possible to redefine the LECs such that the dependence of the physical amplitude on off-shell parameters is cancelled. Thus, we can ignore these parameters from the beginning. However, it is advantageous to keep them in our Lagrangian such that we have a further check on our calculations by demanding later on that the physical amplitudes should be free of off-shell parameters.

In the HB approach, a light spin-3/2 and isospin-3/2 field is defined via

$$T_i^\mu = P_v^+ \xi_{ij}^{3/2} \left(\hat{P}_{33}^{3/2} \right)^{\mu\nu} \Psi_\nu^j e^{imv \cdot x} \tag{A34}$$

with the projection operator

$$\left(\hat{P}_{33}^{3/2} \right)_{\mu\nu} = g_{\mu\nu} - v_\mu v_\nu - \frac{4}{1-d} S_\mu S_\nu , \tag{A35}$$

whereas the other projections are treated as heavy contributions. As mentioned before, we need to consider the HB Lagrangian only up to next-to-leading order explicitly. The HB pion- Δ Lagrangian up to next-to-leading order is given by [24]

$$\begin{aligned}
\hat{\mathcal{L}}_{\pi\Delta}^{(1)} &= -\bar{T}_i^\mu \left[i v \cdot D^{ij} - \Delta_0 \delta^{ij} + \mathbf{g}_1 S \cdot u^{ij} \right] g_{\mu\nu} T_j^\nu , \\
\hat{\mathcal{L}}_{\pi\Delta}^{(2)} &= -\bar{T}_i^\mu \left[c_1^\Delta \langle \chi_+ \rangle g_{\mu\nu} \delta^{ij} + \frac{c_2^\Delta}{4} \langle (v \cdot u)^2 \rangle g_{\mu\nu} \delta^{ij} + \frac{c_3^\Delta}{2} \langle u \cdot u \rangle g_{\mu\nu} \delta^{ij} + \frac{c_4^\Delta}{2} [S^\alpha, S^\beta] [u_\alpha, u_\beta] g_{\mu\nu} \delta^{ij} \right]
\end{aligned}$$

$$\begin{aligned}
& + \frac{c_{11}^\Delta}{2} \langle u^\mu u^\nu \rangle \delta^{ij} + c_{12}^\Delta (w_\mu^i w_\nu^j + w_\mu^j w_\nu^i) - \frac{c_{13}^\Delta}{2} (w_\rho^i w_\lambda^k + w_\lambda^i w_\rho^k) v^\rho v^\lambda \delta^{kj} g_{\mu\nu} \Big] T_j^\nu \\
& + \frac{1}{2m} \bar{T}_\mu^i \Big[[D_\alpha^{ik} D_\beta^{kj} g^{\alpha\beta} - v \cdot D^{ik} v \cdot D^{kj}] g^{\mu\nu} + \mathbf{g}_1 i (S \cdot D^{ik} v \cdot u^{kj} + v \cdot u^{ik} S \cdot D^{kj}) g^{\mu\nu} \\
& - [S^\alpha, S^\beta] (D_\alpha^{ik} D_\beta^{kj} - D_\beta^{ik} D_\alpha^{kj}) g^{\mu\nu} + \frac{\mathbf{g}_1^2}{4} v \cdot u^{ik} v \cdot u^{kj} g^{\mu\nu} \Big] T_\nu^j,
\end{aligned} \tag{A36}$$

where $u_\mu^{ij} = \xi_{3/2}^{il} u_\mu \xi_{3/2}^{lj}$. From the leading-order Lagrangian $\hat{\mathcal{L}}_{\pi\Delta}^{(1)}$ one can deduce the HB Δ propagator, which reads

$$\hat{\mathcal{G}}_{ij,\Delta}^{\mu\nu}(p) = \frac{-1}{v \cdot k - \Delta_0} \left(\hat{P}_{33}^{3/2} \right)^{\mu\nu} \xi_{3/2}^{ij}. \tag{A37}$$

The HB pion-nucleon- Δ Lagrangian up to next-to-leading order reads [24]

$$\begin{aligned}
\hat{\mathcal{L}}_{\pi N \Delta}^{(1)} &= h \bar{T}_i^\mu w_\mu^i N + \text{h.c.}, \\
\hat{\mathcal{L}}_{\pi N \Delta}^{(2)} &= \bar{T}_i^\mu \left[(b_3 + b_6) i w_{\mu\nu}^i v^\nu + b_4 w_\mu^i S \cdot u + b_5 u_\mu S \cdot w^i \right] N + \text{h.c.} \\
&\quad - \frac{1}{2m} \bar{T}_\mu^i \left[\frac{2}{d-1} h \mathbf{g}_1 z_0 u_\mu^\mu \xi^{jk} S \cdot w^k + 2 h i D_{ij}^\mu \xi^{jk} v \cdot w^k \right] N + \text{h.c.} .
\end{aligned} \tag{A38}$$

Finally, one has additional contributions to the pion-nucleon Lagrangian at next-to-leading order [24]

$$\begin{aligned}
\hat{\mathcal{L}}_{\pi N}^{(2)} &= -\frac{h^2}{2m} \bar{N} \left[\frac{4}{d-1} (2z_0 + (d-1)z_0^2) S \cdot w^i \xi^{ij} S \cdot w^j \right. \\
&\quad \left. + \frac{1}{d-1} (4(d-2) + 2(d-3)z_0 - z_0^2) v \cdot w^i \xi^{ij} v \cdot w^j \right] N.
\end{aligned} \tag{A39}$$

Note that we restored the explicit d -dependence in the Lagrangians in Eqs. (A38) and (A39). In Ref. [24] these terms are only given for the case $d = 4$, which is sufficient at tree-level. However, for our loop-level analysis, where we employ dimensional regularization, the explicit d -dependence is necessary. In particular, we restored it by matching covariant and HB amplitudes for the reactions $\pi N \rightarrow \pi N$ and $\pi N \rightarrow \pi\pi N$ at tree-level and for the Δ mass up to loop-level. We already mentioned that the Lagrangian in Ref. [24] is effectively constructed with the choice $A = 0$ for the unphysical off-shell parameter, however, we employ $A = -1$ in the above Lagrangians. The Lagrangian in Ref. [24] can be matched to the one presented here by applying the following relations

$$\hat{z}_0 = -\frac{1}{2}(1 + z_0), \quad \hat{\mathbf{g}}_2 = -\mathbf{g}_1 \quad \hat{\mathbf{g}}_3 = -\mathbf{g}_1, \tag{A40}$$

where the parameters in Ref. [24] are denoted by \hat{z}_0 , $\hat{\mathbf{g}}_2$ and $\hat{\mathbf{g}}_3$.

Appendix B: Redundancy Shifts for the Pion-Nucleon Scattering Amplitude

Treating the Δ resonance as an explicit degree of freedom introduces several new LECs and off-shell parameters in the pion-nucleon scattering amplitude. Fortunately, the majority of these LECs and all of the off-shell parameters turn out to be redundant. In the following we show the necessary redefinitions of LECs to get rid of the redundant dependence on the

LECs $b_3, b_6, h_i, c_i^\Delta$ and the off-shell parameter z_0 . For the sake of brevity, we only show the required shifts in the HB framework and we also suppress the off-shell parameters y_i and z_i for $i \in 1, 2, 3$. Needless to say, we extracted the shifts for the covariant framework as well and including the off-shell parameters y_i and z_i . The issue with the covariant approach is that even after considering further powers of $1/m_N$ in the shifts of the LECs, the amplitude will still depend on the off-shell parameters and the above mentioned redundant LECs at higher chiral orders. These terms can only be cancelled by higher-order LECs. Thus, in the covariant framework we set $b_i = h_i = c_i^\Delta = y_i = z_i = 0$ and demonstrate in the following the independence on these redundant terms only in a strict chiral counting.

At tree-level, the contributions proportional to b_3, b_6 and h_i are cancelled by

$$\begin{aligned}
h &\rightarrow h - (b_3 + b_6)\Delta + M_\pi^2 \left(-2h_4 + 4h_7 + \frac{b_6}{2m_N} \right) \\
&\quad + \left(2(h_{64} + h_{65}) - \frac{b_6}{2m_N} \right) \Delta^2 + \frac{(4b_6c_1 - 2(h_{64} + h_{65}))M_\pi^2\Delta}{m_N} \\
&\quad + \frac{2(h_{64} + h_{65})\Delta^3}{m_N}, \\
c_1 &\rightarrow c_1, \\
c_2 &\rightarrow c_2 + \frac{8}{9}(h_A + \delta h_A^{(3)})(b_3 + b_6) - \frac{4}{9}((b_3 + b_6)^2 + 4h_A(h_{64} + h_{65}))\Delta \\
&\quad - \frac{4h_A(4b_3 + 3b_6)\Delta}{9m_N} + \frac{16}{9}(b_3 + b_6)(h_{64} + h_{65})\Delta^2 + \frac{8h_A(3b_3 + 2b_6)\Delta^2}{9m_N^2} \\
&\quad + \frac{4((b_3 + b_6)(2b_3 + b_6) + 4h_A(h_{64} + h_{65}))\Delta^2}{9m_N}, \\
c_3 &\rightarrow c_3 - \frac{8}{9}(h_A + \delta h_A^{(3)})(b_3 + b_6) + \frac{4}{9}((b_3 + b_6)^2 + 4h_A(h_{64} + h_{65}))\Delta - \frac{4h_Ab_6\Delta}{9m_N} \\
&\quad - \frac{16}{9}(b_3 + b_6)(h_{64} + h_{65})\Delta^2 + \frac{4(b_6(b_3 + b_6) + 4h_A(h_{64} + h_{65}))\Delta^2}{9m_N}, \\
c_4 &\rightarrow c_4 + \frac{4}{9}(h_A + \delta h_A^{(3)})(b_3 + b_6) - \frac{2}{9}((b_3 + b_6)^2 + 4h_A(h_{64} + h_{65}))\Delta + \frac{2h_Ab_6\Delta}{9m_N} \\
&\quad + \frac{8}{9}(b_3 + b_6)(h_{64} + h_{65})\Delta^2 - \frac{2(b_6(b_3 + b_6) + 4h_A(h_{64} + h_{65}))\Delta^2}{9m_N}, \\
d_1 + d_2 &\rightarrow d_1 + d_2 + \frac{1}{9}((b_3 + b_6)^2 - 4h_A(h_{64} + h_{65})) - \frac{2h_Ab_3}{9m_N} + \frac{h_A(8b_3 + 5b_6)\Delta}{18m_N^2} \\
&\quad + \frac{((b_3 + b_6)(3b_3 + b_6) - 4h_A(h_{64} + h_{65}))\Delta}{18m_N}, \\
d_3 &\rightarrow d_3 + \frac{1}{9}(-(b_3 + b_6)^2 + 4h_A(h_{64} + h_{65})) - \frac{h_Ab_6}{9m_N} + \frac{2h_Ab_6\Delta}{9m_N^2} \\
&\quad + \frac{2((b_3 + b_6)^2 - 2h_A(h_{64} + h_{65}))\Delta}{9m_N}, \\
d_5 &\rightarrow d_5 - \frac{h_A(2b_3 + 3b_6)}{18m_N} + \frac{h_A(8b_3 + 7b_6)\Delta}{36m_N^2}
\end{aligned}$$

$$\begin{aligned}
& + \frac{((b_3 + b_6)(b_3 + 3b_6) + 12h_A(h_{64} + h_{65}))\Delta}{36m_N}, \\
d_{14} - d_{15} & \rightarrow d_{14} - d_{15} + \frac{1}{9}(-2(b_3 + b_6)^2 + 8h_A(h_{64} + h_{65})) + \frac{2h_A b_6}{9m_N} \\
& - \frac{2h_A b_6 \Delta}{9m_N^2} + \frac{2(b_3 - b_6)(b_3 + b_6)\Delta}{9m_N}, \\
e_{14} & \rightarrow e_{14} + \frac{h_A(4b_3 + 3b_6)}{72m_N^2} + \frac{b_3^2 - 4b_3 b_6 - 2b_6^2 + 8h_A(h_{64} + h_{65})}{72m_N}, \\
e_{15} & \rightarrow e_{15} + \frac{2}{9}(b_3 + b_6)(h_{64} + h_{65}) + \frac{h_A b_6}{18m_N^2} \\
& + \frac{2b_3^2 + 6b_3 b_6 + b_6^2 - 4h_A(h_{64} + h_{65})}{36m_N}, \\
e_{16} & \rightarrow e_{16} - \frac{2}{9}(b_3 + b_6)(h_{64} + h_{65}) + \frac{b_6^2 - 4h_A(h_{64} + h_{65})}{36m_N}, \\
e_{17} & \rightarrow e_{17} + \frac{h_A b_6}{36m_N^2} + \frac{4b_3^2 + 2b_3 b_6 + b_6^2 - 4h_A(h_{64} + h_{65})}{72m_N}, \\
e_{18} & \rightarrow e_{18} - \frac{1}{9}(b_3 + b_6)(h_{64} + h_{65}) - \frac{h_A b_6}{36m_N^2} \\
& + \frac{-2b_3^2 - b_6^2 + 4h_A(h_{64} + h_{65})}{72m_N}, \\
2e_{19} - e_{22} - e_{36} & \rightarrow 2e_{19} - e_{22} - e_{36} - \frac{4h_A(h_{64} + h_{65})}{9m_N}, \\
e_{20} + e_{35} & \rightarrow e_{20} + e_{35} + \frac{h_A b_6}{18m_N^2} + \frac{2b_3^2 + 4b_3 b_6 + 3b_6^2 - 4h_A(h_{64} + h_{65})}{36m_N}, \\
2e_{21} - e_{37} & \rightarrow 2e_{21} - e_{37} - \frac{h_A b_6}{18m_N^2} + \frac{2h_A(h_{64} + h_{65})}{9m_N}, \\
e_{22} - 4e_{38} & \rightarrow e_{22} - 4e_{38} + \frac{h_A(4b_3 + 5b_6)}{36m_N^2} - \frac{b_3^2}{36m_N}
\end{aligned}$$

and terms proportional to z_0 are cancelled by

$$\begin{aligned}
c_1 & \rightarrow c_1, \\
c_2 & \rightarrow c_2 + \frac{2(h_A^2 + 2h_A \delta h_A^{(3)})z_0(2 + z_0)}{9m_N} - \frac{4h_A^2 z_0(2 + z_0)\Delta}{9m_N^2} + \frac{2h_A^2 z_0(2 + z_0)\Delta^2}{3m_N^3}, \\
c_3 & \rightarrow c_3 - \frac{(h_A^2 + 2h_A \delta h_A^{(3)})z_0(2 + 3z_0)}{9m_N} + \frac{2h_A^2 z_0(1 + 2z_0)\Delta}{9m_N^2} - \frac{h_A^2 z_0(2 + 5z_0)\Delta^2}{9m_N^3}, \\
c_4 & \rightarrow c_4 - \frac{(h_A^2 + 2h_A \delta h_A^{(3)})z_0(2 + 3z_0)}{9m_N} + \frac{2h_A^2 z_0(1 + 2z_0)\Delta}{9m_N^2} - \frac{h_A^2 z_0(2 + 5z_0)\Delta^2}{9m_N^3}, \\
d_1 + d_2 & \rightarrow d_1 + d_2 - \frac{h_A^2 z_0(2 + z_0)}{36m_N^2} + \frac{h_A^2 z_0(2 + z_0)\Delta}{18m_N^3}, \\
d_3 & \rightarrow d_3,
\end{aligned}$$

$$\begin{aligned}
d_5 &\rightarrow d_5 - \frac{h_A^2 z_0}{36m_N^2} + \frac{h_A^2 z_0 \Delta}{18m_N^3} , \\
d_{14} - d_{15} &\rightarrow d_{14} - d_{15} + \frac{h_A^2 z_0(2+z_0)}{9m_N^2} - \frac{2h_A^2 z_0(2+z_0)\Delta}{9m_N^3} , \\
e_{14} &\rightarrow e_{14} + \frac{h_A^2 z_0(2+z_0)}{144m_N^3} , \\
e_{15} &\rightarrow e_{15} , \\
e_{16} &\rightarrow e_{16} , \\
e_{17} &\rightarrow e_{17} - \frac{h_A^2 z_0(2+z_0)}{144m_N^3} , \\
e_{18} &\rightarrow e_{18} , \\
2e_{19} - e_{22} - e_{36} &\rightarrow 2e_{19} - e_{22} - e_{36} - \frac{h_A^2 z_0(2+z_0)}{36m_N^3} , \\
e_{20} + e_{35} &\rightarrow e_{20} + e_{35} , \\
2e_{21} - e_{37} &\rightarrow 2e_{21} - e_{37} - \frac{h_A^2 z_0}{36m_N^3} , \\
e_{22} - 4e_{38} &\rightarrow e_{22} - 4e_{38} + \frac{h_A^2 z_0(2+z_0)}{36m_N^3} .
\end{aligned}$$

Note that we set $d = 4$ in the tree-level contributions above and that the terms proportional to the redundant LECs from $\mathcal{L}_{\pi N \Delta}^{(4)}$ are suppressed.

At loop-level, the contributions proportional to the LECs b_3 , b_6 , c_{11}^Δ , c_{12}^Δ and c_{13}^Δ are cancelled by

$$\begin{aligned}
c_1 &\rightarrow c_1 , \\
c_2 &\rightarrow c_2 + \frac{4(d-2)h_A(b_3+b_6)}{3(d-1)} , \\
c_3 &\rightarrow c_3 - \frac{4(d-2)h_A(b_3+b_6)}{3(d-1)} , \\
c_4 &\rightarrow c_4 + \frac{4h_A(b_3+b_6)}{3(d-1)} , \\
b_4 &\rightarrow b_4 + \frac{((1+3d)g_1 - 3(d-1)g_A)(b_3+b_6)}{3(d-1)} , \\
b_5 &\rightarrow b_5 - \frac{2(d+2)g_1(b_3+b_6)}{3(d-1)} , \\
c_1^\Delta &\rightarrow c_1^\Delta , \\
c_2^\Delta &\rightarrow c_2^\Delta + \frac{-4h_A(b_3+b_6) + 6c_{11}^\Delta + 4c_{12}^\Delta + 2(d-1)c_{13}^\Delta}{3(d-1)} , \\
c_3^\Delta &\rightarrow c_3^\Delta + \frac{2h_A(b_3+b_6) - 3c_{11}^\Delta - 2c_{12}^\Delta}{3(d-1)} ,
\end{aligned}$$

$$c_4^\Delta \rightarrow c_4^\Delta - \frac{2(-7+3d)h_A(b_3+b_6)}{22+d(-3+(-4+d)d)}$$

and the off-shell parameter z_0 contributions are cancelled by

$$\begin{aligned} c_1 &\rightarrow c_1, \\ c_2 &\rightarrow c_2 + \frac{(d-2)h_A^2 z_0(2+z_0)}{3(d-1)m_N}, \\ c_3 &\rightarrow c_3 - \frac{h_A^2 z_0(2+(d-1)z_0)}{3(d-1)m_N}, \\ c_4 &\rightarrow c_4 - \frac{h_A^2 z_0(2+(d-1)z_0)}{3(d-1)m_N}, \\ b_4 &\rightarrow b_4 - \frac{2g_1 h_A z_0}{3(d-1)m_N}, \\ b_5 &\rightarrow b_5 + \frac{g_1 h_A z_0}{(d-1)m_N}. \end{aligned}$$

Finally, terms proportional to the LECs c_i^Δ are cancelled by performing additional shifts for the LECs c_i in the tree-level diagrams

$$\begin{aligned} c_1 &\rightarrow c_1 + \frac{2(d-2)h_A^2 c_1^\Delta (A_0(M_\pi^2) + \Delta J_0(-\Delta))}{F_\pi^2}, \\ c_2 &\rightarrow c_2 + \frac{(d-2)h_A^2 c_2^\Delta (A_0(M_\pi^2) + \Delta J_0(-\Delta))}{F_\pi^2}, \\ c_3 &\rightarrow c_3 + \frac{2(d-2)h_A^2 c_3^\Delta (A_0(M_\pi^2) + \Delta J_0(-\Delta))}{F_\pi^2}, \\ c_4 &\rightarrow c_4 + \frac{10(22-3d-4d^2+d^3)h_A^2 c_4^\Delta (A_0(M_\pi^2) + \Delta J_0(-\Delta))}{9(d-1)^2 F_\pi^2}. \end{aligned}$$

Note that the shifts given above cancel the dependence on z_0 in the pion-nucleon scattering amplitude, however, the renormalization of leading-order couplings is necessary to cancel the terms proportional to $b_3 + b_6$ and c_i^Δ at loop-level. In particular, the renormalization of the coupling constant h_A and the Δ mass m_Δ discussed in Appendix C are needed. We have to emphasize that the LECs b_3 and b_6 should be redundant for every process involving a $\pi\bar{N}\Delta$ -vertex. However, the redundancy of the LECs c_i^Δ seems to be accidental and it is not clear to us why it should hold for any reaction other than $\pi N \rightarrow \pi N$.

In addition, we make use of the following linear combinations of LECs at tree-level

$$\begin{aligned} \bar{c}_1 &\rightarrow \bar{c}_1 + 2M_\pi^2(\bar{e}_{22} - 4\bar{e}_{38} + \bar{c}_1\beta_{l_3}\bar{l}_3/(32\pi^2 F_\pi^2)), \\ \bar{c}_2 &\rightarrow \bar{c}_2 - 8M_\pi^2(\bar{e}_{20} + \bar{e}_{35}), \\ \bar{c}_3 &\rightarrow \bar{c}_3 - 4M_\pi^2(2\bar{e}_{19} - \bar{e}_{22} - \bar{e}_{36}), \\ \bar{c}_4 &\rightarrow \bar{c}_4 - 4M_\pi^2(2\bar{e}_{21} - \bar{e}_{37}). \end{aligned}$$

Note that these linear combinations refer to the renormalized LECs, which is denoted by the bar notation. The renormalization of the bare LECs is discussed in Appendix C.

Appendix C: Renormalization Rules

In this appendix, we list the renormalization rules for the leading-order coupling constants, masses and higher-order LECs. Note that we employ the following integral notation

$$\begin{aligned}
A_0(m_0^2) &= \frac{1}{i} \int \frac{d^d l}{(2\pi)^d} \frac{1}{l^2 - m_0^2} , \\
B_0(p^2, m_0^2, m_1^2) &= \frac{1}{i} \int \frac{d^d l}{(2\pi)^d} \frac{1}{(l^2 - m_0^2)((l+p)^2 - m_1^2)} , \\
J_0(\omega) &= \frac{1}{i} \int \frac{d^d l}{(2\pi)^d} \frac{1}{(l^2 - M_\pi^2)(\omega + v \cdot l)} , \\
C_0(p_1^2, (p_1 - p_2)^2, p_2^2, m_0^2, m_1^2, m_2^2) &= \frac{1}{i} \int \frac{d^d l}{(2\pi)^d} \frac{1}{(l^2 - m_0^2)((l+p_1)^2 - m_1^2)((l+p_2)^2 - m_2^2)}
\end{aligned}$$

where the $+i\epsilon$ prescription was suppressed. In particular, we only show the HB expressions in the following sections, whereas the covariant expressions (as well as the HB ones) can be found in the supplementary material.

1. Mesonic Sector

In the meson sector, the renormalization rules for the pion mass, Z-factor and decay constant are given by

$$\begin{aligned}
M^2 &= M_\pi^2 + \delta M^{(4)} , \\
\delta M^{(4)} &= -\frac{2l_3 M_\pi^4}{F_\pi^2} + \frac{M_\pi^2 A_0(M_\pi^2)}{2F_\pi^2} , \\
Z_\pi &= 1 + \delta Z_\pi^{(4)} , \\
\delta Z_\pi^{(4)} &= -\frac{2l_4 M_\pi^2}{F_\pi^2} - \frac{(-1 + 10\alpha) A_0(M_\pi^2)}{F_\pi^2} , \\
F &= F_\pi + \delta F_\pi^{(4)} , \\
\delta F_\pi^{(4)} &= -\frac{l_4 M_\pi^2}{F_\pi} - \frac{A_0(M_\pi^2)}{F_\pi} .
\end{aligned}$$

2. Heavy Baryon Chiral Perturbation Theory

a. Renormalization of Masses and Couplings

The HB expression for the nucleon mass reads

$$\begin{aligned}
m &= m_N + \delta m^{(2)} + \delta m^{(3)} + \delta m^{(3,\Delta)} + \delta m^{(4,\Delta)} , \\
\delta m^{(2)} &= 4c_1 M_\pi^2 , \\
\delta m^{(3)} &= -\frac{3g_A^2 M_\pi^2 J_0(0)}{4F_\pi^2}
\end{aligned}$$

$$\begin{aligned}
\delta m^{(3,\Delta)} &= -\frac{h_A^2 M_\pi^2 \Delta}{12 F_\pi^2 \pi^2} + \frac{h_A^2 \Delta^3}{18 F_\pi^2 \pi^2} + \frac{4 h_A^2 \Delta A_0(M_\pi^2)}{3 F_\pi^2} + \left(-\frac{4 h_A^2 M_\pi^2}{3 F_\pi^2} + \frac{4 h_A^2 \Delta^2}{3 F_\pi^2} \right) J_0(-\Delta) , \\
\delta m^{(4)} &= M_\pi^4 \left(2e_{115} + 2e_{116} + 16e_{38} - \frac{8c_1 l_3}{F_\pi^2} - \frac{3c_2}{128 F_\pi^2 \pi^2} + \frac{3g_A^2}{64 F_\pi^2 m_N \pi^2} \right) \\
&\quad + M_\pi^2 \left(\frac{32c_1 - 3(c_2 + 4c_3)}{4 F_\pi^2} - \frac{3g_A^2}{4 F_\pi^2 m_N} \right) A_0(M_\pi^2) , \\
\delta m^{(4,\Delta)} &= \frac{49 h_A^2 M_\pi^4}{576 F_\pi^2 m_N \pi^2} - \frac{7 h_A^2 M_\pi^2 \Delta^2}{24 F_\pi^2 m_N \pi^2} + \frac{7 h_A^2 \Delta^4}{36 F_\pi^2 m_N \pi^2} \\
&\quad + \left(\frac{h_A^2 M_\pi^2}{6 F_\pi^2 m_N} + \frac{2 h_A^2 \Delta^2}{3 F_\pi^2 m_N} \right) A_0(M_\pi^2) + \left(-\frac{2 h_A^2 M_\pi^2 \Delta}{3 F_\pi^2 m_N} + \frac{2 h_A^2 \Delta^3}{3 F_\pi^2 m_N} \right) J_0(-\Delta) ,
\end{aligned}$$

the Z-Factor is given by

$$\begin{aligned}
Z_N &= 1 + \delta Z_N^{(3)} + \delta Z_N^{(3,\Delta)} + \delta Z_N^{(4)} + \delta Z_N^{(4,\Delta)} , \\
\delta Z_N^{(3)} &= -\frac{3g_A^2 M_\pi^2}{32 F_\pi^2 \pi^2} + \frac{9g_A^2 A_0(M_\pi^2)}{4 F_\pi^2} , \\
\delta Z_N^{(3,\Delta)} &= -\frac{h_A^2 M_\pi^2}{4 F_\pi^2 \pi^2} + \frac{h_A^2 \Delta^2}{2 F_\pi^2 \pi^2} + \frac{4 h_A^2 A_0(M_\pi^2)}{F_\pi^2} + \frac{4 h_A^2 \Delta J_0(-\Delta)}{F_\pi^2} , \\
\delta Z_N^{(4)} &= -\frac{9g_A^2 M_\pi^2 J_0(0)}{8 F_\pi^2 m_N} , \\
\delta Z_N^{(4,\Delta)} &= M_\pi^2 \left(-\frac{h_A(b_3 + b_6)}{6 F_\pi^2 \pi^2} - \frac{2h_A^2}{3 F_\pi^2 m_N \pi^2} \right) \Delta + \left(\frac{h_A(b_3 + b_6)}{9 F_\pi^2 \pi^2} + \frac{17h_A^2}{18 F_\pi^2 m_N \pi^2} \right) \Delta^3 \\
&\quad + \left(\frac{8h_A(b_3 + b_6)}{3 F_\pi^2} + \frac{8h_A^2}{3 F_\pi^2 m_N} \right) \Delta A_0(M_\pi^2) \\
&\quad + \left(M_\pi^2 \left(-\frac{8h_A(b_3 + b_6)}{3 F_\pi^2} - \frac{2h_A^2}{3 F_\pi^2 m_N} \right) + \left(\frac{8h_A(b_3 + b_6)}{3 F_\pi^2} + \frac{8h_A^2}{3 F_\pi^2 m_N} \right) \Delta^2 \right) J_0(-\Delta) .
\end{aligned}$$

and the effective nucleon axial coupling constant reads

$$\begin{aligned}
g &= g_A + \delta g^{(3)} + \delta g^{(3,\Delta)} + \delta g^{(4)} + \delta g^{(4,\Delta)} , \\
\delta g^{(3)} &= M_\pi^2 \left(-4d_{16} + 2d_{18} + \frac{g_A^3}{16 F_\pi^2 \pi^2} \right) - \frac{(g_A + 2g_A^3) A_0(M_\pi^2)}{F_\pi^2} , \\
\delta g_A^{(3,\Delta)} &= \frac{5(-31g_1 + 63g_A)h_A^2 M_\pi^2}{972 F_\pi^2 \pi^2} + \frac{(155g_1 - 267g_A)h_A^2 \Delta^2}{486 F_\pi^2 \pi^2} + \frac{4(25g_1 - 57g_A)h_A^2 A_0(M_\pi^2)}{81 F_\pi^2} \\
&\quad + \frac{32g_A h_A^2 M_\pi^2 J_0(0)}{27 F_\pi^2 \Delta} + \left(-\frac{32g_A h_A^2 M_\pi^2}{27 F_\pi^2 \Delta} + \frac{4(25g_1 - 57g_A)h_A^2 \Delta}{81 F_\pi^2} \right) J_0(-\Delta) , \\
\delta g^{(4)} &= M_\pi^2 \left(-\frac{4g_A(c_3 - 2c_4)}{3 F_\pi^2} + \frac{g_A + g_A^3}{F_\pi^2 m_N} \right) J_0(0) , \\
\delta g^{(4,\Delta)} &= \frac{5h_A b_4 \Delta (3M_\pi^2 - 2\Delta^2)}{162 F_\pi^2 \pi^2} + \frac{h_A^2 \Delta (-140g_1 M_\pi^2 + 252g_A M_\pi^2 + 195g_1 \Delta^2 - 411g_A \Delta^2)}{486 F_\pi^2 m_N \pi^2} \\
&\quad + \left(-\frac{8h_A(13b_4 + 12b_5)\Delta}{27 F_\pi^2} + \frac{40(5g_1 - 9g_A)h_A^2 \Delta}{243 F_\pi^2 m_N} \right) A_0(M_\pi^2)
\end{aligned}$$

$$\begin{aligned}
& + \frac{8h_A(13b_4 + 12b_5)(M_\pi^2 - \Delta^2)J_0(-\Delta)}{27F_\pi^2} \\
& - \frac{2h_A^2(25g_1(M_\pi^2 - 4\Delta^2) + 9g_A(7M_\pi^2 + 20\Delta^2))J_0(-\Delta)}{243F_\pi^2m_N}.
\end{aligned}$$

The Δ mass reads

$$\begin{aligned}
\mathbf{m} &= m_\Delta + \delta\mathbf{m}^{(2)} + \delta\mathbf{m}^{(3)} + \delta\mathbf{m}^{(4)}, \\
\delta\mathbf{m}^{(2)} &= 4c_1^\Delta M_\pi^2, \\
\delta\mathbf{m}^{(3)} &= -\frac{h_A^2 M_\pi^2 \Delta}{24F_\pi^2 \pi^2} + \frac{h_A^2 \Delta^3}{36F_\pi^2 \pi^2} - \frac{h_A^2 \Delta A_0(M_\pi^2)}{3F_\pi^2} - \frac{25g_1^2 M_\pi^2 J_0(0)}{108F_\pi^2} \\
& + \left(-\frac{h_A^2 M_\pi^2}{3F_\pi^2} + \frac{h_A^2 \Delta^2}{3F_\pi^2} \right) J_0(\Delta), \\
\delta\mathbf{m}^{(4)} &= M_\pi^4 \left(-2e_{115}^\Delta - 2e_{116}^\Delta - 16e_{38}^\Delta - \frac{8c_1^\Delta l_3}{F_\pi^2} - \frac{3c_2^\Delta}{256F_\pi^2 \pi^2} + \frac{25g_1^2 - 3h_A^2}{768F_\pi^2 m_N \pi^2} \right) \\
& + \frac{h_A^2 M_\pi^2 \Delta^2}{24F_\pi^2 m_N \pi^2} - \frac{h_A^2 \Delta^4}{36F_\pi^2 m_N \pi^2} + \left(\frac{5h_A^2 M_\pi^2 \Delta}{6F_\pi^2 m_N} - \frac{5h_A^2 \Delta^3}{6F_\pi^2 m_N} \right) J_0(\Delta) \\
& + \left(M_\pi^2 \left(\frac{64c_1^\Delta - 3(c_2^\Delta + 8c_3^\Delta)}{8F_\pi^2} - \frac{5(g_1^2 + 3h_A^2)}{24F_\pi^2 m_N} \right) + \frac{5h_A^2 \Delta^2}{6F_\pi^2 m_N} \right) A_0(M_\pi^2)
\end{aligned}$$

with the Δ width given by

$$\frac{\Gamma}{2} = \frac{h_A^2 (-M_\pi^2 + \Delta^2)^{3/2}}{12F_\pi^2 \pi} - \frac{5h_A^2 \Delta (-M_\pi^2 + \Delta^2)^{3/2}}{24F_\pi^2 m_N \pi},$$

the Z-Factor is given by

$$\begin{aligned}
Z_\Delta &= 1 + \delta Z_\Delta^{(3)} + \delta Z_\Delta^{(4)}, \\
\delta Z_\Delta^{(3)} &= -\frac{65g_1^2 M_\pi^2}{864F_\pi^2 \pi^2} + \frac{(25g_1^2 + 36h_A^2)A_0(M_\pi^2)}{36F_\pi^2} - \frac{h_A^2 \Delta J_0(\Delta)}{F_\pi^2}, \\
\delta Z_\Delta^{(4)} &= \frac{h_A^2 \Delta (3M_\pi^2 - 14\Delta^2)}{144F_\pi^2 m_N \pi^2} + \frac{h_A(b_3 + b_6)\Delta(3M_\pi^2 - 2\Delta^2)}{36F_\pi^2 \pi^2} \\
& + \left(\frac{2h_A(b_3 + b_6)\Delta}{3F_\pi^2} - \frac{10h_A^2 \Delta}{3F_\pi^2 m_N} \right) A_0(M_\pi^2) - \frac{25g_1^2 M_\pi^2 J_0(0)}{72F_\pi^2 m_N} \\
& + \left(-\frac{5h_A^2 (M_\pi^2 - 4\Delta^2)}{6F_\pi^2 m_N} + \frac{2h_A(b_3 + b_6)(M_\pi^2 - \Delta^2)}{3F_\pi^2} \right) J_0(\Delta).
\end{aligned}$$

and the effective nucleon- Δ axial coupling constant is given by

$$\begin{aligned}
h &= h_A + \delta h^{(3)} + \delta h^{(4)}, \\
\delta h^{(3)} &= M_\pi^2 \left(\frac{h_A(155g_1^2 - 390g_1g_A + 459g_A^2 + 624h_A^2)}{5184F_\pi^2 \pi^2} \right)
\end{aligned}$$

$$\begin{aligned}
& + \left(-\frac{h_A (-5g_1^2 + 27g_A^2 + 240h_A^2)}{972F_\pi^2\pi^2} \right) \Delta^2 \\
& - \frac{h_A (475g_1^2 - 1350g_1g_A + 9(216 + 171g_A^2 + 532h_A^2)) A_0(M_\pi^2)}{1944F_\pi^2} \\
& + \frac{(25g_1^2 - 81g_A^2) h_A M_\pi^2 J_0(0)}{243F_\pi^2\Delta} \\
& + \left(-\frac{(50g_1^2 h_A + 9h_A^3) M_\pi^2}{486F_\pi^2\Delta} + \frac{(50g_1^2 h_A - 963h_A^3) \Delta}{486F_\pi^2} \right) J_0(-\Delta) \\
& + \left(\frac{(18g_A^2 h_A + h_A^3) M_\pi^2}{54F_\pi^2\Delta} + \frac{(-9g_A^2 h_A + 13h_A^3) \Delta}{27F_\pi^2} \right) J_0(\Delta) , \\
\delta h^{(4)} = & \frac{h_A(189h_A(b_3 + b_6) - 2(24c_{11}^\Delta + 36c_{12}^\Delta + 18c_3 - 18c_3^\Delta - 9c_4 + 5c_4^\Delta))\Delta(3M_\pi^2 - 2\Delta^2)}{1296F_\pi^2\pi^2} \\
& - \frac{5h_A\Delta(3(36 + 16g_1^2 - 165h_A^2)M_\pi^2 - 2(36 + 16g_1^2 - 327h_A^2)\Delta^2)}{7776F_\pi^2m_N\pi^2} \\
& + \frac{h_A(15c_{11}^\Delta + 45c_{12}^\Delta - 18c_3 + 18c_3^\Delta + 9c_4 - 25c_4^\Delta)\Delta A_0(M_\pi^2)}{27F_\pi^2} \\
& + \frac{h_A(25g_1^2 - 81g_A^2 + 60(-3 + h_A^2))\Delta A_0(M_\pi^2)}{162F_\pi^2m_N} \\
& + \frac{(25g_1b_4 + 25g_1^2(b_3 + b_6) - 9g_A(-13b_4 - 12b_5 + 9g_A(b_3 + b_6)))M_\pi^2 J_0(0)}{108F_\pi^2} \\
& + \frac{(875g_1^2 - 1350g_1g_A + 1539g_A^2)h_A M_\pi^2 J_0(0)}{3888F_\pi^2m_N} \\
& + \frac{h_A(9h_A(b_3 + b_6) - 15c_{11}^\Delta - 45c_{12}^\Delta - 18c_3^\Delta + 25c_4^\Delta)(M_\pi^2 - \Delta^2)J_0(-\Delta)}{27F_\pi^2} \\
& + \frac{h_A((360 - 50g_1^2 + 93h_A^2)M_\pi^2 + (-360 + 50g_1^2 - 417h_A^2)\Delta^2)J_0(-\Delta)}{324F_\pi^2m_N} \\
& + \frac{h_A(h_A(b_3 + b_6) - 2c_3 + c_4)(M_\pi^2 - \Delta^2)J_0(\Delta)}{3F_\pi^2} \\
& + \frac{(h_A^3(44M_\pi^2 - 179\Delta^2) - 54g_A^2 h_A(M_\pi^2 - \Delta^2))J_0(\Delta)}{108F_\pi^2m_N}
\end{aligned}$$

with the imaginary parts

$$\begin{aligned}
\text{Im } \delta h_A^{(3)} &= \frac{h_A \sqrt{-M_\pi^2 + \Delta^2}}{216F_\pi^2\pi\Delta} \left(18g_A^2 (M_\pi^2 - \Delta^2) + h_A^2 (M_\pi^2 + 26\Delta^2) \right) , \\
\text{Im } \delta h_A^{(4)} &= \frac{h_A(2c_3 - c_4)(-M_\pi^2 + \Delta^2)^{3/2}}{12F_\pi^2\pi} \\
&\quad - \frac{h_A \sqrt{-M_\pi^2 + \Delta^2}}{432F_\pi^2m_N\pi} \left(54g_A^2 (M_\pi^2 - \Delta^2) + h_A^2 (-44M_\pi^2 + 179\Delta^2) \right) .
\end{aligned}$$

We emphasize that in the expressions above we have already performed all the redundancy shifts discussed in Appendix B. Note that the quantities Z_N , Z_Δ and h_A however still depend

on the linear combination $b_3 + b_6$. This is crucial for the explicit redundancy of these LECs in the renormalized pion-nucleon scattering amplitude.

b. Renormalization of LECs

Next, we discuss the renormalization of the LECs c_i , d_i and e_i in the HB framework, see Eqs. (19) and (20). In particular, we list in the following the β -functions and the additional finite shifts. The employed β -functions at order Q^3 read

$$\begin{aligned}
\beta_{d_1} &= -\frac{g_A^4}{6} , & \beta_{d_2} &= \frac{1}{12} (-1 - 5g_A^2) , \\
\beta_{d_3} &= \frac{1}{6} (3 + g_A^4) , & \beta_{d_4} &= 0 , \\
\beta_{d_5} &= \frac{1}{24} (1 + 5g_A^2) , & \beta_{d_{10}} &= \frac{1}{2} (g_A + 5g_A^3 + 4g_A^5) , \\
\beta_{d_{11}} &= \frac{1}{6} (3g_A - 9g_A^3 - 4g_A^5) , & \beta_{d_{12}} &= -g_A (2 + g_A^2 + 2g_A^4) , \\
\beta_{d_{13}} &= g_A^3 + \frac{2g_A^5}{3} , & \beta_{d_{14}} &= \frac{g_A^4}{3} , \\
\beta_{d_{15}} &= 0 , & \beta_{d_{16}} &= \frac{g_A}{2} + g_A^3 , \\
\beta_{d_{18}} &= 0
\end{aligned}$$

and at order Q^4 we get

$$\begin{aligned}
\beta_{e_{10}} &= -\frac{1}{6} g_A (3 + 8g_A^2) c_4 - \frac{g_A (3 + 19g_A^2 + 13g_A^4)}{24m_N} , \\
\beta_{e_{11}} &= -\frac{g_A c_4}{3} + \frac{g_A (-7 + 35g_A^2 + 12g_A^4)}{48m_N} , \\
\beta_{e_{12}} &= \frac{4}{3} g_A (1 + g_A^2) c_4 + \frac{g_A (61 + 57g_A^2 + 26g_A^4)}{48m_N} , \\
\beta_{e_{13}} &= -\frac{2}{3} (g_A + 2g_A^3) c_4 - \frac{g_A (73 + 54g_A^2 + 21g_A^4)}{24m_N} , \\
\beta_{e_{14}} &= \frac{1}{12} (-c_2 - 6c_3) - \frac{g_A^2 (3 + g_A^2)}{12m_N} , \\
\beta_{e_{15}} &= \frac{9 + 2g_A^2 + 11g_A^4}{24m_N} , \\
\beta_{e_{16}} &= \frac{-3 - 2g_A^2 - 2g_A^4}{4m_N} , \\
\beta_{e_{17}} &= -\frac{c_4}{12} + \frac{-1 + 7g_A^2 + 4g_A^4}{48m_N} , \\
\beta_{e_{18}} &= -\frac{2g_A^2 c_4}{3} - \frac{g_A^2 (3 + 4g_A^2)}{12m_N} , \\
2\beta_{e_{19}} - \beta_{e_{22}} - \beta_{e_{36}} &= 2c_1 - \frac{5c_2}{24} + \frac{3c_3}{4} + \frac{-1 + g_A^2 - 6g_A^4}{8m_N} ,
\end{aligned}$$

$$\begin{aligned}
\beta_{e_{20}} + \beta_{e_{35}} &= \frac{c_2}{2} + \frac{6 + 16g_A^2 + 15g_A^4}{24m_N}, \\
2\beta_{e_{21}} - \beta_{e_{37}} &= \frac{1}{3} (2 + 9g_A^2) c_4 + \frac{2 + 16g_A^2 + 9g_A^4}{12m_N}, \\
\beta_{e_{22}} - 4\beta_{e_{38}} &= \frac{1}{4} (-12c_1 + c_2 + 3c_3), \\
\beta_{e_{34}} &= \frac{2g_A c_4}{3} + \frac{g_A - 7g_A^3 - 6g_A^5}{24m_N}.
\end{aligned}$$

Treating the Δ resonance as an explicit degree of freedom gives additional β functions for the LECs c_i at ε^3

$$\begin{aligned}
\beta_{c_i}^\Delta &= 0 \\
\beta_{c_1}^{(3,\Delta)} &= 2h_A^2 \Delta, \\
\beta_{c_2}^{(3,\Delta)} &= -\frac{80(5g_1 - 9g_A)^2 h_A^2 \Delta}{2187}, \\
\beta_{c_3}^{(3,\Delta)} &= \frac{16(125g_1^2 - 450g_1g_A + 81(9 + 5g_A^2)) h_A^2 \Delta}{2187}, \\
\beta_{c_4}^{(3,\Delta)} &= -\frac{2h_A^2(972 + 125g_1^2 - 2250g_1g_A + 2349g_A^2 + 1152h_A^2) \Delta}{2187}
\end{aligned}$$

and the contributions at order ε^4 read

$$\begin{aligned}
\beta_{c_1}^{(4,\Delta)} &= -16h_A^2 c_1 \Delta^2 + \frac{h_A^2 \Delta^2}{m_N}, \\
\beta_{c_2}^{(4,\Delta)} &= -\frac{16}{243} h_A (-25g_1 b_4 + 9(13g_A b_4 + 12g_A b_5 + 27h_A c_2)) \Delta^2 \\
&\quad - \frac{8h_A^2 (-72 + 40g_1^2 - 150g_1g_A - 63g_A^2 + 260h_A^2) \Delta^2}{243m_N}, \\
\beta_{c_3}^{(4,\Delta)} &= \frac{16}{243} h_A (-25g_1 b_4 + 9(13g_A b_4 + 12g_A b_5 - 27h_A c_3)) \Delta^2 \\
&\quad + \frac{2h_A^2 (1025g_1^2 - 4050g_1g_A + 9(252 - 63g_A^2 + 640h_A^2)) \Delta^2}{2187m_N}, \\
\beta_{c_4}^{(4,\Delta)} &= -\frac{4}{243} h_A (-25g_1(23b_4 + 24b_5) + 45g_A(27b_4 + 28b_5) + 684h_A c_4) \Delta^2 \\
&\quad + \frac{h_A^2 (-275g_1^2 + 1350g_1g_A + 9(36 + 405g_A^2 - 832h_A^2)) \Delta^2}{2187m_N}.
\end{aligned}$$

Additionally, one has corresponding finite shifts at ε^3

$$\begin{aligned}
\delta \bar{c}_{1,f}^{(3,\Delta)} &= 0, \\
\delta \bar{c}_{2,f}^{(3,\Delta)} &= -\frac{(3575g_1^2 - 8910g_1g_A + 6399g_A^2) h_A^2 \Delta}{52488\pi^2}, \\
\delta \bar{c}_{3,f}^{(3,\Delta)} &= \frac{(3575g_1^2 - 8910g_1g_A + 6399g_A^2) h_A^2 \Delta}{52488\pi^2}, \\
\delta \bar{c}_{4,f}^{(3,\Delta)} &= \frac{h_A^2 (-4775g_1^2 + 28350g_1g_A + 27(180 - 1317g_A^2 + 64h_A^2)) \Delta}{104976\pi^2}
\end{aligned}$$

and at ε^4

$$\begin{aligned}
\delta\bar{c}_{1,f}^{(4,\Delta)} &= \frac{h_A^2 \Delta^2}{16m_N \pi^2}, \\
\delta\bar{c}_{2,f}^{(4,\Delta)} &= \frac{5(7g_1 - 3g_A)h_A b_4 \Delta^2}{486\pi^2} \\
&\quad + \frac{h_A^2 (-4015g_1^2 + 12510g_1 g_A - 9(240 + 1839g_A^2 - 304h_A^2)) \Delta^2}{34992m_N \pi^2}, \\
\delta\bar{c}_{3,f}^{(4,\Delta)} &= \frac{5(-7g_1 + 3g_A)h_A b_4 \Delta^2}{486\pi^2} \\
&\quad + \frac{h_A^2 (11405g_1^2 - 33210g_1 g_A + 27(744 + 1263g_A^2 - 16h_A^2)) \Delta^2}{104976m_N \pi^2}, \\
\delta\bar{c}_{4,f}^{(4,\Delta)} &= \frac{5h_A(71g_1 b_4 + 9g_A b_4 + 68g_1 b_5 + 48g_A b_5 - 48h_A c_4) \Delta^2}{1944\pi^2} \\
&\quad + \frac{h_A^2 (-10355g_1^2 + 81270g_1 g_A - 81(4 + 1611g_A^2 - 144h_A^2)) \Delta^2}{209952m_N \pi^2}.
\end{aligned}$$

Analogously, for the LECs d_i we obtain at ε^3

$$\begin{aligned}
\beta_{d_i}^\Delta &= 0 \\
\beta_{d_1}^{(3,\Delta)} + \beta_{d_2}^{(3,\Delta)} &= -\frac{h_A^2 (125g_1^2 - 450g_1 g_A - 9(90 + 27g_A^2 - 32h_A^2))}{2187}, \\
\beta_{d_3}^{(3,\Delta)} &= \frac{h_A^2 (125g_1^2 - 450g_1 g_A - 243g_A^2 + 288h_A^2)}{2187}, \\
\beta_{d_5}^{(3,\Delta)} &= -\frac{5h_A^2}{27}, \\
\beta_{d_{14}}^{(3,\Delta)} - \beta_{d_{15}}^{(3,\Delta)} &= \frac{2h_A^2 (125g_1^2 - 450g_1 g_A - 243g_A^2 + 288h_A^2)}{2187}
\end{aligned}$$

and at ε^4

$$\begin{aligned}
\beta_{d_1}^{(4,\Delta)} + \beta_{d_2}^{(4,\Delta)} &= \frac{4}{243} h_A (100g_1 b_4 - 252g_A b_4 + 75g_1 b_5 - 198g_A b_5 + 36h_A c_4) \Delta \\
&\quad + \frac{h_A^2 (-175g_1^2 + 750g_1 g_A + 3(792 + 531g_A^2 - 512h_A^2)) \Delta}{1458m_N}, \\
\beta_{d_3}^{(4,\Delta)} &= -\frac{4}{243} h_A (100g_1 b_4 - 252g_A b_4 + 75g_1 b_5 - 198g_A b_5 + 36h_A c_4) \Delta \\
&\quad + \frac{h_A^2 (275g_1^2 - 750g_1 g_A - 9(180 + 129g_A^2 - 128h_A^2)) \Delta}{729m_N}, \\
\beta_{d_5}^{(4,\Delta)} &= -\frac{h_A^2 (360 + 125g_1^2 - 250g_1 g_A - 243g_A^2 + 256h_A^2) \Delta}{972m_N}, \\
\beta_{d_{14}}^{(4,\Delta)} - \beta_{d_{15}}^{(4,\Delta)} &= -\frac{8}{243} h_A (100g_1 b_4 - 252g_A b_4 + 75g_1 b_5 - 198g_A b_5 + 36h_A c_4) \Delta \\
&\quad + \frac{8h_A^2 (50g_1^2 - 27(6 + 33g_A^2 - 16h_A^2)) \Delta}{2187m_N}.
\end{aligned}$$

Additionally, the finite shifts at ε^3 have the form

$$\delta\bar{d}_{1,f}^{(3,\Delta)} + \delta\bar{d}_{2,f}^{(3,\Delta)} = \frac{h_A^2 (-925g_1^2 + 3870g_1 g_A - 27(-78 + 189g_A^2 + 8h_A^2))}{104976\pi^2},$$

$$\begin{aligned}\delta\bar{d}_{3,f}^{(3,\Delta)} &= \frac{h_A^2 (925g_1^2 - 3870g_1g_A + 5103g_A^2 + 216h_A^2)}{104976\pi^2}, \\ \delta\bar{d}_{5,f}^{(3,\Delta)} &= -\frac{13h_A^2}{1296\pi^2}, \\ \delta\bar{d}_{14,f}^{(3,\Delta)} - \delta\bar{d}_{15,f}^{(3,\Delta)} &= \frac{h_A^2 (3425g_1^2 - 9090g_1g_A + 5589g_A^2 + 432h_A^2)}{104976\pi^2}\end{aligned}$$

and at ε^4

$$\begin{aligned}\delta\bar{d}_{1,f}^{(4,\Delta)} + \delta\bar{d}_{2,f}^{(4,\Delta)} &= \frac{h_A(5g_1(38b_4 + 31b_5) - 6(49g_Ab_4 + 31g_Ab_5 + 8h_Ac_4))\Delta}{1944\pi^2} \\ &\quad - \frac{h_A^2(4535g_1^2 - 19950g_1g_A + 27(-232 + 965g_A^2 + 64h_A^2))\Delta}{139968m_N\pi^2}, \\ \delta\bar{d}_{3,f}^{(4,\Delta)} &= \frac{h_A(-5g_1(38b_4 + 31b_5) + 6(49g_Ab_4 + 31g_Ab_5 + 8h_Ac_4))\Delta}{1944\pi^2} \\ &\quad + \frac{h_A^2(2605g_1^2 - 10650g_1g_A + 9(504 + 1641g_A^2 + 64h_A^2))\Delta}{69984m_N\pi^2}, \\ \delta\bar{d}_{5,f}^{(4,\Delta)} &= \frac{h_A^2(-1272 - 75g_1^2 + 150g_1g_A - 387g_A^2 + 64h_A^2)\Delta}{31104m_N\pi^2}, \\ \delta\bar{d}_{14,f}^{(4,\Delta)} - \delta\bar{d}_{15,f}^{(4,\Delta)} &= \frac{h_A(393g_Ab_4 + 312g_Ab_5 - 5g_1(33b_4 + 16b_5) + 12h_Ac_4)\Delta}{972\pi^2} \\ &\quad + \frac{h_A^2(7715g_1^2 - 21150g_1g_A + 81(32 + 191g_A^2 - 32h_A^2))\Delta}{104976m_N\pi^2}.\end{aligned}$$

Finally, the additional β -functions of the LECs e_i at ε^3 read

$$\begin{aligned}\beta_{e_{14}}^\Delta &= \frac{2h_A^2}{27m_N} + \frac{5h_A^2}{27\Delta}, \\ \beta_{e_{15}}^\Delta &= 0, \\ \beta_{e_{16}}^\Delta &= 0, \\ \beta_{e_{17}}^\Delta &= -\frac{h_A^2}{54\Delta}, \\ \beta_{e_{18}}^\Delta &= -\frac{4g_A^2h_A^2}{27\Delta}, \\ 2\beta_{e_{19}}^\Delta - \beta_{e_{22}}^\Delta - \beta_{e_{36}}^\Delta &= -\frac{h_A^2}{27m_N} + \frac{(-33 + 25g_1^2 - 50g_1g_A + 81g_A^2)h_A^2}{162\Delta}, \\ \beta_{e_{20}}^\Delta + \beta_{e_{35}}^\Delta &= \frac{(25g_1^2 - 50g_1g_A + 81g_A^2)h_A^2}{162m_N} - \frac{(25g_1^2 - 50g_1g_A + 81g_A^2)h_A^2}{324\Delta}, \\ 2\beta_{e_{21}}^\Delta - \beta_{e_{37}}^\Delta &= \frac{(-24 - 25g_1^2 + 50g_1g_A + 135g_A^2)h_A^2}{324\Delta}, \\ \beta_{e_{22}}^\Delta - 4\beta_{e_{38}}^\Delta &= -\frac{2h_A^2}{9m_N} - \frac{2h_A^2}{9\Delta}\end{aligned}$$

and at ε^4

$$\beta_{e_{14}}^{(4,\Delta)} = -\frac{h_A^2(125g_1^2 - 450g_1g_A + 9(135 - 27g_A^2 + 32h_A^2))}{4374m_N} - \frac{5h_A^2}{27\Delta},$$

$$\begin{aligned}
\beta_{e_{15}}^{(4,\Delta)} &= \frac{h_A^2 (1375g_1^2 - 4950g_1g_A - 9(72 + 297g_A^2 - 352h_A^2))}{8748m_N}, \\
\beta_{e_{16}}^{(4,\Delta)} &= \frac{h_A^2 (-125g_1^2 + 450g_1g_A + 9(36 + 27g_A^2 - 32h_A^2))}{729m_N}, \\
\beta_{e_{17}}^{(4,\Delta)} &= \frac{h_A^2 (125g_1^2 - 450g_1g_A + 9(90 - 243g_A^2 + 128h_A^2))}{17496m_N} + \frac{h_A^2}{54\Delta}, \\
\beta_{e_{18}}^{(4,\Delta)} &= \frac{1}{486}h_A(5(5g_1 - 9g_A)(7b_4 + 8b_5) + 288h_Ac_4) \\
&\quad - \frac{h_A^2 (-648 + 125g_1^2 + 150g_1g_A - 1971g_A^2 + 384h_A^2)}{2916m_N} + \frac{4g_A^2h_A^2}{27\Delta}, \\
2\beta_{e_{19}}^{(4,\Delta)} - \beta_{e_{22}}^{(4,\Delta)} - \beta_{e_{36}}^{(4,\Delta)} &= 2h_A^2(-2c_1 + c_3) \\
&\quad + \frac{h_A^2 (2025 + 20(-35g_1^2 + 90g_1g_A + 81g_A^2) - 1872h_A^2)}{2916m_N} \\
&\quad + \frac{(33 - 25g_1^2 + 50g_1g_A - 81g_A^2)h_A^2}{162\Delta}, \\
\beta_{e_{20}}^{(4,\Delta)} + \beta_{e_{35}}^{(4,\Delta)} &= h_A^2c_2 + \frac{h_A^2 (5(37g_1^2 - 210g_1g_A - 351g_A^2) + 1152(-1 + h_A^2))}{1944m_N} \\
&\quad + \frac{(25g_1^2 - 50g_1g_A + 81g_A^2)h_A^2}{324\Delta}, \\
2\beta_{e_{21}}^{(4,\Delta)} - \beta_{e_{37}}^{(4,\Delta)} &= \frac{1}{162}h_A(-25g_1(7b_4 + 8b_5) + 9(31g_Ab_4 + 44g_Ab_5 + 4h_Ac_4)) \\
&\quad + \frac{h_A^2 (575g_1^2 + 450g_1g_A - 9(360 + 873g_A^2 - 272h_A^2))}{5832m_N} \\
&\quad + \frac{(24 + 25g_1^2 - 50g_1g_A - 135g_A^2)h_A^2}{324\Delta}, \\
\beta_{e_{22}}^{(4,\Delta)} - 4\beta_{e_{38}}^{(4,\Delta)} &= -4h_A^2c_1 - \frac{h_A^2}{6m_N} + \frac{2h_A^2}{9\Delta}
\end{aligned}$$

The finite pieces at ε^3 are given by

$$\begin{aligned}
\delta\bar{e}_{14,f}^{(4,\Delta)} &= -\frac{h_A^2 (2725g_1^2 - 8730g_1g_A + 81(216 + 141g_A^2 + 16h_A^2))}{839808m_N\pi^2} \\
&\quad - \frac{13h_A^2}{1296\pi^2\Delta}, \\
\delta\bar{e}_{15,f}^{(4,\Delta)} &= \frac{h_A(-25g_1b_4 + 9g_A(13b_4 + 12b_5))}{11664\pi^2} \\
&\quad + \frac{h_A^2 (35725g_1^2 - 116730g_1g_A + 81(64 + 1421g_A^2 + 256h_A^2))}{1679616m_N\pi^2} \\
&\quad + \frac{(1225g_1^2 - 4050g_1g_A + 3969g_A^2)h_A^2}{839808\pi^2\Delta}, \\
\delta\bar{e}_{16,f}^{(4,\Delta)} &= \frac{h_A(25g_1b_4 - 9g_A(13b_4 + 12b_5))}{11664\pi^2} \\
&\quad - \frac{h_A^2 (34325g_1^2 - 116010g_1g_A + 27(864 + 4695g_A^2 + 832h_A^2))}{1679616m_N\pi^2}
\end{aligned}$$

$$\begin{aligned}
& - \frac{(1225g_1^2 - 4050g_1g_A + 3969g_A^2)h_A^2}{839808\pi^2\Delta}, \\
\delta\bar{e}_{17,f}^{(4,\Delta)} &= \frac{h_A^2(2125g_1^2 - 10890g_1g_A + 27(66 + 999g_A^2 + 16h_A^2))}{1679616m_N\pi^2} \\
& + \frac{h_A^2}{5184\pi^2\Delta}, \\
\delta\bar{e}_{18,f}^{(4,\Delta)} &= -\frac{5h_A(-98g_1b_4 + 162g_Ab_4 - 107g_1b_5 + 171g_Ab_5 + 36h_Ac_4)}{11664\pi^2} \\
& - \frac{h_A^2(8075g_1^2 - 5670g_1g_A + 81(315g_A^2 + 64(3 + h_A^2)))}{1679616m_N\pi^2} \\
& - \frac{h_A^2(425g_1^2 - 450g_1g_A + 4617g_A^2 + 3456h_A^2)}{839808\pi^2\Delta}, \\
2\delta\bar{e}_{19,f}^{(4,\Delta)} - \delta\bar{e}_{22,f}^{(4,\Delta)} - \delta\bar{e}_{36,f}^{(4,\Delta)} &= \frac{h_A(25g_1b_4 - 9g_A(13b_4 + 12b_5) + 162h_A(-2c_1 + c_3))}{1296\pi^2} \\
& - \frac{h_A^2(-2484 + 1255g_1^2 - 5070g_1g_A + 1647g_A^2 + 3696h_A^2)}{93312m_N\pi^2} \\
& + \frac{(450 - 65g_1^2 + 930g_1g_A + 567g_A^2)h_A^2}{46656\pi^2\Delta}, \\
\delta\bar{e}_{20,f}^{(4,\Delta)} + \delta\bar{e}_{35,f}^{(4,\Delta)} &= \frac{h_A(-25g_1b_4 + 9(13g_Ab_4 + 12g_Ab_5 + 18h_Ac_2))}{2592\pi^2} \\
& + \frac{h_A^2(1584 + 2195g_1^2 - 8310g_1g_A + 9531g_A^2 + 5712h_A^2)}{186624m_N\pi^2} \\
& + \frac{(65g_1^2 - 930g_1g_A - 567g_A^2)h_A^2}{93312\pi^2\Delta}, \\
2\delta\bar{e}_{21,f}^{(4,\Delta)} - \delta\bar{e}_{37,f}^{(4,\Delta)} &= \frac{h_A(-5g_1(307b_4 + 308b_5) + 9(319g_Ab_4 + 296g_Ab_5 + 232h_Ac_4))}{15552\pi^2} \\
& + \frac{h_A^2(2880 + 355g_1^2 - 870g_1g_A + 3699g_A^2 + 3648h_A^2)}{186624m_N\pi^2} \\
& + \frac{h_A^2(24 - 95g_1^2 + 590g_1g_A - 567g_A^2 + 384h_A^2)}{31104\pi^2\Delta}, \\
\delta\bar{e}_{22,f}^{(4,\Delta)} - 4\delta\bar{e}_{38,f}^{(4,\Delta)} &= -\frac{h_A^2c_1}{4\pi^2} + \frac{7h_A^2}{432\pi^2\Delta}.
\end{aligned}$$

Appendix D: Tables

$O(1/m_N)$	$\Gamma[\text{MeV}]$	$\text{Re } h_A$	$\text{Im } h_A$	
0	$0.079h_A^2$	1.12	$-0.242h_A + 0.288h_A^3$	$0.000h_{Ac2} + 0.079h_{Ac3} - 0.040h_{Ac4}$
1	$0.022h_A^2$	2.14	$-0.137h_A + 0.022h_A^3$	$-0.023h_{Ac2} + 0.022h_{Ac3} - 0.011h_{Ac4}$
2	$0.054h_A^2$	1.36	$-0.174h_A + 0.208h_A^3$	$-0.009h_{Ac2} + 0.054h_{Ac3} - 0.027h_{Ac4}$
3	$0.038h_A^2$	1.62	$-0.162h_A + 0.098h_A^3$	$-0.016h_{Ac2} + 0.038h_{Ac3} - 0.019h_{Ac4}$
4	$0.045h_A^2$	1.49	$-0.166h_A + 0.156h_A^3$	$-0.013h_{Ac2} + 0.045h_{Ac3} - 0.023h_{Ac4}$
5	$0.042h_A^2$	1.54	$-0.164h_A + 0.128h_A^3$	$-0.014h_{Ac2} + 0.042h_{Ac3} - 0.021h_{Ac4}$
6	$0.043h_A^2$	1.52	$-0.165h_A + 0.141h_A^3$	$-0.014h_{Ac2} + 0.043h_{Ac3} - 0.022h_{Ac4}$
7	$0.043h_A^2$	1.52	$-0.165h_A + 0.135h_A^3$	$-0.014h_{Ac2} + 0.043h_{Ac3} - 0.022h_{Ac4}$
Cov	$0.043h_A^2$	1.52	$-0.165h_A + 0.137h_A^3$	$-0.014h_{Ac2} + 0.043h_{Ac3} - 0.022h_{Ac4}$

TABLE I: Convergence in $1/m_N$ of the quantities Γ , $\text{Re } h_A$, and $\text{Im } h_A$, where $\text{Re } h_A$ is matched to the decay width $\Gamma_{\Delta \rightarrow \pi N} = 100 \text{ MeV}$ [52], which is extracted from the complex-valued pole position of the Δ resonances. The column for $\text{Im } h_A$ is divided in the contribution at order ε^3 (left) and ε^4 (right).

	HB-NN		HB- π N		Cov	
ε^2	π N	π N+RS	π N	π N+RS	π N	π N+RS
h_A	1.34(0)	1.34(0)	1.37(0)	1.36(0)	1.40(0)	1.40(0)
c_1	-1.02(3)	-1.01(3)	-0.79(2)	-0.81(2)	-0.86(2)	-0.87(2)
c_2	0.27(5)	0.28(5)	0.80(5)	0.80(5)	0.45(3)	0.45(3)
c_3	-0.99(4)	-0.99(4)	-0.99(3)	-1.01(3)	-0.71(3)	-0.72(3)
c_4	0.51(3)	0.52(3)	1.09(3)	1.08(3)	0.87(2)	0.87(2)
$\chi^2_{\pi N}/\text{dof}$	0.65	0.64	0.61	0.61	0.55	0.56
$\bar{\chi}^2_{\pi N}/\text{dof}$	14.1	14.0	3.7	3.7	2.9	3.0
ε^3	π N	π N+RS	π N	π N+RS	π N	π N+RS
h_A	1.46(1)	1.46(1)	1.45(1)	1.46(1)	1.46(1)	1.46(1)
c_1	-1.81(1)	-1.81(1)	-1.98(1)	-1.97(1)	-1.51(1)	-1.50(1)
c_2	1.69(9)	1.67(9)	1.20(6)	1.17(6)	0.67(3)	0.69(3)
c_3	-3.91(9)	-3.89(9)	-3.74(7)	-3.70(7)	-2.67(7)	-2.63(6)
c_4	1.71(5)	1.70(5)	1.50(4)	1.48(4)	1.26(5)	1.22(5)
d_{1+2}	0.23(6)	0.21(5)	0.59(6)	0.57(6)	0.57(5)	0.55(4)
d_3	-1.55(6)	-1.53(6)	-1.40(5)	-1.39(6)	-1.78(3)	-1.78(3)
d_5	0.82(3)	0.82(3)	0.53(3)	0.54(3)	0.70(3)	0.72(3)
d_{14-15}	-0.87(13)	-0.83(13)	-1.14(12)	-1.11(12)	-0.75(8)	-0.72(7)
g_1	-2.74(15)	-2.74(14)	-2.82(13)	-2.74(14)	-0.67(29)	-0.38(29)
$\chi^2_{\pi N}/\text{dof}$	1.16	1.15	1.26	1.26	1.20	1.19
$\bar{\chi}^2_{\pi N}/\text{dof}$	2.1	2.1	2.0	2.0	1.95	1.95
ε^4	π N	π N+RS	π N	π N+RS	π N	π N+RS
h_A	1.38(1)	1.37(1)	1.39(1)	1.38(1)	1.42(1)	1.40(1)
c_1	-1.45(5)	-1.39(3)	-1.29(5)	-1.30(4)	-1.50(4)	-1.32(3)
c_2	0.39(13)	0.51(10)	1.66(13)	1.61(10)	0.52(7)	0.86(5)
c_3	-2.14(7)	-2.12(6)	-2.37(5)	-2.34(5)	-1.98(7)	-1.98(6)
c_4	2.47(10)	2.29(5)	2.56(10)	2.43(6)	2.31(7)	2.28(4)
d_{1+2}	2.12(7)	2.07(6)	1.98(7)	1.94(6)	1.67(5)	1.74(5)
d_3	-2.61(6)	-2.62(5)	-1.97(4)	-1.96(4)	-3.13(4)	-3.07(4)
d_5	0.36(3)	0.39(3)	0.13(3)	0.15(3)	0.90(3)	0.81(3)
d_{14-15}	-3.38(13)	-3.53(12)	-2.75(11)	-2.76(10)	-2.94(10)	-3.16(9)
e_{14}	2.10(15)	2.30(13)	1.76(14)	1.92(12)	1.76(12)	1.61(10)
e_{15}	-3.41(45)	-4.13(26)	-1.92(50)	-2.61(31)	-2.27(19)	-2.50(17)
e_{16}	2.55(48)	2.70(28)	-1.23(56)	-0.65(37)	1.40(18)	0.88(9)
e_{17}	-0.63(23)	-0.53(20)	-0.59(21)	-0.71(19)	-0.96(15)	-0.87(14)
e_{18}	-0.82(43)	-0.11(15)	-0.36(42)	0.30(21)	0.82(18)	1.03(10)
g_1	-2.41(20)	-2.52(19)	-2.55(19)	-2.60(17)	-2.35(21)	-2.32(20)
b_4	-1.33(34)	-1.45(29)	-1.44(31)	-1.56(28)	1.07(43)	1.55(28)
b_5	-1.24(37)	-1.39(32)	-1.31(35)	-1.39(32)	0.81(65)	1.35(32)
$\chi^2_{\pi N}/\text{dof}$	1.73	1.73	1.80	1.80	1.78	1.80
$\bar{\chi}^2_{\pi N}/\text{dof}$	1.91	1.92	1.92	1.92	1.91	1.93

TABLE II: K -matrix approach: LECs extracted from fits at order ε^2 , ε^3 , and ε^4 with $T_\pi < 125$ MeV. The labels π N and π N+RS denote fits without and with additional constraints χ^2_{RS} , see Eqs. (44) and (48), respectively. The labels HB-NN, HB- π N, and Cov (covariant) denote the different counting schemes of $1/m_N$ contributions, see section III.

	HB-NN		HB- π N		Cov	
ε^2	π N	π N+RS	π N	π N+RS	π N	π N+RS
h_A	1.26(0)	1.26(0)	1.29(0)	1.29(0)	1.30(0)	1.30(0)
c_1	-0.88(2)	-0.89(2)	-0.68(2)	-0.69(2)	-0.80(1)	-0.80(1)
c_2	0.52(3)	0.52(3)	0.99(4)	0.98(4)	0.59(2)	0.59(2)
c_3	-1.16(3)	-1.16(3)	-1.13(2)	-1.13(2)	-0.90(2)	-0.90(2)
c_4	0.74(3)	0.73(3)	1.21(3)	1.20(3)	1.02(2)	1.01(2)
$\chi^2_{\pi N}/\text{dof}$	0.66	0.66	0.58	0.58	0.50	0.51
$\bar{\chi}^2_{\pi N}/\text{dof}$	35.6	35.8	7.1	7.1	4.9	4.9
ε^3	π N	π N+RS	π N	π N+RS	π N	π N+RS
h_A	1.37(0)	1.37(0)	1.37(0)	1.37(0)	1.42(0)	1.43(0)
c_1	-1.82(1)	-1.82(1)	-2.01(1)	-2.01(1)	-1.51(1)	-1.50(1)
c_2	1.66(5)	1.66(5)	1.04(3)	1.03(3)	0.51(2)	0.51(2)
c_3	-4.00(5)	-3.99(5)	-3.71(4)	-3.70(4)	-2.44(2)	-2.43(2)
c_4	1.83(2)	1.83(2)	1.48(2)	1.48(2)	1.14(2)	1.13(2)
d_{1+2}	0.10(3)	0.09(3)	0.47(3)	0.46(3)	0.39(2)	0.37(2)
d_3	-1.22(4)	-1.21(4)	-1.02(4)	-1.01(4)	-1.57(2)	-1.56(2)
d_5	0.68(2)	0.68(2)	0.35(2)	0.35(2)	0.66(1)	0.66(1)
d_{14-15}	-0.69(7)	-0.67(7)	-0.70(7)	-0.67(7)	-0.46(4)	-0.44(4)
g_1	-3.05(10)	-3.04(10)	-2.90(9)	-2.85(9)	-0.42(7)	-0.41(7)
$\chi^2_{\pi N}/\text{dof}$	0.97	0.97	1.04	1.02	0.98	0.98
$\bar{\chi}^2_{\pi N}/\text{dof}$	2.5	2.5	2.4	2.4	1.87	1.87
ε^4	π N	π N+RS	π N	π N+RS	π N	π N+RS
h_A	1.47(0)	1.47(0)	1.63(0)	1.63(0)	1.45(0)	1.45(0)
c_1	-1.55(2)	-1.48(2)	-1.31(2)	-1.14(2)	-1.63(2)	-1.52(2)
c_2	-0.81(6)	-0.66(5)	-0.66(8)	-0.09(6)	-0.13(3)	0.02(2)
c_3	-1.00(4)	-0.99(4)	0.85(3)	0.95(2)	-1.30(3)	-1.21(3)
c_4	1.76(5)	1.84(4)	0.90(6)	1.29(4)	1.78(3)	1.82(3)
d_{1+2}	1.32(4)	1.39(3)	-1.15(6)	-0.82(5)	1.43(3)	1.38(2)
d_3	-1.89(3)	-1.93(3)	0.09(3)	-0.06(3)	-3.10(3)	-3.00(2)
d_5	0.34(2)	0.32(1)	0.62(2)	0.52(1)	1.01(1)	0.98(1)
d_{14-15}	-2.19(6)	-2.32(5)	2.13(9)	1.73(7)	-2.90(5)	-2.86(5)
e_{14}	2.25(9)	2.13(8)	1.01(10)	0.39(8)	1.56(6)	1.44(5)
e_{15}	-4.90(18)	-4.63(16)	-0.47(26)	1.16(21)	-3.32(9)	-3.18(8)
e_{16}	4.64(15)	4.21(13)	-0.24(27)	-2.24(20)	2.85(8)	2.43(6)
e_{17}	-1.00(8)	-0.97(8)	-0.82(7)	-0.66(7)	-0.07(5)	-0.05(5)
e_{18}	0.99(15)	0.79(10)	0.99(15)	0.40(12)	1.33(6)	1.28(5)
g_1	-2.63(18)	-2.73(17)	-2.01(21)	-3.08(12)	-2.13(13)	-2.27(12)
b_4	1.32(28)	1.36(23)	2.88(13)	3.09(12)	3.01(12)	3.26(11)
b_5	-0.85(51)	-1.14(36)	2.37(17)	2.48(16)	2.37(16)	2.45(16)
$\chi^2_{\pi N}/\text{dof}$	1.48	1.48	1.59	1.59	1.62	1.62
$\bar{\chi}^2_{\pi N}/\text{dof}$	1.80	1.80	1.84	1.86	1.87	1.88

TABLE III: Complex mass approach: LECs extracted from fits at order ε^2 , ε^3 , and ε^4 with $T_\pi < 200$ MeV. The labels π N and π N+RS denote fits without and with additional constraints χ^2_{RS} , see Eqs. (44) and (48), respectively. The labels HB-NN, HB- π N, and Cov (covariant) denote the different counting schemes of $1/m_N$ contributions, see section III.

K	h_A	c_1	c_2	c_3	c_4	d_{1+2}	d_3	d_5	$d_{14-15}e_{14}$	e_{15}	e_{16}	e_{17}	e_{18}	g_1	b_4	b_5
h_A	1	-14	-29	45	-44	-89	71	39	93	33	15	-17	2	-12	-21	-18
c_1	0	12	77	20	21	17	-5	-20	-10	-5	-1	-65	-10	0	0	14
c_2	-2	26	94	-44	9	19	-8	-20	-20	9	13	-76	-5	2	43	-8
c_3	2	5	-28	42	6	-25	23	8	36	-5	-21	17	-7	-8	-67	23
c_4	-2	4	4	2	24	68	-30	-59	-43	-27	-9	7	-60	1	-20	-1
d_{1+2}	-5	4	12	-10	21	40	-79	-44	-86	-35	-14	17	-20	7	-2	34
d_3	3	-1	-4	8	-8	-27	30	-19	74	23	15	-23	-14	8	-2	-40
d_5	1	-2	-5	1	-8	-7	-3	7	33	22	-1	7	48	-22	5	-5
d_{14-15}	10	-4	-24	29	-26	-68	50	11	154	30	12	-17	-7	-2	-2	-35
e_{14}	4	-2	11	-4	-17	-28	16	8	48	163	-67	10	13	-13	-1	-20
e_{15}	3	-1	34	-37	-11	-23	22	0	41	-227	700	-58	-2	3	11	-12
e_{16}	-4	-64	-211	30	9	31	-36	5	-59	38	-439	805	2	5	-14	13
e_{17}	0	-7	-9	-9	-57	-25	-15	25	-17	33	-9	9	392	-66	4	8
e_{18}	-1	0	3	-7	1	6	6	-9	-4	-23	13	20	-191	216	2	-2
g_1	-3	0	77	-81	-18	-2	-2	3	-5	-2	54	-73	14	6	344	-3
b_4	-7	14	-23	44	-1	62	-63	1	-128	-74	-90	111	48	-8	-18	845
b_5	-5	10	-15	30	40	44	-34	-4	-70	-49	-65	74	43	-65	-2	-62
C	h_A	c_1	c_2	c_3	c_4	d_{1+2}	d_3	d_5	$d_{14-15}e_{14}$	e_{15}	e_{16}	e_{17}	e_{18}	g_1	b_4	b_5
h_A	0	-39	16	-58	0	-27	31	0	34	40	-8	6	6	-25	45	-23
c_1	0	5	65	33	30	40	-31	-22	-26	-35	22	-63	-8	-10	-15	8
c_2	0	8	30	-50	-14	-1	1	-6	-2	-9	28	-70	-6	9	48	10
c_3	0	3	-12	18	58	50	-35	-25	-28	-27	-11	15	-1	-29	-76	-6
c_4	0	4	-4	13	27	76	-41	-62	-52	-24	3	-6	0	-75	-51	-34
d_{1+2}	0	4	0	8	15	15	-82	-46	-77	-38	22	-27	-4	-48	-66	-7
d_3	0	-2	0	-5	-7	-10	10	-10	63	30	-21	23	5	18	57	-7
d_5	0	-1	0	-2	-5	-3	-1	2	42	21	-8	16	-3	51	24	19
d_{14-15}	0	-4	-1	-8	-17	-19	13	4	41	38	-27	26	-4	30	57	-1
e_{14}	1	-7	-4	-10	-11	-13	8	3	21	75	-87	64	0	8	21	-9
e_{15}	0	9	28	-9	2	16	-12	-2	-32	-138	339	-82	2	5	-5	7
e_{16}	0	-22	-60	9	-5	-16	11	4	25	85	-232	239	2	-3	-1	-8
e_{17}	0	-1	-3	0	0	-1	1	0	-2	0	3	3	64	-53	0	-1
e_{18}	-1	-3	8	-19	-61	-29	9	12	30	10	13	-8	-66	240	20	11
g_1	1	-6	47	-58	-48	-46	33	7	65	32	-18	-2	0	57	323	15
b_4	-1	5	16	-7	-49	-8	-6	8	-2	-20	37	-36	-2	49	74	760
b_5	0	12	0	25	34	-33	39	-1	99	-45	13	-5	-13	72	182	-834

TABLE IV: The upper and lower table correspond to the K -matrix (K) and complex mass approach (C), respectively. Correlation (upper triangle) and covariance (lower triangle) matrices for the fits denoted by $\pi N + RS$ (K) and πN (C) at order ε^4 in the HB-NN counting. The units of the correlation and covariance values are 10^{-2} and 10^{-4} , respectively.

K	h_A	c_1	c_2	c_3	c_4	d_{1+2}	d_3	d_5	$d_{14-15}e_{14}$	e_{15}	e_{16}	e_{17}	e_{18}	g_1	b_4	b_5	
h_A	1	-8	0	42	-31	-89	74	59	95	24	37	-32	4	-14	-19	-24	-16
c_1	0	15	86	19	26	18	-4	-22	-4	-10	15	-70	-10	-10	-2	11	8
c_2	0	32	92	-10	29	13	7	-23	-1	-2	36	-86	-7	-12	-32	-8	-6
c_3	2	4	-5	25	6	-31	32	16	46	-8	-10	6	-9	-10	-27	34	25
c_4	-2	6	16	2	35	64	-24	-63	-31	-28	4	-12	-36	-42	-29	-4	19
d_{1+2}	-5	4	7	-9	23	36	-74	-72	-85	-31	-25	17	-18	-8	6	24	18
d_3	2	-1	2	6	-5	-16	13	8	75	14	33	-29	-15	12	-27	-30	-16
d_5	1	-2	-6	2	-10	-12	1	7	53	31	5	3	38	-3	11	-6	-9
d_{14-15}	8	-2	-1	24	-19	-52	28	15	107	22	31	-26	-8	-1	-18	-27	-14
e_{14}	2	-5	-2	-5	-20	-22	6	10	28	150	-62	20	20	-6	10	-16	-11
e_{15}	10	18	107	-15	7	-47	38	4	100	-241	990	-72	-5	-7	-29	-13	-9
e_{16}	-10	-100	-307	11	-27	38	-40	3	-101	93	-843	1371	2	16	27	11	7
e_{17}	1	-8	-12	-8	-41	-20	-11	20	-16	46	-29	16	367	-57	5	7	6
e_{18}	-3	-9	-25	-10	-53	-11	9	-2	-2	-17	-44	128	-234	453	6	0	-8
g_1	-3	-1	-50	-23	-28	6	-16	5	-30	20	-151	164	17	19	273	-3	-1
b_4	-6	12	-20	46	-6	40	-30	-5	-76	-55	-114	109	39	1	-16	761	-3
b_5	-4	10	-18	39	36	34	-18	-8	-45	-43	-91	87	37	-53	-7	-30	1009
C	h_A	c_1	c_2	c_3	c_4	d_{1+2}	d_3	d_5	$d_{14-15}e_{14}$	e_{15}	e_{16}	e_{17}	e_{18}	g_1	b_4	b_5	
h_A	0	-9	-8	15	4	-48	61	21	65	13	22	-20	6	-43	8	-37	-21
c_1	0	6	83	39	52	59	-53	-47	-48	-44	42	-71	10	-17	-50	23	15
c_2	0	16	60	45	70	80	-70	-66	-70	-65	68	-90	13	-13	-86	25	12
c_3	0	3	9	7	81	49	-28	-54	-26	-41	35	-44	23	-60	-65	22	24
c_4	0	8	33	13	37	77	-54	-79	-59	-61	54	-65	23	-62	-80	20	21
d_{1+2}	-1	8	36	7	27	33	-92	-80	-93	-67	48	-61	17	-15	-83	40	23
d_3	0	-4	-18	-2	-11	-18	11	52	89	54	-34	47	-8	-7	68	-43	-20
d_5	0	-2	-9	-2	-8	-8	3	3	72	62	-49	57	-23	37	71	-24	-17
d_{14-15}	1	-10	-47	-6	-31	-46	26	11	75	60	-37	47	-9	-4	70	-39	-18
e_{14}	0	-11	-52	-11	-38	-40	19	11	54	108	-90	78	-16	19	68	-27	-17
e_{15}	1	28	139	25	87	74	-30	-23	-85	-248	701	-91	16	-21	-69	15	9
e_{16}	-1	-48	-189	-32	-107	-96	43	27	111	220	-653	740	-17	24	79	-19	-10
e_{17}	0	2	7	4	10	7	-2	-3	-6	-12	30	-33	52	-64	-17	5	3
e_{18}	-1	-6	-16	-24	-58	-14	-4	10	-5	30	-87	99	-71	237	21	2	0
g_1	0	-26	-138	-36	-100	-99	47	26	126	147	-380	446	-25	67	430	-27	-16
b_4	-1	7	26	8	16	31	-19	-6	-45	-37	54	-69	5	4	-76	178	-12
b_5	-1	6	16	11	22	22	-12	-5	-27	-31	40	-48	4	0	-57	-26	293

TABLE V: The upper and lower table correspond to the K -matrix (K) and complex mass approach (C), respectively. Correlation (upper triangle) and covariance (lower triangle) matrices for the fits denoted by $\pi N + RS$ (K) and πN (C) at order ε^4 in the HB- πN counting. The units of the correlation and covariance values are 10^{-2} and 10^{-4} , respectively.

K	h_A	c_1	c_2	c_3	c_4	d_{1+2}	d_3	d_5	$d_{14-15}e_{14}$	e_{15}	e_{16}	e_{17}	e_{18}	g_1	b_4	b_5	
h_A	1	-31	-54	35	-27	-69	54	34	86	47	20	-6	-5	-7	-32	-40	-17
c_1	-1	7	78	26	12	3	34	-41	-10	-22	-38	-50	2	-7	15	28	9
c_2	-2	10	25	-35	12	35	-8	-42	-42	2	-41	-39	-4	4	38	4	-1
c_3	2	5	-12	45	14	-34	65	-8	35	-26	-2	-27	12	-22	-65	45	11
c_4	-1	1	3	4	19	49	-14	-35	-47	-23	-8	-9	-50	0	-39	-7	25
d_{1+2}	-3	0	8	-11	10	22	-54	-58	-81	-20	-15	10	-17	15	-12	8	-19
d_3	2	3	-2	17	-2	-10	15	-33	58	6	-3	-40	-6	4	-34	6	-11
d_5	1	-3	-5	-1	-4	-7	-3	7	38	19	18	25	27	-24	22	-11	29
d_{14-15}	6	-2	-18	21	-18	-33	19	8	76	31	16	-5	0	-4	-2	-20	-16
e_{14}	5	-7	1	-20	-11	-11	3	6	31	130	-55	35	2	-3	-4	-48	-17
e_{15}	3	-17	-34	-3	-6	-12	-2	8	24	-105	287	-40	-4	6	-1	-5	-3
e_{16}	0	-12	-18	-17	-4	4	-14	6	-4	37	-63	87	-7	14	18	-19	-2
e_{17}	-1	1	-3	11	-32	-12	-4	10	-1	3	-10	-9	215	-71	3	36	17
e_{18}	-1	-2	2	-15	0	7	2	-6	-4	-4	11	14	-107	105	5	-26	-14
g_1	-5	7	37	-85	-33	-11	-26	11	-3	-8	-5	32	9	10	377	-12	0
b_4	-17	38	10	155	-15	20	12	-14	-89	-279	-43	-90	268	-136	-117	2593	-11
b_5	-5	8	-1	23	35	-29	-13	25	-46	-63	-16	-7	80	-46	0	-184	1061
C	h_A	c_1	c_2	c_3	c_4	d_{1+2}	d_3	d_5	$d_{14-15}e_{14}$	e_{15}	e_{16}	e_{17}	e_{18}	g_1	b_4	b_5	
h_A	0	7	-7	12	-18	-43	24	17	57	37	-22	10	-12	0	14	-9	-2
c_1	0	4	85	35	11	-19	56	-60	14	-34	14	-78	3	-14	4	20	11
c_2	0	5	8	-11	14	21	15	-57	-14	-12	5	-64	-12	-7	19	7	1
c_3	0	2	-1	12	30	-56	76	-19	12	-48	19	-49	39	-26	-68	30	7
c_4	0	1	1	3	10	30	-14	-11	-66	-21	0	-24	-1	-65	-46	-5	0
d_{1+2}	0	-1	2	-5	2	7	-76	-23	-68	8	-5	17	-14	-12	9	-21	-41
d_3	0	3	1	7	-1	-5	7	-41	45	-35	18	-55	25	5	-30	29	11
d_5	0	-2	-2	-1	0	-1	-1	2	16	34	-16	52	-8	9	5	-12	25
d_{14-15}	0	1	-2	2	-11	-9	6	1	27	13	-2	6	3	22	42	22	16
e_{14}	0	-4	-2	-9	-4	1	-5	3	4	33	-87	72	-28	18	26	-26	-14
e_{15}	0	2	1	6	0	-1	4	-2	-1	-42	73	-64	23	-2	-14	18	10
e_{16}	0	-12	-14	-13	-6	3	-11	5	2	31	-41	57	-25	18	31	-30	-11
e_{17}	0	0	-2	6	0	-2	3	-1	1	-8	9	-9	23	-48	-37	14	17
e_{18}	0	-2	-1	-5	-12	-2	1	1	6	6	-1	8	-13	33	13	-12	-6
g_1	0	1	7	-29	-19	3	-10	1	27	19	-15	29	-22	9	159	-5	18
b_4	0	5	3	13	-2	-7	10	-2	14	-18	19	-28	8	-8	-7	152	-22
b_5	0	4	1	4	0	-17	5	5	14	-13	14	-14	13	-6	38	-44	266

TABLE VI: The upper and lower table correspond to the K -matrix (K) and complex mass approach (C), respectively. Correlation (upper triangle) and covariance (lower triangle) matrices for the fits denoted by πN +RS (K) and πN (C) at order ε^4 in the covariant counting. The units of the correlation and covariance values are 10^{-2} and 10^{-4} , respectively.

ε^4	K -matrix approach		Complex mass approach		
	πN	$\pi N+RS$	πN	$\pi N+RS$	RS
$d_{00}^+[M_\pi^{-1}]$	-1.15(7)(9)	-1.15(4)(9)	-0.71(3)(5)	-1.07(3)(9)	-1.36(3)
$d_{10}^+[M_\pi^{-3}]$	1.14(11)(13)	1.10(6)(13)	0.50(4)(5)	0.84(4)(10)	1.16(2)
$d_{01}^+[M_\pi^{-3}]$	1.24(3)(1)	1.19(2)(0)	1.07(1)(0)	1.22(1)(1)	1.16(2)
$d_{20}^+[M_\pi^{-5}]$	0.04(5)(6)	0.07(3)(5)	0.30(2)(1)	0.29(1)(2)	0.196(3)
$d_{11}^+[M_\pi^{-5}]$	0.10(2)(2)	0.14(1)(1)	0.21(1)(0)	0.22(1)(1)	0.185(3)
$d_{02}^+[M_\pi^{-5}]$	0.046(4)(3)	0.052(3)(3)	0.052(2)(3)	0.045(2)(3)	0.0336(6)
$b_{00}^+[M_\pi^{-3}]$	-1.88(10)(24)	-2.24(1)(16)	-1.77(8)(16)	-2.95(6)(9)	-3.45(7)
$d_{00}^-[M_\pi^{-2}]$	1.03(1)(9)	1.06(1)(9)	0.95(1)(9)	1.03(1)(9)	1.41(1)
$d_{10}^-[M_\pi^{-4}]$	0.21(2)(10)	0.17(2)(9)	0.27(1)(10)	0.17(1)(9)	-0.159(4)
$d_{01}^-[M_\pi^{-4}]$	-0.155(3)(3)	-0.158(3)(3)	-0.139(3)(4)	-0.189(2)(6)	-0.141(5)
$b_{00}^-[M_\pi^{-2}]$	11.31(43)(13)	10.51(11)(5)	9.08(20)(16)	10.12(11)(9)	10.49(11)
$b_{10}^-[M_\pi^{-4}]$	-0.50(30)(22)	-0.01(11)(12)	0.82(11)(2)	0.75(7)(3)	1.00(3)
$b_{01}^-[M_\pi^{-4}]$	0.24(8)(3)	0.22(7)(2)	0.36(3)(5)	0.32(3)(5)	0.21(2)
<hr/>					
$d_{00}^+[M_\pi^{-1}]$	-1.35(8)(20)	-1.28(5)(18)	-0.58(5)(6)	-0.96(4)(14)	-1.36(3)
$d_{10}^+[M_\pi^{-3}]$	1.47(13)(27)	1.33(8)(24)	0.42(7)(8)	0.97(5)(19)	1.16(2)
$d_{01}^+[M_\pi^{-3}]$	1.23(3)(3)	1.19(2)(2)	0.88(2)(4)	1.00(1)(2)	1.16(2)
$d_{20}^+[M_\pi^{-5}]$	-0.10(6)(9)	-0.03(4)(7)	0.14(3)(5)	-0.044(20)(86)	0.196(3)
$d_{11}^+[M_\pi^{-5}]$	0.11(3)(2)	0.15(2)(1)	0.18(1)(1)	0.10(1)(3)	0.185(3)
$d_{02}^+[M_\pi^{-5}]$	0.051(4)(3)	0.056(3)(3)	0.037(2)(3)	0.024(2)(6)	0.0336(6)
$b_{00}^+[M_\pi^{-3}]$	-0.70(10)(53)	-0.91(9)(49)	0.37(6)(77)	0.36(6)(76)	-3.45(7)
$d_{00}^-[M_\pi^{-2}]$	0.93(1)(11)	0.94(1)(10)	0.85(1)(11)	0.89(1)(10)	1.41(1)
$d_{10}^-[M_\pi^{-4}]$	0.51(2)(15)	0.49(2)(15)	0.60(1)(17)	0.50(1)(15)	-0.159(4)
$d_{01}^-[M_\pi^{-4}]$	-0.059(3)(24)	-0.063(3)(23)	0.016(2)(42)	0.01(2)(40)	-0.141(5)
$b_{00}^-[M_\pi^{-2}]$	11.28(42)(34)	10.59(20)(20)	7.51(17)(33)	8.23(14)(19)	10.49(11)
$b_{10}^-[M_\pi^{-4}]$	0.17(30)(9)	0.63(15)(1)	1.66(11)(16)	1.33(9)(9)	1.00(3)
$b_{01}^-[M_\pi^{-4}]$	0.28(7)(4)	0.32(6)(5)	0.28(2)(4)	0.23(2)(3)	0.21(2)
<hr/>					
$d_{00}^+[M_\pi^{-1}]$	-1.06(5)(1)	-1.23(2)(2)	-0.84(2)(5)	-0.98(2)(2)	-1.36(3)
$d_{10}^+[M_\pi^{-3}]$	0.99(6)(2)	1.16(3)(4)	0.61(2)(5)	0.76(2)(2)	1.16(2)
$d_{01}^+[M_\pi^{-3}]$	1.22(1)(0)	1.20(1)(0)	1.21(1)(0)	1.21(1)(0)	1.16(2)
$d_{20}^+[M_\pi^{-5}]$	0.12(2)(2)	0.10(1)(2)	0.30(1)(1)	0.27(0)(0)	0.196(3)
$d_{11}^+[M_\pi^{-5}]$	0.13(1)(0)	0.15(1)(0)	0.24(0)(1)	0.23(0)(1)	0.185(3)
$d_{02}^+[M_\pi^{-5}]$	0.048(3)(3)	0.044(2)(2)	0.042(1)(2)	0.039(1)(2)	0.0336(6)
$b_{00}^+[M_\pi^{-3}]$	-2.68(7)(13)	-2.84(6)(9)	-4.41(4)(13)	-4.36(4)(13)	-3.45(7)
$d_{00}^-[M_\pi^{-2}]$	1.39(1)(3)	1.38(1)(3)	1.47(0)(2)	1.46(0)(2)	1.41(1)
$d_{10}^-[M_\pi^{-4}]$	-0.05(0)(3)	-0.07(0)(3)	-0.12(0)(2)	-0.12(0)(2)	-0.159(4)
$d_{01}^-[M_\pi^{-4}]$	-0.117(2)(5)	-0.120(2)(4)	-0.178(2)(4)	-0.173(2)(3)	-0.141(5)
$b_{00}^-[M_\pi^{-2}]$	11.17(27)(11)	10.79(11)(5)	10.36(12)(5)	10.45(8)(5)	10.49(11)
$b_{10}^-[M_\pi^{-4}]$	0.64(13)(8)	0.87(7)(3)	1.29(4)(2)	1.27(3)(1)	1.00(3)
$b_{01}^-[M_\pi^{-4}]$	0.35(5)(2)	0.32(5)(2)	0.01(2)(4)	0.00(2)(4)	0.21(2)

TABLE VII: Comparison of the subthreshold parameters determined at order ε^4 with the RS values [38] in both unitarization approaches. The LECs from Tables II and III are taken as input. The results in the HB-NN, HB- πN , and covariant counting are given in the upper, middle, and lower table, respectively. The first and second bracket denote the statistical and theoretical uncertainty, respectively.

	K -matrix approach		Complex mass approach		
ε^4	πN	$\pi N+RS$	πN	$\pi N+RS$	RS
$a_{0+}^+[M_\pi^{-1}10^{-3}]$	3.8(6)(6)	2.8(5)(8)	7.4(4)(4)	4.5(4)(8)	-0.9(1.4)
$a_{0+}^-[M_\pi^{-1}10^{-3}]$	86.1(2)(3)	86.1(2)(3)	85.1(1)(3)	85.0(1)(3)	85.4(9)
$a_{1+}^+[M_\pi^{-3}10^{-3}]$	128.7(3)(3)	129.1(3)(3)	123.1(3)(2)	135.1(3)(5)	131.2(1.7)
$a_{1+}^-[M_\pi^{-3}10^{-3}]$	-79.4(4)(3)	-78.9(2)(2)	-77.1(2)(2)	-82.0(2)(3)	-80.3(1.1)
$a_{1-}^+[M_\pi^{-3}10^{-3}]$	-45.9(4)(3)	-47.0(3)(3)	-50.9(3)(4)	-47.5(2)(3)	-50.9(1.9)
$a_{1-}^-[M_\pi^{-3}10^{-3}]$	-7.0(8)(9)	-8.7(3)(5)	-10.9(4)(4)	-9.3(3)(4)	-9.9(1.2)
$b_{0+}^+[M_\pi^{-3}10^{-3}]$	-59.7(2.2)(2.0)	-57.2(1.6)(2.5)	-64.7(1.2)(1.6)	-61.9(1.1)(2.0)	-45.0(1.0)
$b_{0+}^-[M_\pi^{-3}10^{-3}]$	15.3(3)(1.2)	15.1(3)(1.2)	16.6(1)(1.1)	17.0(1)(1.1)	4.9(8)
$a_{0+}^+[M_\pi^{-1}10^{-3}]$	3.4(6)(1.0)	3.4(6)(1.0)	6.1(4)(9)	4.3(4)(1.2)	-0.9(1.4)
$a_{0+}^-[M_\pi^{-1}10^{-3}]$	85.8(2)(1.0)	85.8(2)(1.0)	84.6(1)(9)	84.5(1)(9)	85.4(9)
$a_{1+}^+[M_\pi^{-3}10^{-3}]$	128.5(3)(4)	128.4(3)(5)	115.4(3)(3.5)	117.0(3)(3.2)	131.2(1.7)
$a_{1+}^-[M_\pi^{-3}10^{-3}]$	-79.3(3)(2)	-79.0(2)(2)	-73.5(2)(1.3)	-74.7(2)(1.1)	-80.3(1.1)
$a_{1-}^+[M_\pi^{-3}10^{-3}]$	-45.9(4)(6)	-46.7(3)(4)	-55.9(3)(1.3)	-55.0(2)(1.2)	-50.9(1.9)
$a_{1-}^-[M_\pi^{-3}10^{-3}]$	-6.7(7)(1.0)	-8.0(4)(8)	-12.7(4)(2)	-11.4(3)(4)	-9.9(1.2)
$b_{0+}^+[M_\pi^{-3}10^{-3}]$	-59.6(2.2)(3.8)	-60.1(1.9)(3.6)	-62.5(1.1)(4.0)	-57.1(1.1)(5.0)	-45.0(1.0)
$b_{0+}^-[M_\pi^{-3}10^{-3}]$	15.9(3)(4)	15.9(3)(4)	15.1(1)(4)	15.2(1)(4)	4.9(8)
$a_{0+}^+[M_\pi^{-1}10^{-3}]$	3.5(6)(4)	0.9(4)(5)	5.4(4)(4)	3.5(3)(4)	-0.9(1.4)
$a_{0+}^-[M_\pi^{-1}10^{-3}]$	88.8(2)(7)	88.2(2)(7)	89.4(1)(7)	89.0(1)(7)	85.4(9)
$a_{1+}^+[M_\pi^{-3}10^{-3}]$	131.1(3)(6)	131.4(3)(6)	140.2(3)(9)	140.2(2)(10)	131.2(1.7)
$a_{1+}^-[M_\pi^{-3}10^{-3}]$	-80.0(3)(5)	-79.9(2)(5)	-83.6(2)(5)	-83.6(2)(5)	-80.3(1.1)
$a_{1-}^+[M_\pi^{-3}10^{-3}]$	-48.6(4)(7)	-49.1(3)(6)	-51.9(2)(6)	-51.7(2)(6)	-50.9(1.9)
$a_{1-}^-[M_\pi^{-3}10^{-3}]$	-7.5(7)(3)	-8.4(3)(2)	-11.2(3)(3)	-10.7(3)(2)	-9.9(1.2)
$b_{0+}^+[M_\pi^{-3}10^{-3}]$	-58.5(2.0)(7)	-50.0(1.2)(2.0)	-66.1(1.0)(1.1)	-60.0(8)(8)	-45.0(1.0)
$b_{0+}^-[M_\pi^{-3}10^{-3}]$	4.6(4)(1.6)	6.1(3)(1.3)	3.7(2)(2.0)	4.5(2)(1.8)	4.9(8)

TABLE VIII: Comparison of the threshold parameters determined at order ε^4 with the RS values [38] in both unitarization approaches. The LECs from Tables II and III are taken as input. The results in the HB-NN, HB- πN , and covariant counting are given in the upper, middle, and lower table, respectively. The first and second bracket denote the statistical and theoretical uncertainty, respectively.

Appendix E: Figures

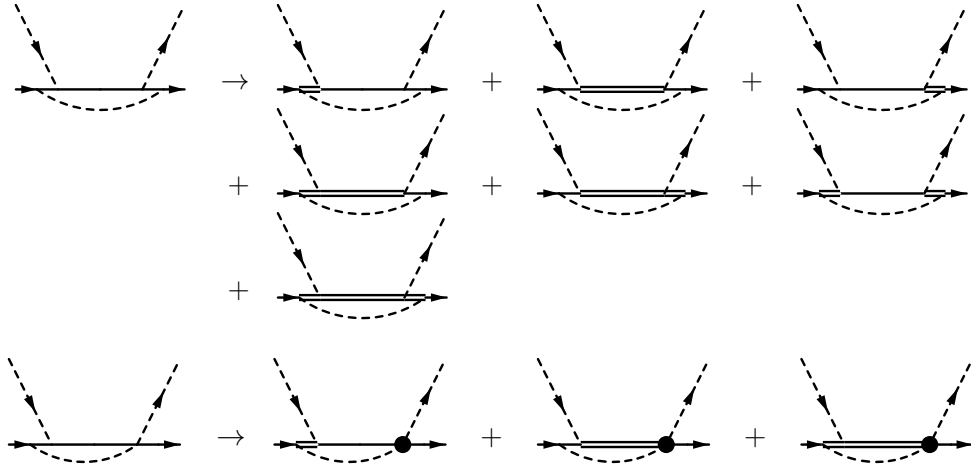


FIG. 1: Examples of transitions from Δ -less to Δ -ful graphs at leading and next-to-leading order. An insertion of the c_i or b_i vertices is denoted by a black blob. Dashed, solid, and double solid lines refer to pions, nucleons, and Δ resonances, respectively. Crossed and redundant diagrams are not shown.

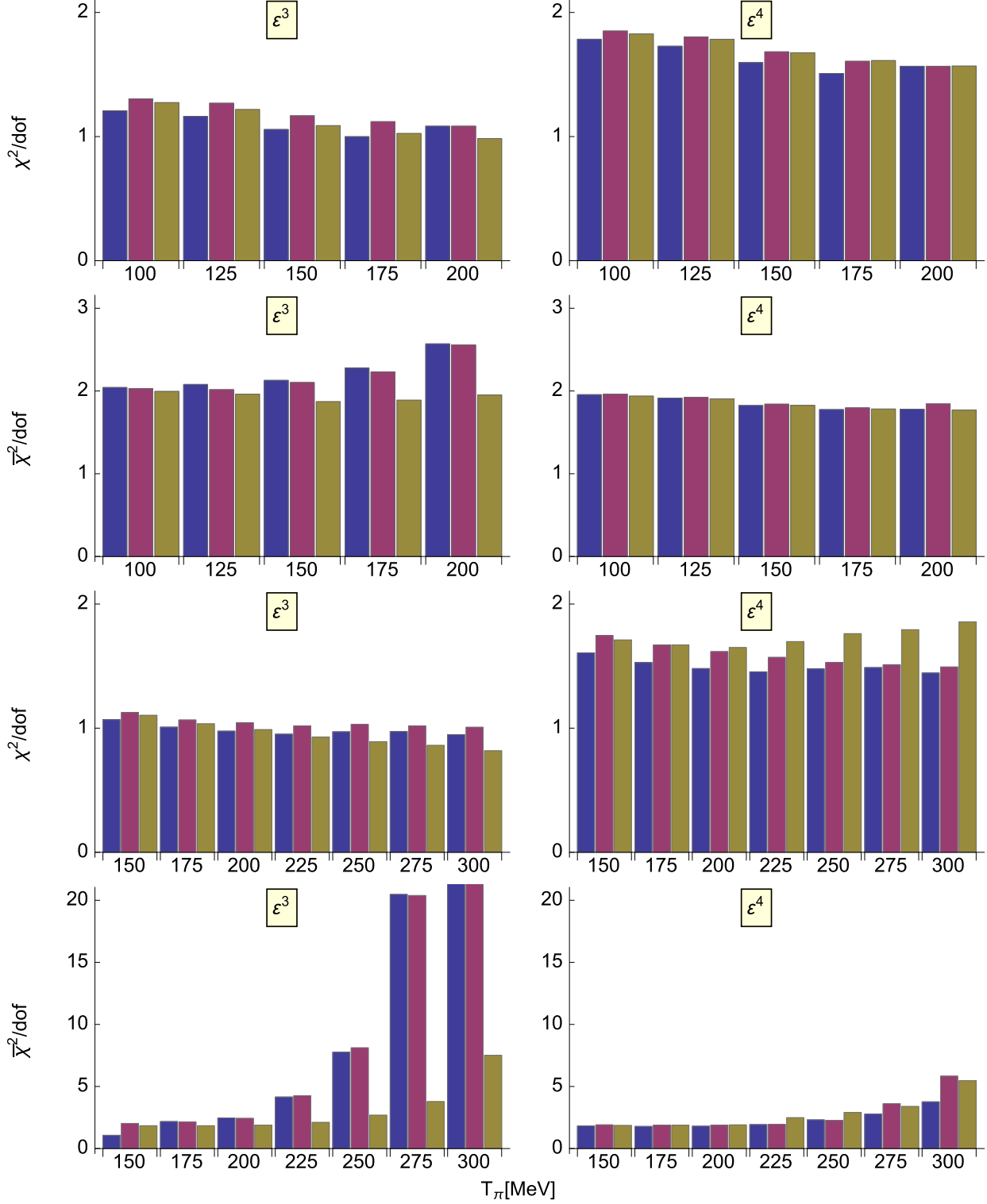


FIG. 2: Reduced χ^2 (with theoretical error) and $\bar{\chi}^2$ (without theoretical error) as functions of the maximum fit energy T_π , see Eq. (44). The results for the HB-NN, HB- π N, and covariant counting are denoted by blue, red, and green bars. The upper two rows refer to fits in the K -matrix approach, whereas the lower two rows refer to fits in the complex mass approach.

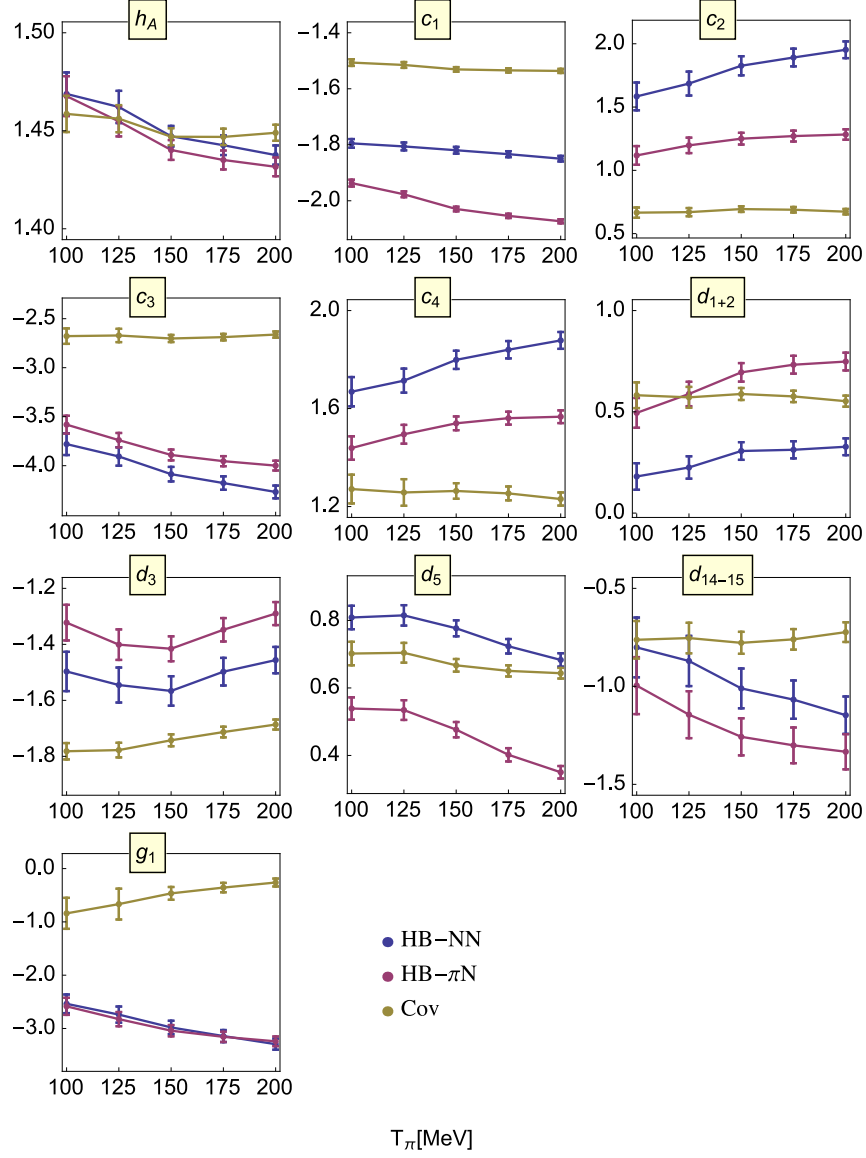


FIG. 3: K -matrix approach: LECs extracted at order ε^3 as functions of the maximum fit energy T_π , see Eq. (44). The labels HB-NN, HB- π N, and Cov (covariant) denote the different counting schemes of $1/m_N$ contributions, see section III.

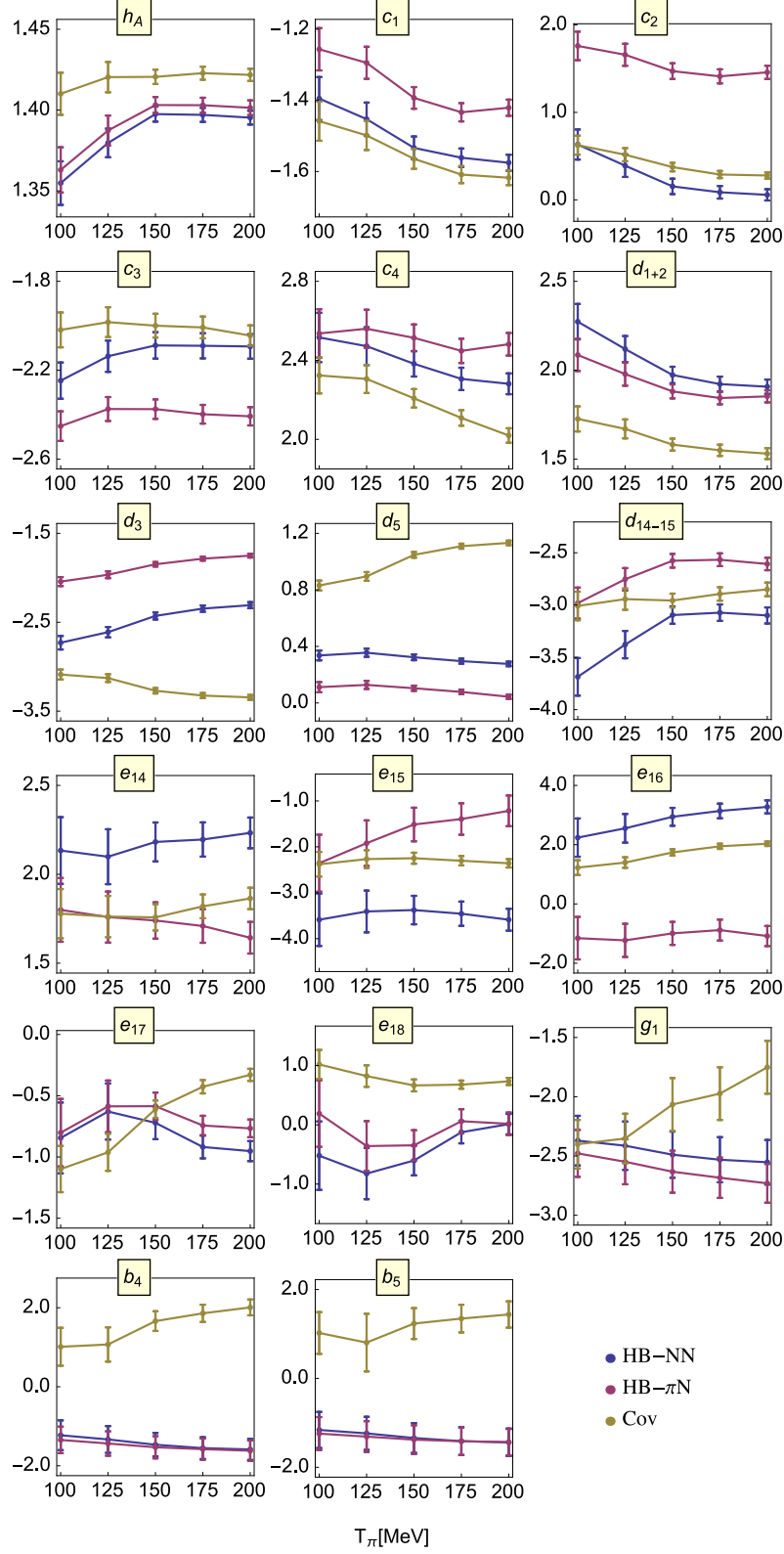


FIG. 4: K -matrix approach: LECs extracted at order ε^4 as functions of the maximum fit energy T_π , see Eq. (44). The labels HB-NN, HB- π N, and Cov (covariant) denote the different counting schemes of $1/m_N$ contributions, see section III.

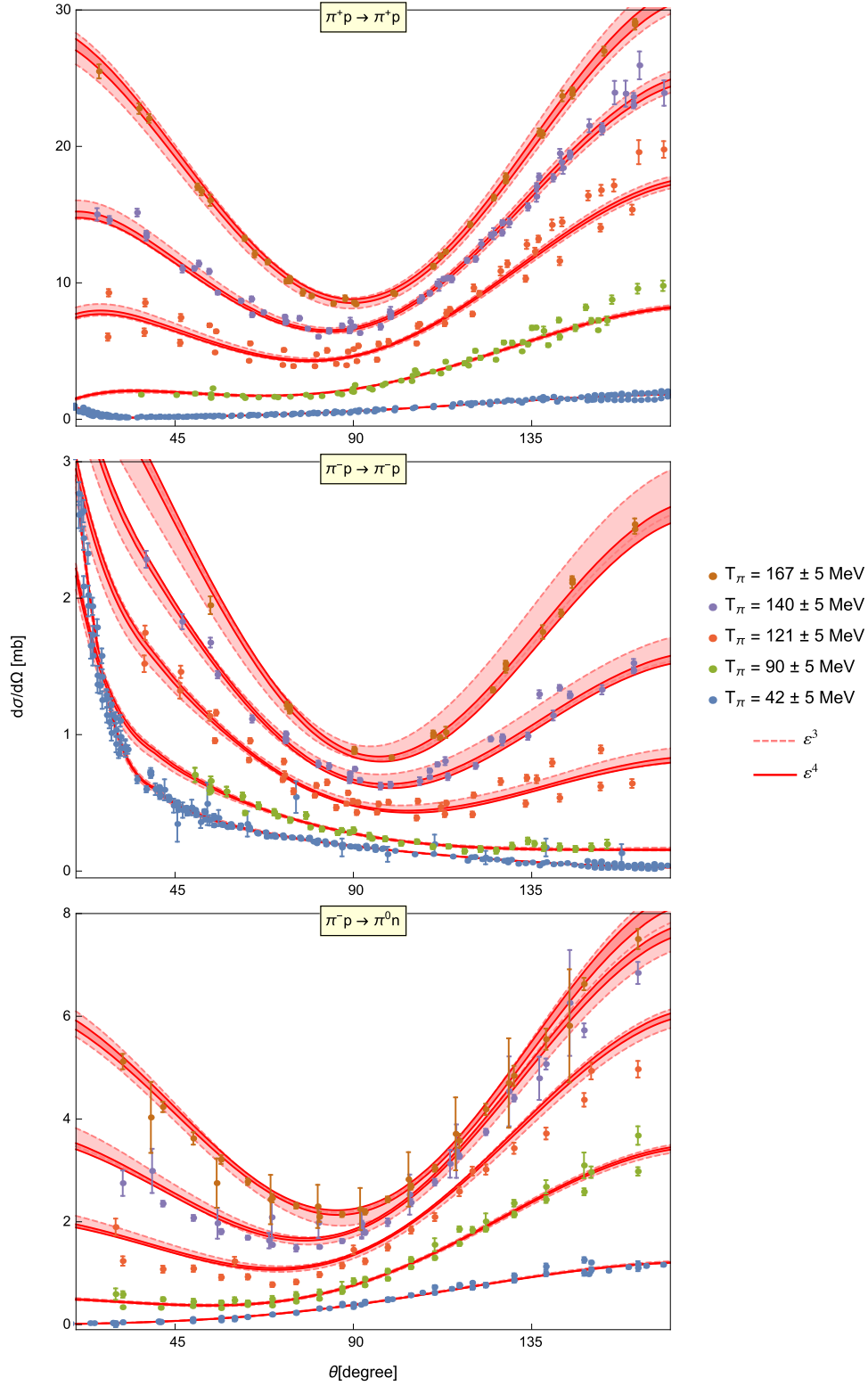


FIG. 5: *K*-matrix approach: Covariant predictions for the differential cross sections $d\sigma/d\Omega$ up to pion energies $T_\pi = 170$ MeV. The pink and red (dashed and solid) bands refer to ε^3 and ε^4 results including theoretical uncertainties, respectively. The experimental data are taken from the GWU-SAID data base [53].

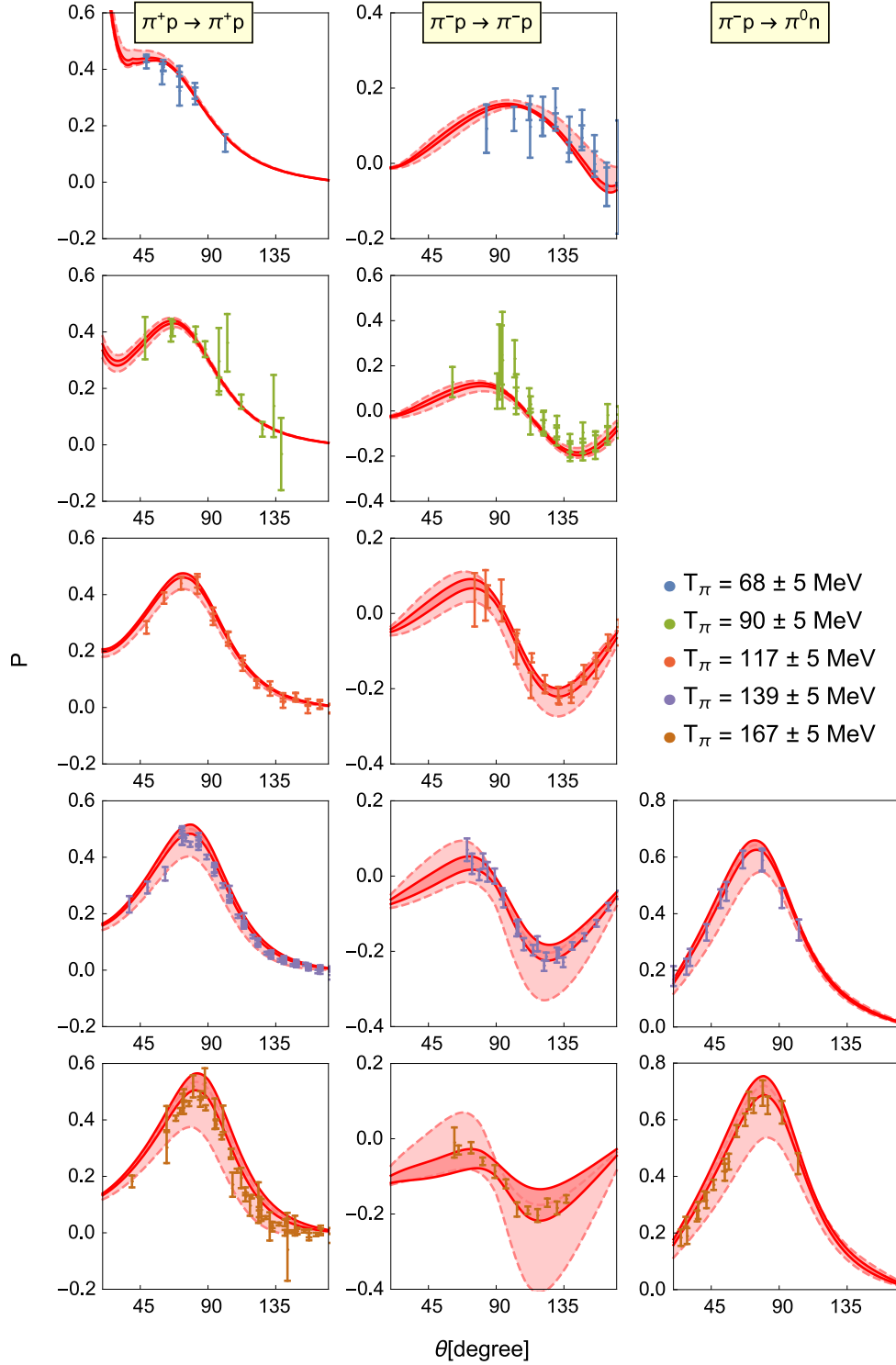


FIG. 6: K -matrix approach: Covariant predictions for the polarizations P up to pion energies $T_\pi = 170$ MeV. The pink and red (dashed and solid) bands refer to ε^3 and ε^4 results including theoretical uncertainties, respectively. The experimental data are taken from the GWU-SAID data base [53].

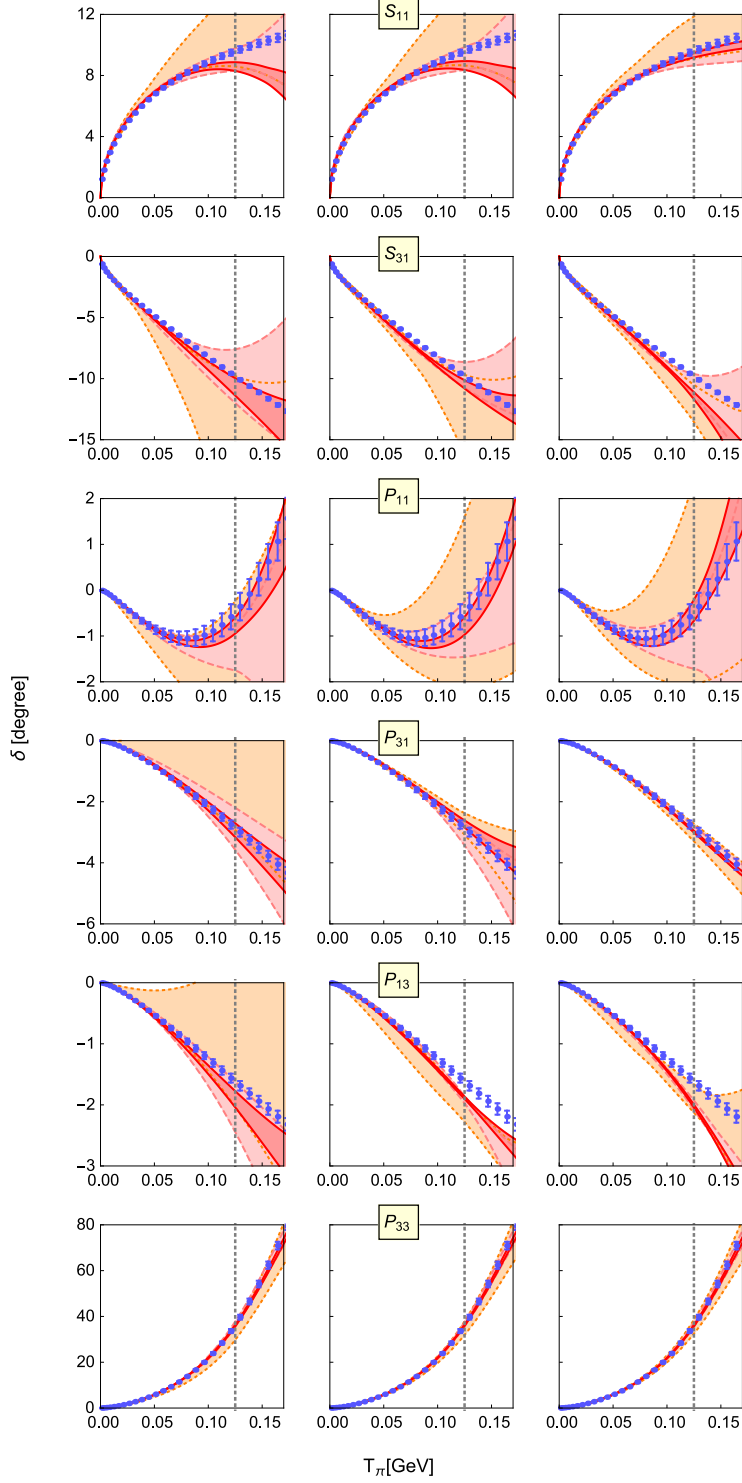


FIG. 7: K -matrix approach: Predicted S - and P -wave phase shifts up to pion energies $T_\pi = 170$ MeV. The predictions in the HB-NN, HB- π N, and covariant counting are given in the columns from left to right, respectively. The orange, pink, and red (dotted, dashed, and solid) bands refer to ε^2 , ε^3 , and ε^4 results including theoretical uncertainties, respectively. The gray dotted vertical line marks the fitting limit. The data are taken from the RS analysis [38].

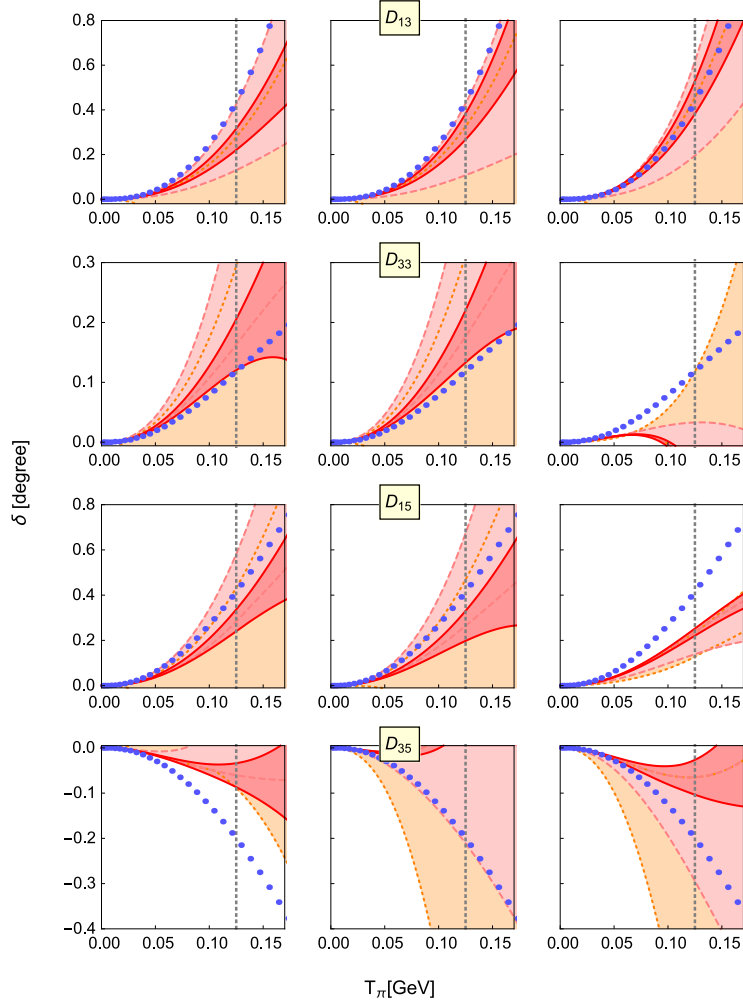


FIG. 8: K -matrix approach: Predicted D -wave phase shifts including theoretical uncertainties up to pion energies $T_\pi = 170$ MeV. The data are taken from the GWU-SAID PWA [53, 60]. For notations see Fig. 7.

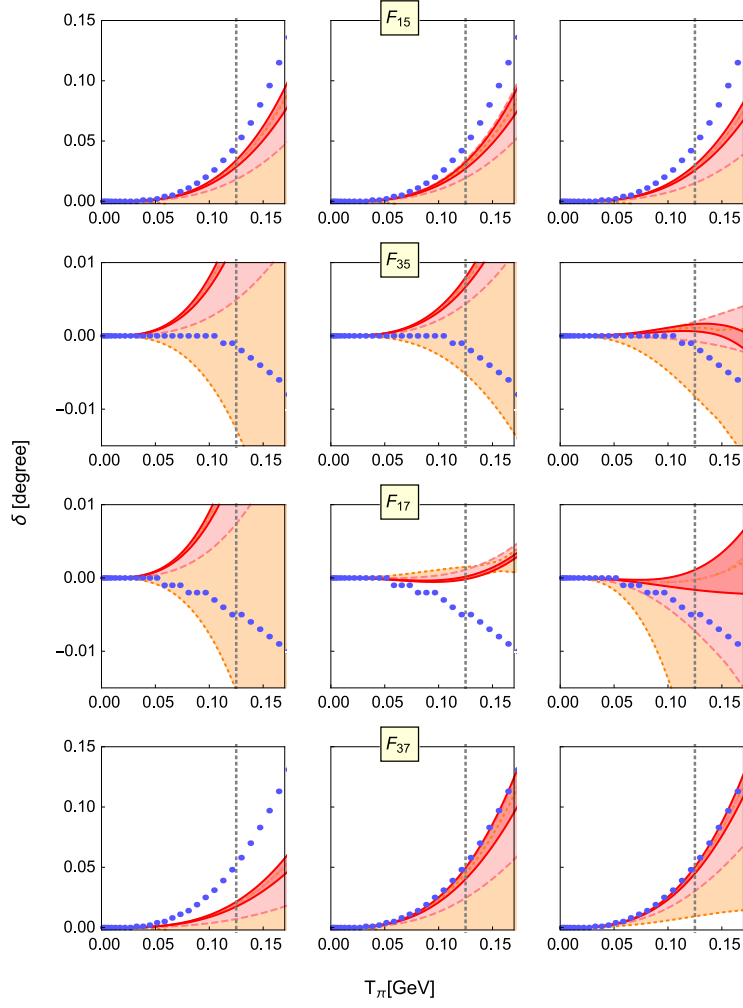


FIG. 9: K -matrix approach: Predicted F -wave phase shifts including theoretical uncertainties up to pion energies $T_\pi = 170$ MeV. The data are taken from the GWU-SAID PWA [53, 60]. For notations see Fig. 7.

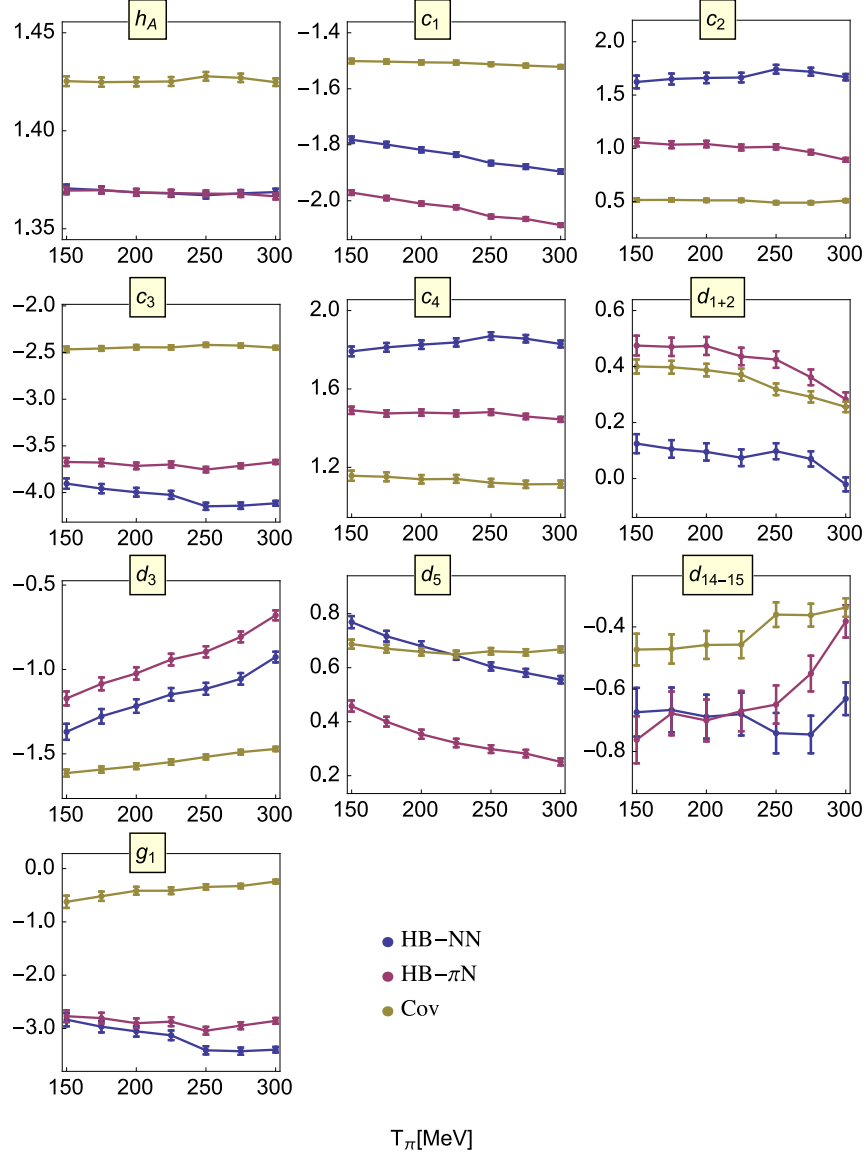


FIG. 10: Complex mass approach: LECs extracted at order ε^3 as functions of maximum fit energy T_π , see Eq. (44). The labels HB-NN, HB- π N, and Cov (covariant) denote the different counting schemes of $1/m_N$ contributions, see section III.

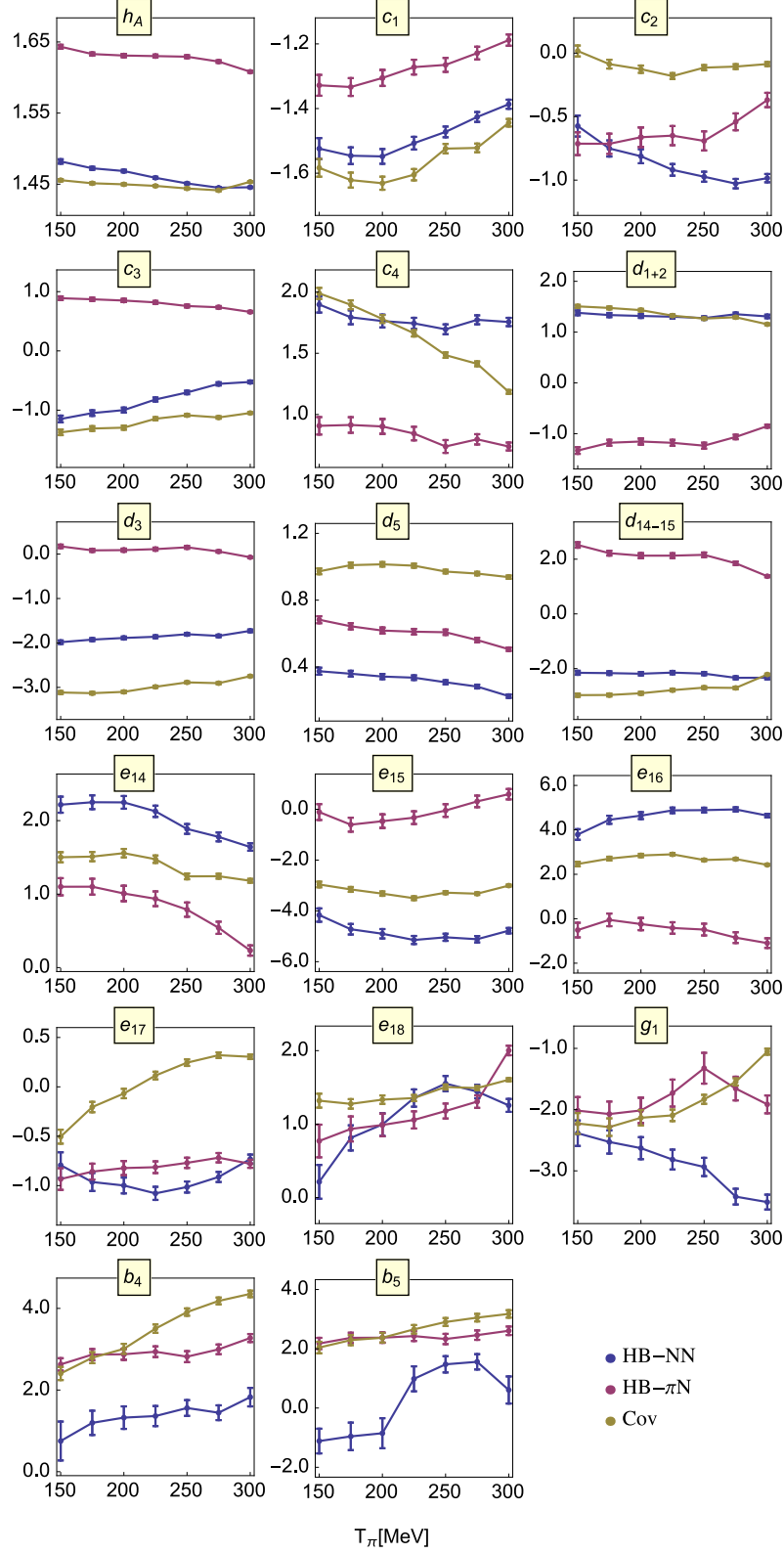


FIG. 11: Complex mass approach: LECs extracted at order ε^4 as functions of maximum fit energy T_π , see Eq. (44). The labels HB-NN, HB- π N, and Cov (covariant) denote the different counting schemes of $1/m_N$ contributions, see section III.

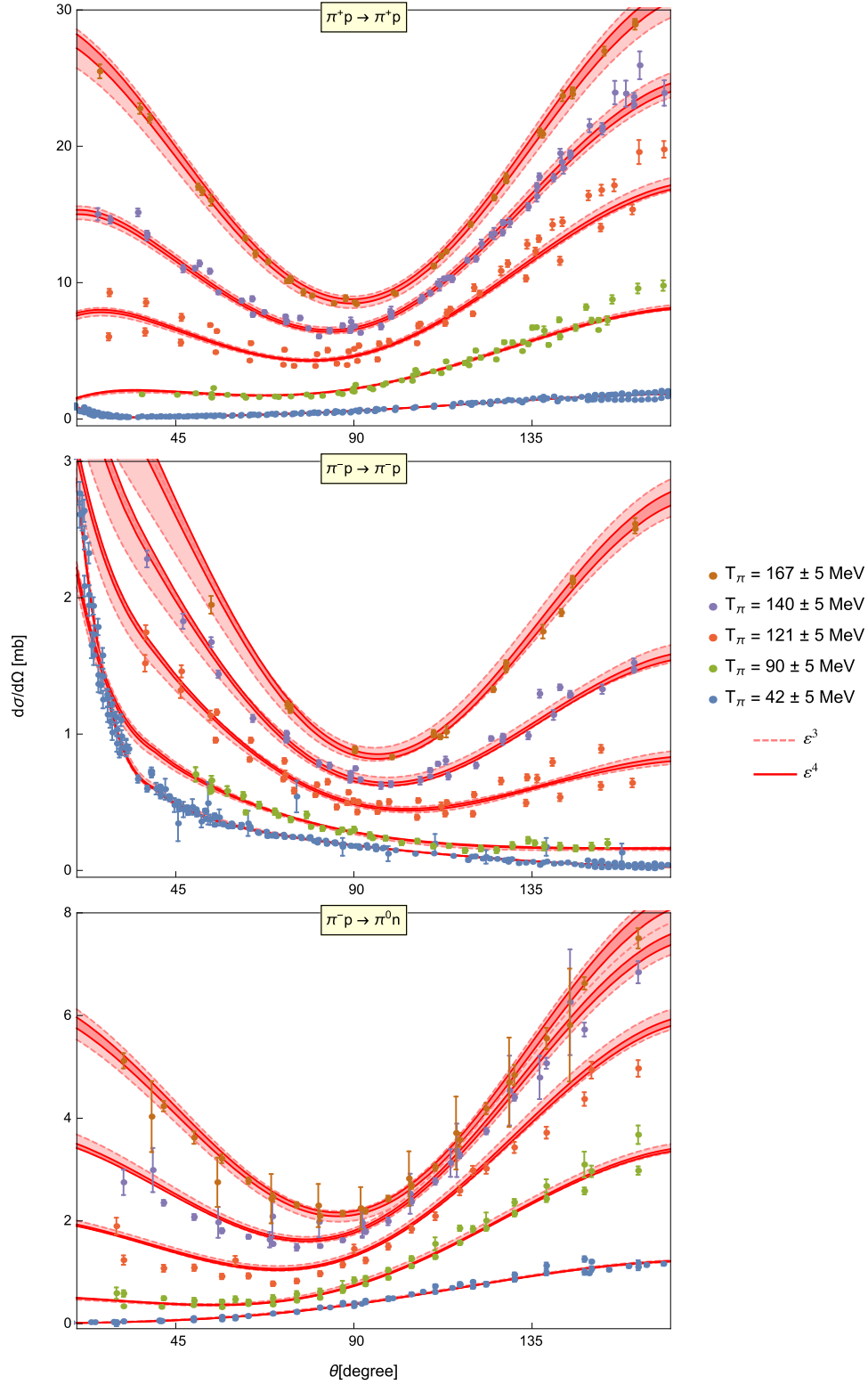


FIG. 12: Complex mass approach: Covariant predictions for the differential cross sections $d\sigma/d\Omega$ up to pion energies $T_\pi = 170$ MeV. The pink and red (dashed and solid) bands refer to ε^3 and ε^4 results including theoretical uncertainties, respectively. The experimental data are taken from the GWU-SAID data base [53].

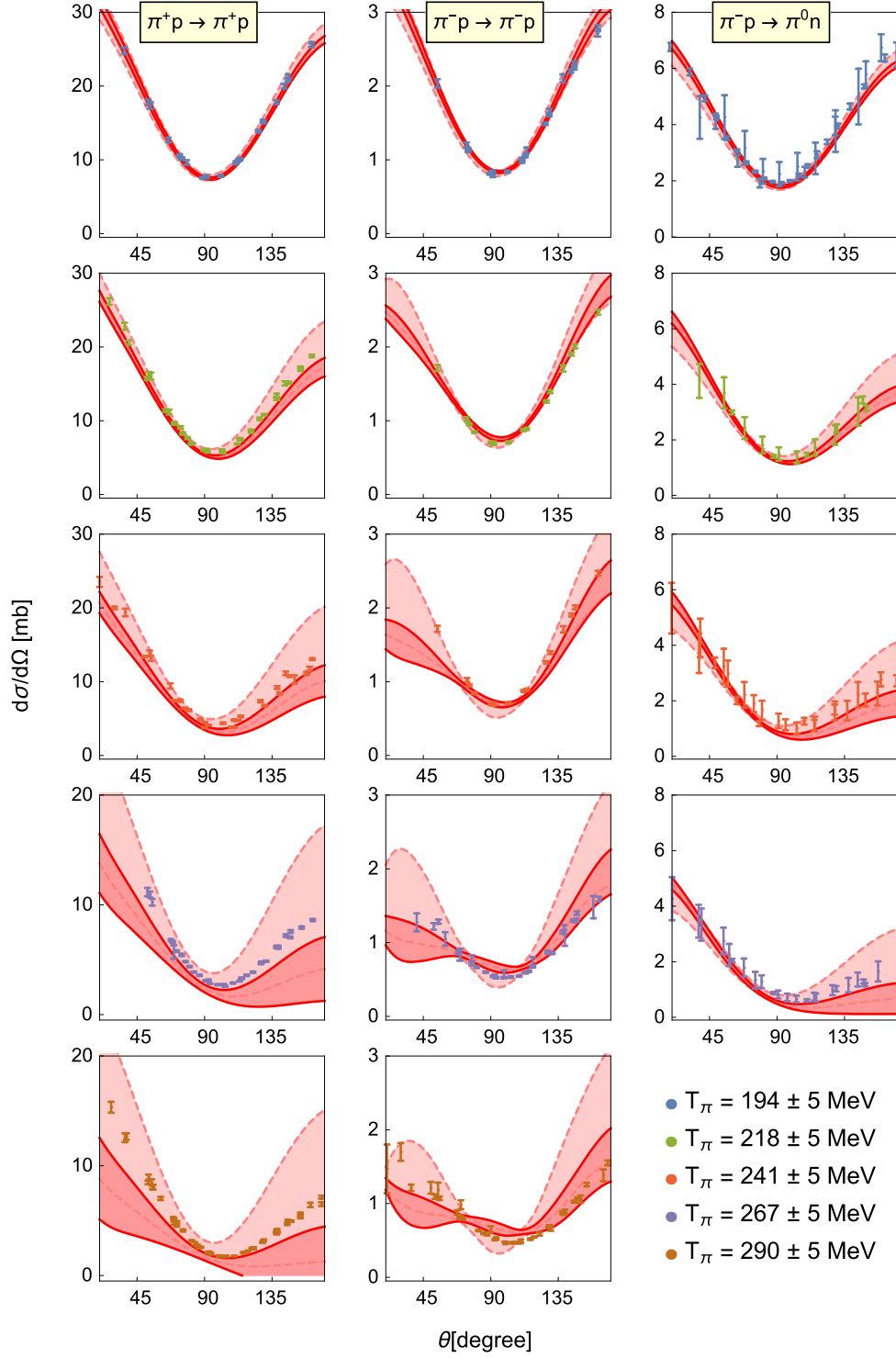


FIG. 13: Complex mass approach: Covariant predictions for the differential cross sections $d\sigma/d\Omega$ up to pion energies $T_\pi = 300$ MeV. The pink and red (dashed and solid) bands refer to ε^3 and ε^4 results including theoretical uncertainties, respectively. The experimental data are taken from the GWU-SAID data base [53].

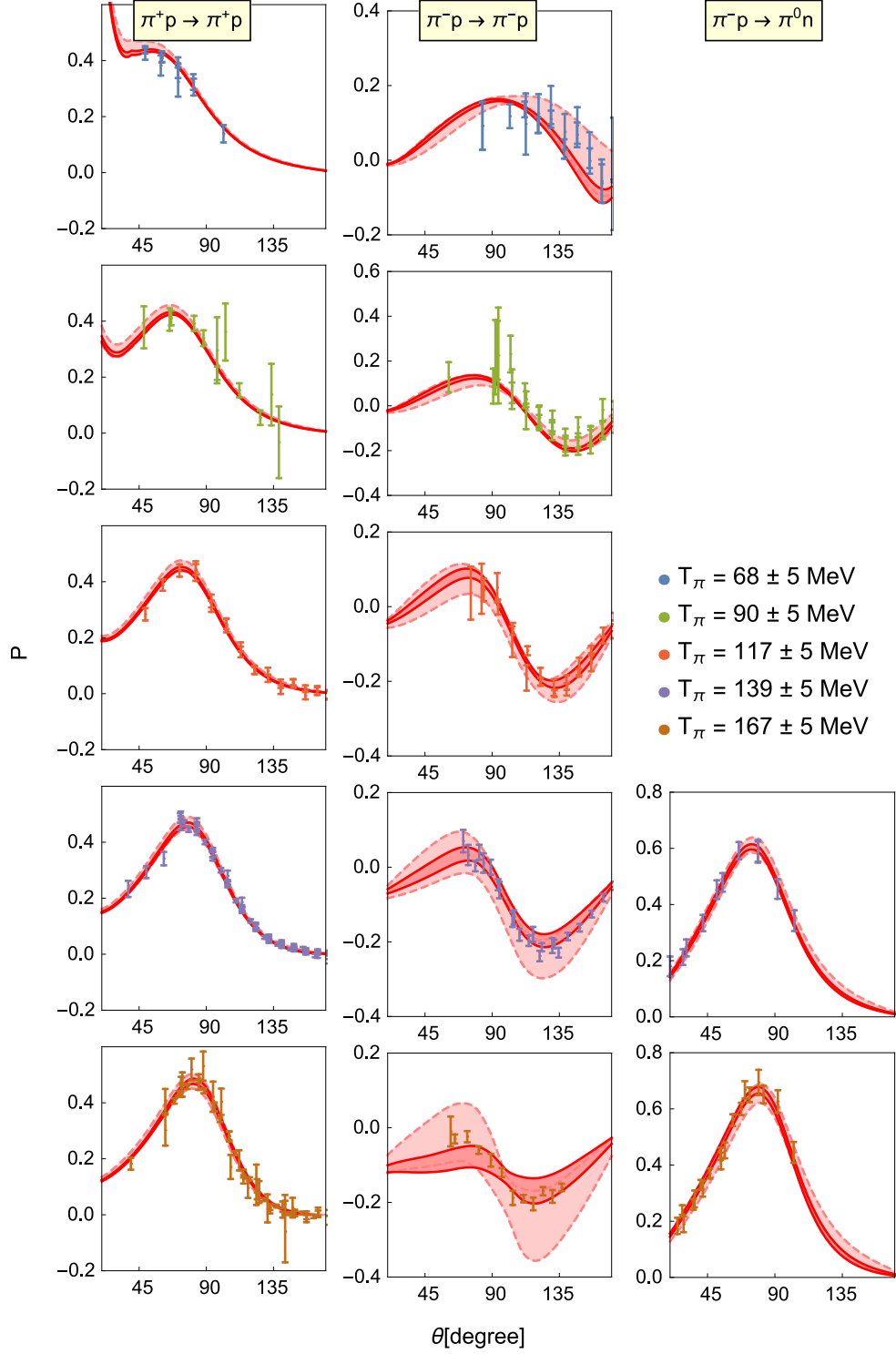


FIG. 14: Complex mass approach: Covariant predictions for the polarizations P up to pion energies $T_\pi = 170$ MeV. The pink and red (dashed and solid) bands refer to ϵ^3 and ϵ^4 results including theoretical uncertainties, respectively. The experimental data are taken from the GWU-SAID data base [53].

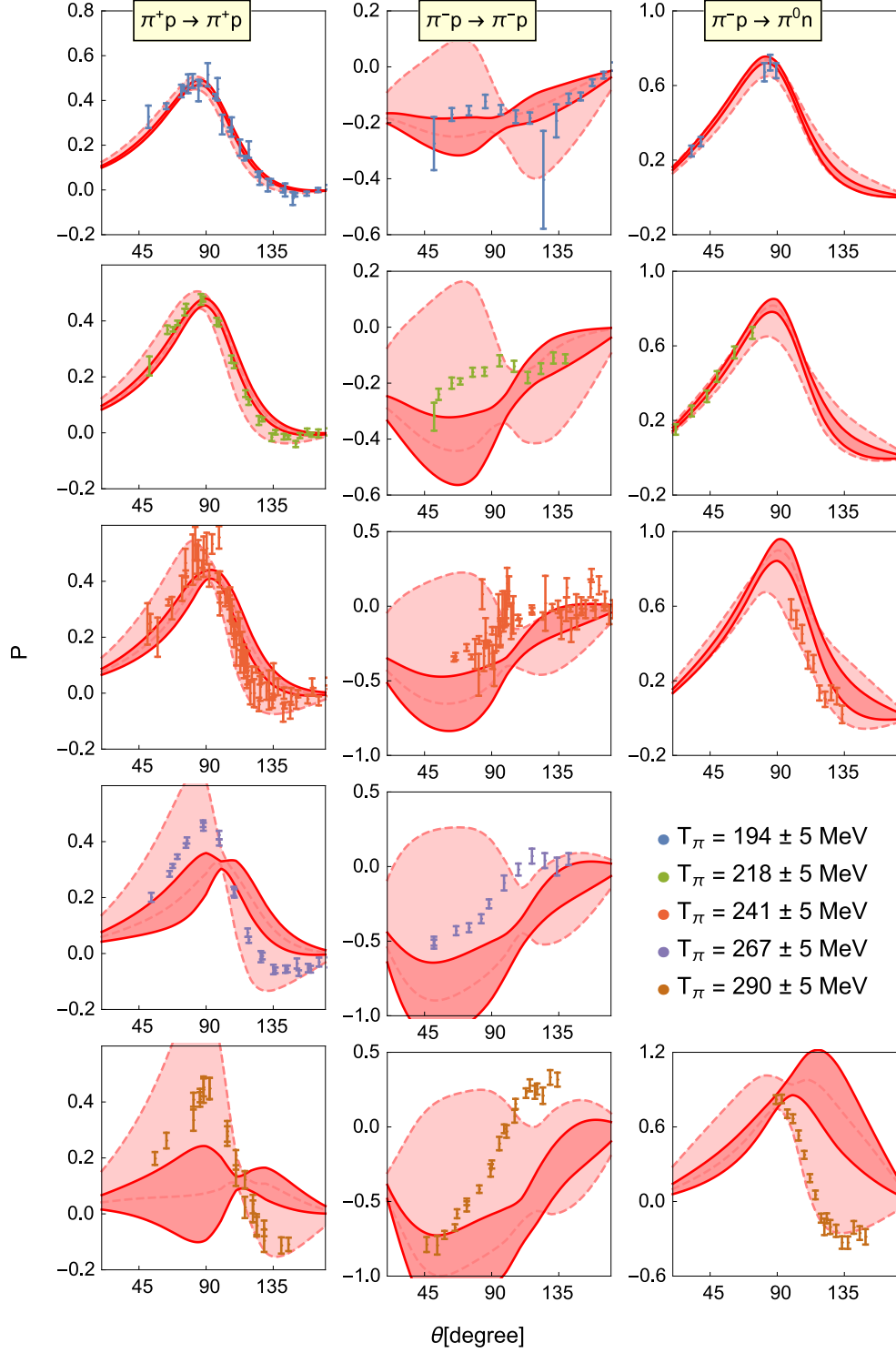


FIG. 15: Complex mass approach: Covariant predictions for the polarizations P up to pion energies $T_\pi = 300$ MeV. The pink and red (dashed and solid) bands refer to ϵ^3 and ϵ^4 results including theoretical uncertainties, respectively. The experimental data are taken from the GWU-SAID data base [53].

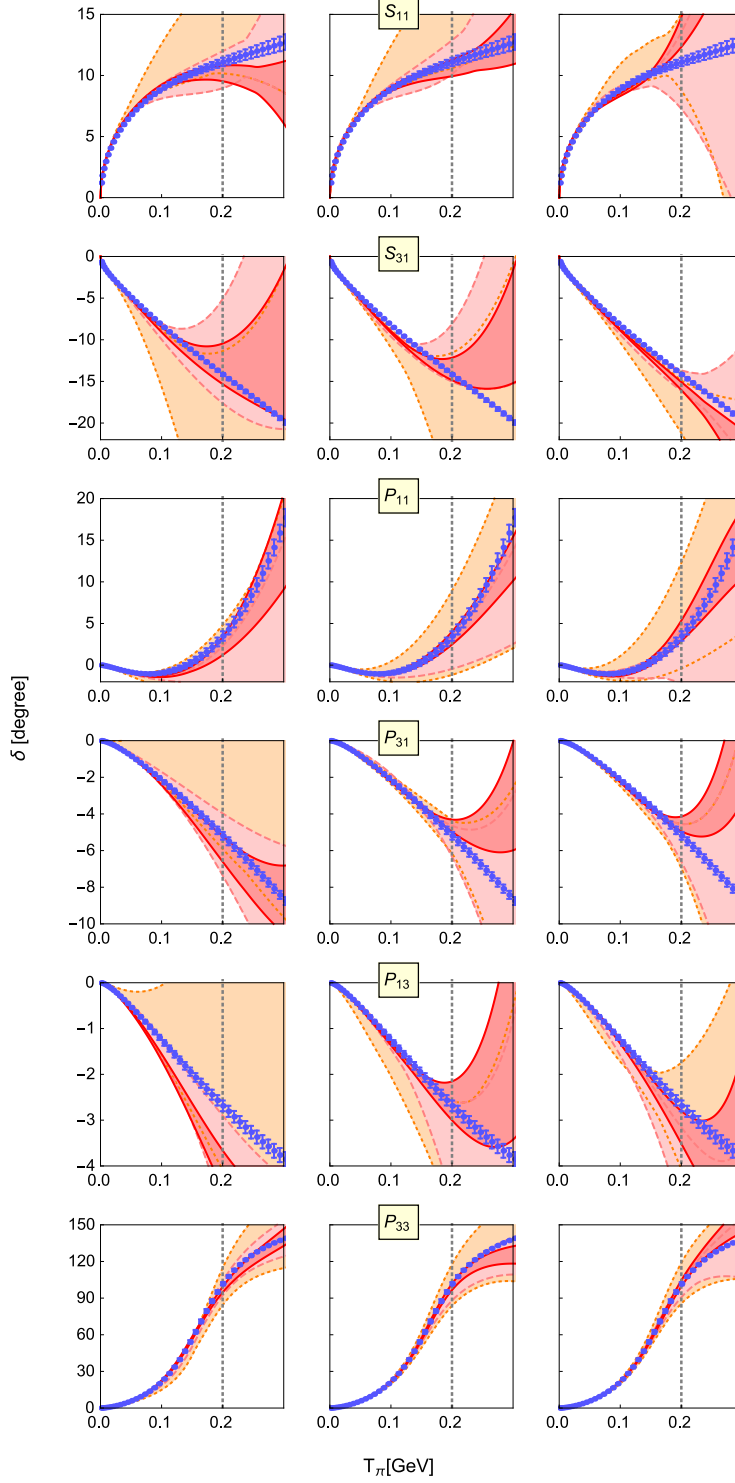


FIG. 16: Complex mass approach: Predicted S - and P -wave phase shifts up to pion energies $T_\pi = 300$ MeV. The predictions in the HB-NN, HB- π N, and covariant counting are given in the columns from left to right, respectively. The orange, pink, and red (dotted, dashed, and solid) bands refer to ε^2 , ε^3 , and ε^4 results including theoretical uncertainties, respectively. The gray dotted vertical line marks the fitting limit. The data are taken from the RS analysis [38].

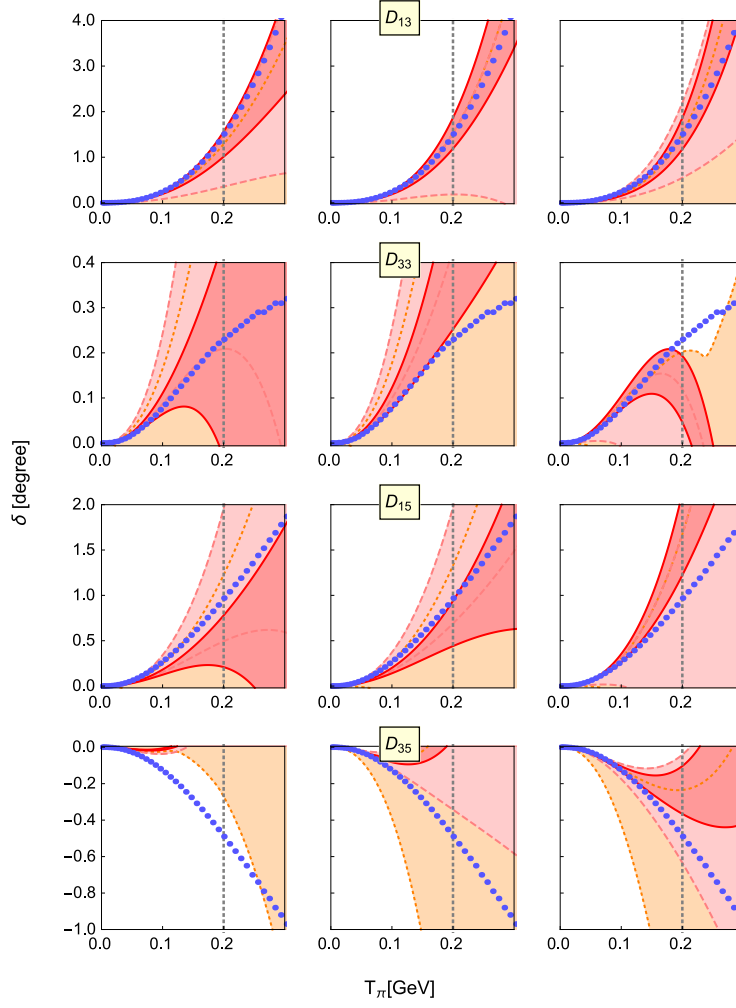


FIG. 17: Complex mass approach: Predicted D -wave phase shifts including theoretical uncertainties up to pion energies $T_\pi = 300$ MeV. The data are taken from the GWU-SAID PWA [53, 60]. For notations see Fig. 16.

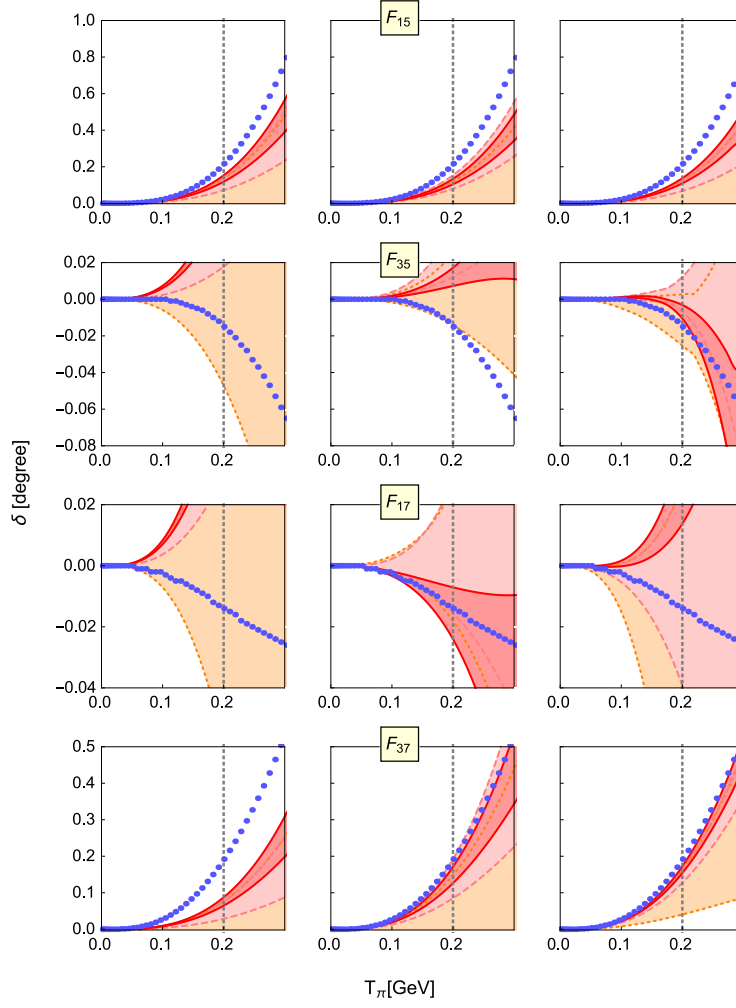


FIG. 18: Complex mass approach: Predicted F -wave phase shifts including theoretical uncertainties up to pion energies $T_\pi = 300$ MeV. The data are taken from the GWU-SAID PWA [53, 60]. For notations see Fig. 16.